



# Clinical Applications of MR Perfusion Imaging

# 5

Seyed Ali Nabavizadeh and Ronald L. Wolf

## Introduction

Perfusion is a physiologic term describing the delivery of blood flow to an organ or tissue. This is expressed in units of blood volume per tissue weight per time (ml/g/min) and in the brain corresponds to cerebral blood flow (CBF). Clinically, however, the term perfusion is often used more generally to describe other hemodynamic parameters in the brain including cerebral blood volume (CBV) and transit measures such as time to peak (TTP), mean transit time (MTT), or time to peak of residue function (Tmax). Several techniques are available for assessing brain perfusion or hemodynamics in a clinical setting, in general falling into two basic categories: those using *diffusible* versus *nondiffusible* tracers.  $H_2^{15}O$  positron emission tomography (PET),  $^{99m}Tc$ -HMPAO or  $^{99m}Tc$ -ECD single photon emission computed tomography (SPECT), stable xenon computed tomography (CT), and arterial spin labeled magnetic resonance imaging (MRI) are examples of diffusible tracer techniques, where the tracer is not confined to the vessels and enters the tissue. The major nondiffusible tracer techniques in use are bolus contrast CT and MR perfusion methods, where the tracer remains within the vasculature as long as the blood–brain barrier (BBB) is intact [1]. Clinical experience in MRI is greatest for bolus contrast or dynamic susceptibility contrast (DSC) perfusion MRI, although application of dynamic contrast-enhanced (DCE) and arterial spin labeled (ASL) perfusion MRI is increasing in the clinical setting [2].

Bolus contrast perfusion techniques, for MRI primarily dynamic susceptibility contrast (DSC), are more extensively used in daily clinical practice. One reason for this is the simple fact that DSC perfusion MRI has been in use longer and experience in using this approach is thus greater. In addition,

this approach is easier to implement, more widely available on clinical scanners, and many postprocessing packages are readily available on- and offline, many of which are now U.S. Food and Drug Administration (FDA)-approved. Compared to ASL perfusion MRI, DSC perfusion MRI has higher signal-to-noise ratio (SNR) and acquisition time is shorter. In addition to CBF, relatively straightforward calculation of perfusion metrics such as CBV and TTP is available with DSC perfusion MRI as compared to ASL methods, though there are potential solutions for the latter [3, 4]. Disadvantages include need for intravenous (IV) contrast and adequate IV access for rapid infusion, conspicuity of large vessels, and the need to address breakdown of the BBB in acquisition and/or postprocessing.

On the other hand, ASL perfusion MRI techniques have several advantages compared to DSC techniques. A primary advantage is that ASL methods are completely noninvasive. Another is that absolute quantitation is possible. In addition, ASL methods are relatively insensitive to permeability effects, and are less affected by large vessel signal. Multiple (and unlimited) repeated measurements can be obtained and CBF measurements can be repeated immediately with ASL, such that changes with one or more interventions can easily be studied. CBF maps can be obtained with temporal resolution as fast as 3–8 s for perfusion-based functional MRI—as opposed to relying on the (blood oxygen level dependent) BOLD effect [5–7]. Finally, it is possible to selectively label vascular territories or even individual vessels noninvasively, which is impossible to accomplish with DSC perfusion MRI [8–10]. Disadvantages include lower SNR, longer acquisition time, and artifacts from prolonged transit times.

Improvements such as higher field strength scanners, pulse sequence design, background suppression, parallel imaging, coil technology, and postprocessing techniques have led to improvements for both DSC and ASL perfusion MRI. Practical utility of perfusion methodology has been demonstrated for several applications, including acute and chronic cerebrovascular disease, central nervous system (CNS) neoplasms, epilepsy, and aging and neurodegenera-

S. A. Nabavizadeh · R. L. Wolf (✉)  
Department of Radiology, Division of Neuroradiology, Perelman  
School of Medicine at the University of Pennsylvania,  
Philadelphia, PA, USA  
e-mail: [ali.nabavizadeh@pennmedicine.upenn.edu](mailto:ali.nabavizadeh@pennmedicine.upenn.edu);  
[ronald.wolf@pennmedicine.upenn.edu](mailto:ronald.wolf@pennmedicine.upenn.edu)

tive disorders [1, 2, 11, 12]. This chapter focuses primarily on practical clinical applications of perfusion imaging in cerebrovascular diseases and CNS neoplasms, using selected examples to illustrate strengths, weaknesses, or complementary roles of these perfusion MRI approaches. Other applications for perfusion MRI including neuropsychiatric, epilepsy, and neurodegenerative diseases will not be discussed in this chapter revision.

## Principles

### Dynamic Susceptibility Contrast Perfusion MRI

DSC implementations use some form of snapshot imaging such as echo-planar imaging (EPI) to follow the first pass of an injected contrast agent, allowing for the acquisition of baseline data prior to arrival of the bolus. When the BBB is intact, the injected contrast agent (the tracer) remains intravascular and microscopic susceptibility gradients are created around vessels as the tracer passes through. This creates signal loss, which depends on the concentration of the tracer. Though the relationship of signal loss to concentration is nonlinear, the time-intensity curve can be used to estimate a time-concentration curve. Parametric maps describing perfusion can be created from these data, including CBV and estimates of delay such as TTP. With more sophisticated analysis accounting for dispersion in the arterial input function (AIF), CBF, MTT, and other parametric maps including T<sub>max</sub> can be created. The acquisition strategy has an effect on the signal change in such experiments, where gradient echo or spin echo EPI sequences can be used to obtain T<sub>2</sub>\*-weighted or T<sub>2</sub>-weighted image data, respectively, with the T<sub>2</sub>-weighted approach yielding less signal change for a given concentration of tracer but less sensitivity to large vessels [13].

In practice, the assumption of an intact BBB is often violated causing unwanted T<sub>1</sub> and T<sub>2</sub>\* relaxation effects leading to inaccurate relative CBV (rCBV) measurements [14]. There are several strategies for correcting for this pitfall; however, preload contrast injection to reduce any T<sub>1</sub> changes followed by postprocessing correction for leakage a voxel-wise basis and dual-echo spiral-based acquisition are considered to be the most effective techniques [15]. Another approach is replacing gadolinium-based contrast agent with blood pool agents that remain intravascular regardless of leakiness of BBB. Multiple investigators used ferumoxytol, which is an ultrasmall superparamagnetic iron oxide nanoparticle in DSC perfusion imaging. Ferumoxytol is FDA approved for iron replacement therapy and can act as a blood pool agent. In an animal study, Gahramanov et al. compared DSC perfusion using a gadolinium-based contrast

agent without preload, with single-dose preload, and with double-dose preload to DSC perfusion using ferumoxytol. They demonstrated that tumor rCBV was underestimated without preload and became dose dependent with preload correction, while ferumoxytol provided consistent assessment of tumor rCBV [16]. The same group also studied 14 patients with glioblastoma multiforme (GBM) following chemoradiation who underwent DSC perfusion with gadoteridol on day 1 and ferumoxytol on day 2 and demonstrated that gadoteridol-DSC showed low rCBV in 3 patients and high rCBV in 4 patients, whereas ferumoxytol-DSC showed high rCBV in 7 patients with active tumor. They concluded that ferumoxytol may better differentiate tumor progression from pseudoprogression [17]. Despite these preliminary promising results, use of ferumoxytol is not suitable for repeated follow-up studies because of potential iron overload [18]. Another limiting factor would be hypersensitivity reactions and/or hypotension that can occur in a small percentage of patients receiving intravenous ferumoxytol [19]. In addition, contrast enhancement on follow-up studies can be altered by the presence of residual ferumoxytol such that short interval follow-up studies can be difficult to interpret.

### Dynamic Contrast-Enhanced Perfusion MRI

This technique is based on relaxivity measurements using a steady-state T<sub>1</sub>-weighted sequence during gadolinium contrast administration. In brief, basic data acquisition involves the use of a three-dimensional (3D) T<sub>1</sub>-weighted sequence with temporal resolution on the order of 5 s, imaging at baseline and during and after a contrast bolus over a period of several minutes to obtain time-concentration curves. DCE perfusion MRI can be analyzed using 2 general approaches. The first approach, which is frequently used in non-CNS tumors such as breast but also can be used in CNS neoplasms, is model-free analysis of the area under the time-signal intensity curve (AUC) during a selected part of the curve. The approach is straightforward and does not require complex postprocessing models. The second approach to analyze DCE data is to use pharmacokinetic models, most commonly a modified Tofts model where each voxel contains 3 components: an intracellular space, an intravascular space, and an extracellular extravascular space (EES). Typical calculated parameters include: K<sub>trans</sub>, which is a measure of microvascular permeability; K<sub>ep</sub>, which is the reflux rate of gadolinium from the EES back into plasma; total plasma space volume (V<sub>p</sub>); and total extravascular-extracellular space volume (V<sub>e</sub>), [20, 21]. This approach is addressed in further detail in Chap. 7.

## Arterial Spin Labeled Perfusion MRI

ASL perfusion MRI uses the patient's own water molecules in blood as an internal contrast agent to measure tissue perfusion. In brief, arterial blood water is labeled and allowed to flow into the imaging plane(s), during which time there is T1 decay of the label. Subtraction of labeled images from unlabeled control images yields a difference image, in which measured signal change is proportional to CBF. Multiple labeled/control image pairs are typically acquired and averaged since the SNR is inherently low with this technique, with a signal change of only a few percent between labeled and control images. ASL studies require no IV contrast and no delay between acquisitions [22, 23]. There are many strategies for acquiring ASL data with pulsed, continuous, and more recently pseudocontinuous labeling, all based on the same basic principle. In routine clinical practice, pulsed and pseudocontinuous ASL are readily available on most of the current MR scanners, the latter labeling strategy supplanting continuous ASL.

---

## Clinical Applications

### Cerebrovascular Disorders

The primary goals of perfusion techniques in acute and subacute cerebrovascular disorders are to determine presence and extent of tissue that is either dead or likely injured despite intervention and presence and extent of tissue that is at risk but salvageable. For chronic cerebrovascular disease, the primary goal is to evaluate impaired perfusion leading to impaired function (transient or chronic) and to assess future risk of ischemic injury. Several perfusion techniques have been applied in this setting, including SPECT, bolus contrast CT perfusion (CTP), stable xenon CT, and MR perfusion techniques. This section discusses the use of MR perfusion techniques in the evaluation of cerebrovascular disorders, with a focus on non-acute ischemia (outside treatment windows for tissue plasminogen activator [tPA] and/or mechanical thrombolysis). Perfusion in acute ischemic stroke is briefly addressed here, but this topic is covered in more detail in Chap. 6.

### Acute Ischemia

#### MR Perfusion and Acute Ischemic Syndrome

MR and CT perfusion (MRP and CTP) techniques are well suited for the evaluation of acute ischemic injury and are the most commonly used perfusion methods in the United States in this setting. MRP can also be easily combined with diffusion-weighted imaging (DWI) and MR angiography (MRA) for a comprehensive ischemic stroke evaluation. The superior contrast resolution in MRI, particularly the avail-

ability of DWI, is a distinct advantage compared to CT. The addition of MRP and MRA to a basic MRI evaluation of the brain (e.g., DWI, gradient echo or susceptibility-weighted sequence, and FLAIR) provides a comprehensive evaluation for ischemic stroke and can be completed in as little as 6 min [24]. For bolus contrast or ASL MR perfusion, one advantage over CTP is the lack of ionizing radiation. Allergic reactions and renal dysfunction are less of a problem with gadolinium-based contrast agents; however, these agents are not without risk as allergic reactions do occur and other rare reactions including nephrogenic systemic fibrosis (NSF) have been described [25]. Gadolinium deposition in neural tissues in patients with normal renal function have also been described in many publications, although the clinical significance of this phenomenon remains to be determined [26].

Access to the unstable patient is not optimal in MRI, and simply preparing and moving a critically ill patient to the MR scanner is not always trivial due to issues such as logistics related to the MR environment including adjustment of lines for IV recombinant tPA (rtPA) administration and clearing the aphasic patient for MRI. Relative and absolute contraindications to MRI such as pacemakers/defibrillators and other devices must also be taken into account, and though one can still obtain MRI in many of these cases, unacceptable delays may occur.

CTP can be easily combined with noncontrast head CT (NECT) and CT angiography (CTA) of the head and neck to obtain a fast and comprehensive evaluation of the acute ischemic stroke patient. It is less expensive than MRI and more widely available at all hours of the day in most centers. Quantitation of perfusion parameters is more easily obtained for bolus contrast CT than MR perfusion, where the concentration of iodine and attenuation are linearly related, while the concentration of gadolinium is not linearly related to signal intensity. There are some disadvantages to CTP such as exposure to ionizing radiation, iodinated contrast and potential impact on renal function, and potential allergic reaction. Limited coverage (2–4 cm), which used to be a limiting factor on the older version of multidetector scanners (4–64 channels) but this is less of an issue with current multidetector scanner configurations, and whole brain CTP is now considered the standard of care. Other alternatives for routine clinical perfusion imaging include SPECT and stable xenon CT. An excellent discussion of the relevant literature as well as a summary of the strengths and weaknesses of these techniques in acute ischemic stroke can be found in multiple resources for interested readers [27–29].

The primary goal of perfusion imaging in this setting is to evaluate tissue viability. MRI with DWI is superior to CTP for demonstration of infarct core, but CTP can estimate core using CBV or CBF as a surrogate. MRP can be combined with DWI to estimate hypoperfused but viable tissue at risk for infarction (i.e., penumbra) (Fig. 5.1) though quantitation

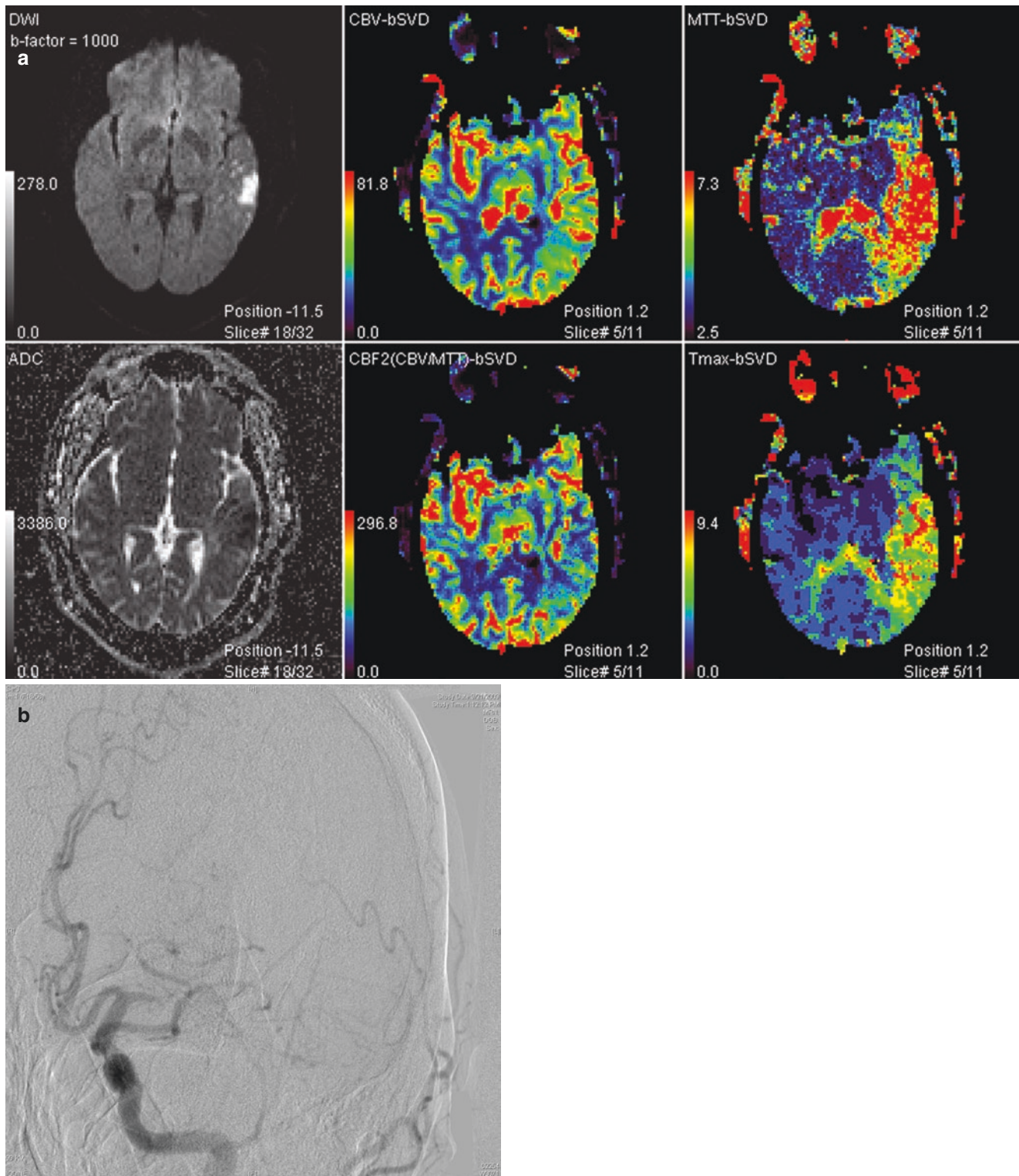


**Fig. 5.1** (a, b) DSC perfusion MRI in acute ischemia: a 56-year-old with gradual onset expressive aphasia approximately 8 h prior. Diffusion-perfusion mismatch is evident on left with prolonged  $T_{max} > 5$  s, decreased  $rCBF = 0.80$ , increased  $rCBV = 1.15$ , and prolonged

MTT. Chemical thrombolysis (IA-tPA) was performed with successful recanalization. \*DSC perfusion using “PMA” image analysis software (copyright owner: Kohsuke Kudo) provided by ASIST-JAPAN

of metrics such as CBF is not as straightforward. Nevertheless, using DSC MR perfusion, hemodynamic parameters including TTP, MTT, and Tmax can be used to evaluate tissue at risk. Tmax is a relatively robust marker of hypoperfusion and has been used in multiple stroke trials in the past 10–15 years [30–32]. Application of automated postprocessing streamlines workflow, increases speed and efficiency, and decreases variability between different centers. Despite the widespread application of Tmax in acute stroke clinical trials, there is still not consensus on which value should be used in mismatch analysis. For example, in the DEFUSE trial (Diffusion and perfusion imaging Evaluation For Understanding Stroke Evolution), a mismatch was a priori defined as a ratio greater than 1.2 between the hypoperfused regions with Tmax >2 s and restricted diffusion [32]; however, a post-hoc analysis of DEFUSE trial data demonstrated that a Tmax threshold between 4 and 6 s was more optimal for early identification of critically hypoperfused tissue [33]. In the DEFUSE 2 trial, a Tmax > 6 s was used to define the target mismatch volume [30]. Overall, despite the lack of consensus, more recent clinical trials moved toward using stricter thresholds for Tmax (> 6 s rather than 2 s) in order to avoid overestimation of penumbra volume [34, 35]. This includes the very recently published DEFUSE 3 trial, which indicated the superiority of endovascular thrombectomy plus medical therapy compared to medical therapy alone for ischemic stroke 6–16 h after the patients were last known to be well [35].

ASL imaging has also been used to evaluate the penumbra in multiple studies and several studies reported concordant results in comparison to DSC perfusion [36–38]. In addition, focal curvilinear bright signal on ASL images can be used to help identify the level of vascular occlusion [39, 40]. It can be particularly helpful when normal or hyperperfusion is present, indicating lack of perfusion-diffusion mismatch or helping identify an AIS mimic [41].

DSC MR perfusion has been used to determine the collateral state in patients with acute stroke in multiple studies predominantly focusing on measures of delayed transit. Olivot et al. demonstrated that a smaller hypoperfusion intensity ratio (volume Tmax > 6-second/Tmax > 10-second delay) was associated with good collateral status [42]. Lee et al. demonstrated that severely delayed perfusion with a Tmax of 16–22 s is associated with poor collateral state [43]. Recently, Nael et al. applied a multiparametric approach and demonstrated that Perfusion Collateral Index—defined as volume of ATD (arterial tissue delay)<sup>2-6s</sup> × rCBV<sup>2-6s</sup>—provides an accurate estimation of baseline collateral status in patients with anterior circulation proximal arterial occlusion [44]. ASL perfusion has also been used to assess collateral circulation in acute ischemic stroke. De Havenon et al. demonstrated that the subjects with ASL collaterals have better neurological outcome at hospital discharge [45]. Lyu et al. used 3D pseudocontinuous ASL in patients with unilateral

middle cerebral artery (MCA) stenosis with postlabeling delays of 1.5 and 2.5 s and demonstrated moderate to strong correlation with cerebral angiography for estimation of antegrade and collateral flow [46].

Lou et al. applied a multidelay ASL technique and demonstrated that higher leptomeningeal collateral scores can be predictive of clinical outcome in patients with acute MCA ischemic stroke after endovascular treatment [47].

### Luxury Perfusion and Reperfusion Injury

Reperfusion after recanalization can lead to edema and hemorrhage, as well as neuronal injury in the penumbra [11, 48]. A potential indicator for hemorrhagic transformation includes extent of parenchymal injury on CT [49], and this is also true for extent of diffusion and perfusion abnormalities [50–53]. In a retrospective study based on xenon CT perfusion [54], it was found that CBF values below 10 and perhaps even less than 15 cc/100 g/min in aggressively managed acute MCA infarct patients could be associated with increased risk of hemorrhage, edema, and herniation with or without reperfusion. MRI-derived permeability measurements have also been applied in this setting [55–58]. Finally, hyperperfusion on ASL can be a predictive biomarker for prediction of post-ischemic hemorrhagic transformation in acute infarction [59].

### Subacute and Chronic Ischemia

As in the acute setting, the significance of a particular patient's cervicocranial stenotic-occlusive disease is modified by many factors. In the head, quality of collaterals, autoregulation and cerebrovascular reserve (CVR), metabolic rate of oxygen (CMRO<sub>2</sub>) and oxygen extraction fraction (OEF) modify the impact of a particular lesion. Extracranially, modifying factors include blood pressure, cardiac status, and type of plaque (i.e., “vulnerable” plaque). While most cerebrovascular events are probably thromboembolic, perfusional or low-flow events also result in symptoms and can modify the impact of a thromboembolic event [60]. Perfusion imaging is thus a logical approach in assessing the hemodynamic status of the brain or the hemodynamic significance of a particular lesion.

An instructive model of hemodynamic failure divides increasing severity into stages: (stage 0) cerebral perfusion pressure and other hemodynamic parameters are normal; (stage 1) cerebral perfusion pressure (CPP) decreases but autoregulation allows compensatory vasodilation, which maintains CBF, OEF and CMRO<sub>2</sub>; (stage 2) CBF cannot be maintained and begins to decrease and OEF increases to maintain CMRO<sub>2</sub>; (Stage 3) CBF decreases enough that CBV, OEF, and CMRO<sub>2</sub> decrease and anaerobic metabolism increases. Depending on the duration of hemodynamic status in stage III, ischemia develops and cell death occurs [61, 62]. There is likely to be some blurring between stages; for example, autoregulatory vasodilation and increased OEF may occur together [63, 64].

This model illustrates that a simple measurement of baseline CBF is inadequate for assessment of hemodynamic compromise. Absolute CBF values can be informative in the sense that thresholds have been reported for suppression of electrical activity in neurons (CBF about 20–40% of normal) and cell death (CBF <20% of normal), modified by duration [65]; however, not only can hemodynamically stressed tissue maintain normal CBF in the face of abnormal CPP, but CBF can be low in tissue, which is not at risk in some situations such as when metabolic rate is low (e.g., with some anesthetic agents). In addition, absolute measures of CBF are not necessarily straightforward. As noted previously, the relationship between gadolinium concentration and signal intensity is nonlinear; and thus, while reasonable estimates of CBF are possible, a relative measure is often used. Qualitative analysis comparing abnormal side to contralateral side can be useful, but may be misleading when both sides are abnormal or when more global perfusion impairment is present as with moyamoya or poor cardiac output. ASL techniques provide a better estimate of absolute blood flow, but can be misleading when long delays are present leading to transit artifacts.

Typical strategies to more completely assess hemodynamic compromise using perfusion methods such as MRP fall into two main categories: (1) CBF measures before and after a vasodilatory challenge (e.g., hypercapnea or acetazolamide) and (2) measuring CBV and other perfusion parameters in addition to CBF (Fig. 5.2). A third strategy would be to measure OEF directly using PET, though this is not trivial and not widely available. In recent years, MRI techniques such as susceptibility-based oximetry (SBO) and T2-relaxation-under-spin-tagging (TRUST) were developed for quantifying the cerebral metabolic rate of oxygen (CMRO<sub>2</sub>) and oxygen extraction fraction (OEF) [66–68], but their added value in the context of cerebral ischemia still needs to be validated. Finally, MR perfusion strategies can provide an indirect assessment of OEF; for example, there is a negative correlation of CO<sub>2</sub> reactivity and OEF such that regions of the brain with impaired CVR and prolonged CBV/CBF ratio (MTT) show the highest OEF values [62, 69].

### Perfusion Patterns in Stenotic-Occlusive Disease

There are many reports describing detectable differences in hemodynamic parameters in cerebral vascular territories and/or border zones on the side of high-grade carotid stenosis or occlusion. Many of these studies report asymmetric increase in TTP or MTT on the side of stenosis/occlusion with more variable results regarding changes in CBF or CBV [70–79]. It makes sense that detection of a delay in transit can be a sensitive and early indicator of hemodynamic disturbance, but this is not necessarily specific or predictive of hemodynamic compromise and likely overestimates risk [80, 81]. Note is made that many of these studies were also performed with symptomatic patients (recent infarcts or transient ischemic attacks [TIAs]), and interpretation in the

setting of recent ischemia is more complex [61, 62]. Also, improvements in perfusion analysis including delay-insensitive methods should refine understanding in the setting of transit delays and feeding vessel dispersion [13, 82, 83]. Olivot et al. [84] studied patients with subacute or chronic ischemia and found that Tmax correlated better than MTT with absolute CBF measured with stable xenon CT MTT, with Tmax greater than 4 s and MTT greater than 10 s associated with Xe-CT CBF less than 20 mL/100 g/min.

Historically most MR-based studies of subacute or chronic cerebrovascular disease to date have employed DSC PWI techniques, but ASL techniques were subsequently being applied to acute and chronic cerebrovascular disease [85–87]. Here again, transit delays were a primary issue [88–91]; for example, Wolf et al. [90] studied patients with acute/subacute or chronic cerebrovascular with continuous ASL and spin-echo DSC perfusion MRI, finding that perfusion deficits on ASL correlated best with prolonged TTP in the presence of a major transit delay related to stenotic occlusive disease. CBF measurements for both techniques correlated best when major transit delay cases were excluded. Kimura et al. [89] used a CASL technique to measure CBF and compared to O15-labeled CO<sub>2</sub> PET measurements of CBF, also estimating arterial and tissue transit times. Though ASL and PET CBF measurements correlated well, the slope of the regression lines varied and they concluded that long transit time in occlusive cerebrovascular disease may underestimate CBF on the affected side.

Simply incorporating a postlabeling delay reduces sensitivity to transit artifact and improves accuracy [92]. For PASL methods, limiting the bolus width decreases sensitivity to variable transit times. Long postlabeling delay times are increasingly feasible with improvements in technique including improved labeling schemes such as pseudocontinuous ASL (pCASL), phased array coils, 3D techniques with background suppression, and use of higher field strength with associated T1 prolongation and longer label lifetime [12, 93, 94]. Postlabeling delays of 2400 ms or longer are feasible (Fig. 5.3). Techniques with multiple delay (inversion) times can be used to generate CBF measurements accounting for variable transit times as well as calculating the transit times and arterial blood volume [3, 95]. Using such a technique, Hendrikse et al. [96] studied patients with carotid occlusion and reported decreased CBF in the ipsilateral MCA territory compared to the contralateral hemisphere and to control subjects. In another study, ASL with multiple delays was used to show border zones based on prolonged arterial transit times in normal volunteers, also measuring differences in CBF and arterial blood volume (decreased values) in the border zones [97]. Bokkers et al. [98, 99] studied patients with symptomatic ICA stenosis or occlusion using ASL PWI with multiple delay times, finding decreased regional and border zone CBF and prolonged transit time and trailing edge of the label in the hemisphere ipsilateral to the occlusion compared to control

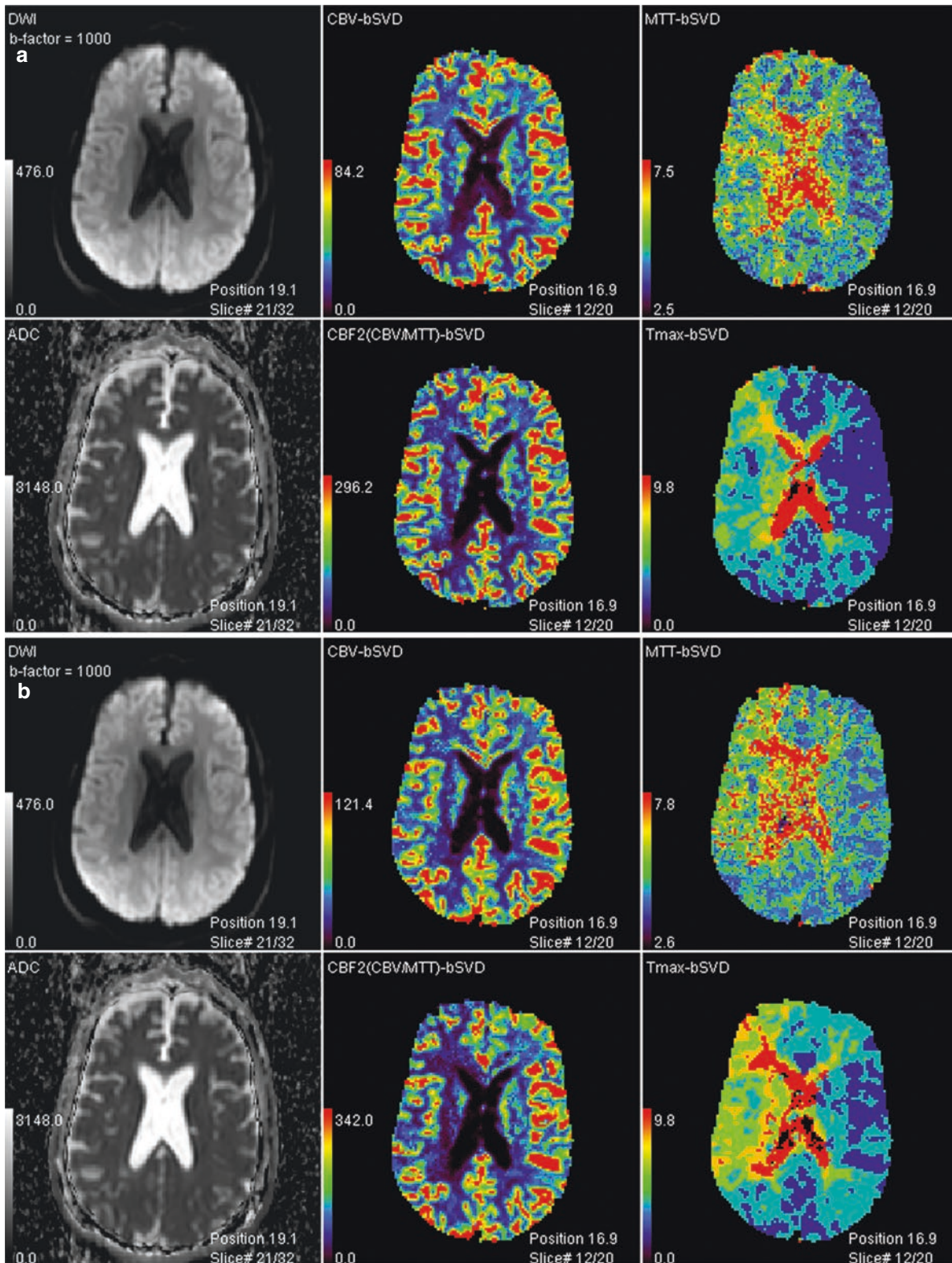


**Fig. 5.2** DSC perfusion MRI before and after acetazolamide for assessing CVR: a 44-year-old with occluded right ICA, left intracranial ICA stenosis, and worsening left-sided weakness without territorial infarct, prior history of surgery and radiation for suprasellar neoplasm. At baseline (*top image*), right MCA territory perfusion parameters compared to left were  $rCBF = 0.86$ ,  $rCBV = 1.06$ , and  $rMTT = 1.14$ .

$T_{max} = 5$  s on right and 3 s on left. After acetazolamide (*bottom image*),  $rCBF = 0.64$ ,  $rCBV = 0.75$ , and  $rMTT = 1.22$ .  $T_{max} = 6.4$  s on right and 3.4 s on left. The left intracranial ICA stenosis was stented with improvement in symptoms. \*DSC perfusion using "PMA" image analysis software (copyright owner: Kohsuke Kudo) provided by ASIST-JAPAN

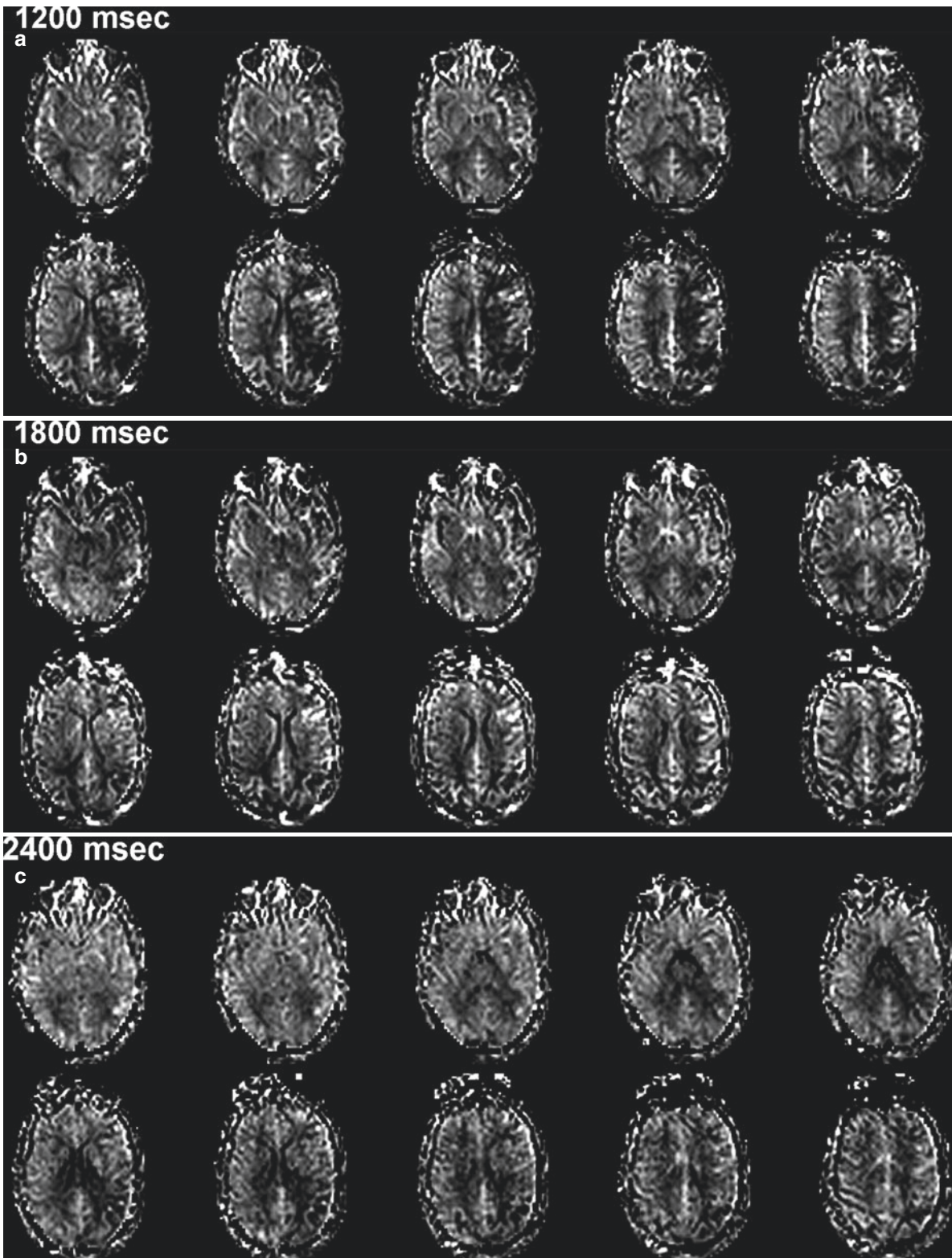


**Fig. 5.3** Improved quantification of absolute CBF using 3D ASL technique based on GRASE with background suppression and pseudocontinuous labeling (pCASL): a 60-year-old status post STA-MCA bypass for left MCA stenosis, now asymptomatic. (a) Perfusion acquisition at

post-labeling delays of 1200 ms shows watershed perfusion deficit with large vessel signal indicating transit delay artifact. Longer postlabeling delays of (b) 1800 ms and (c) 2400 ms show progressive loss of large vessel transit artifact and improved depiction of cortical blood flow



subjects. ASL measurement of white matter CBF may be less accurate, but this is also of interest not only in the setting of border zone hemodynamics [100] but also with regard to the potential relationship of white matter hypoperfusion and ischemic leukoaraiosis [101, 102].

### Cerebrovascular Reserve (CVR)

CVR can provide prognostic information in chronic cerebrovascular disease [64, 103–105], and this can be accomplished with MR perfusion techniques in addition to PET, SPECT, xenon CT, and TCD techniques. Typically, paired measures are obtained, one baseline acquisition at rest and another after a vasodilatory challenge with acetazolamide, CO<sub>2</sub> inhalation or physiologic task such as motor activity or breath-holding. The problem with these challenges is that it is difficult to generate standard stimuli that can be compared between individuals or in the same individual over time [106]. For example, in the case of acetazolamide injection, the dose, rate of injection, and volume of distribution will affect the blood concentration. In addition, there is variability

in different subject's response to acetazolamide [107]. The same unpredictable response applies to administration of a fixed inspired concentration of CO<sub>2</sub> [108]. The most effective technique to standardize the vasodilatory challenge is to control the partial pressure of end-tidal CO<sub>2</sub> [107]. Interested readers can refer to a detailed review by Fisher comparing these two methods [108].

DSC perfusion MRI acquisitions can be repeated (e.g., after a challenge as with acetazolamide) and this approach has been used in several studies (Fig. 5.2) [109, 110]; however, there are certain limitations including total gadolinium dose in multiple repeated acquisitions and the potential for the contrast agent to change the relaxation properties of the blood for a relatively long period of time making it less reliable to compare the serial perfusion measurements during the same MRI session. ASL perfusion MRI is particularly attractive in this setting since it is not dose-limited and repeated measures can be more efficiently obtained [111, 112] (Fig. 5.4). The limitation of ASL imaging in CVR in steno-occlusive disease is inaccuracies in flow measure-

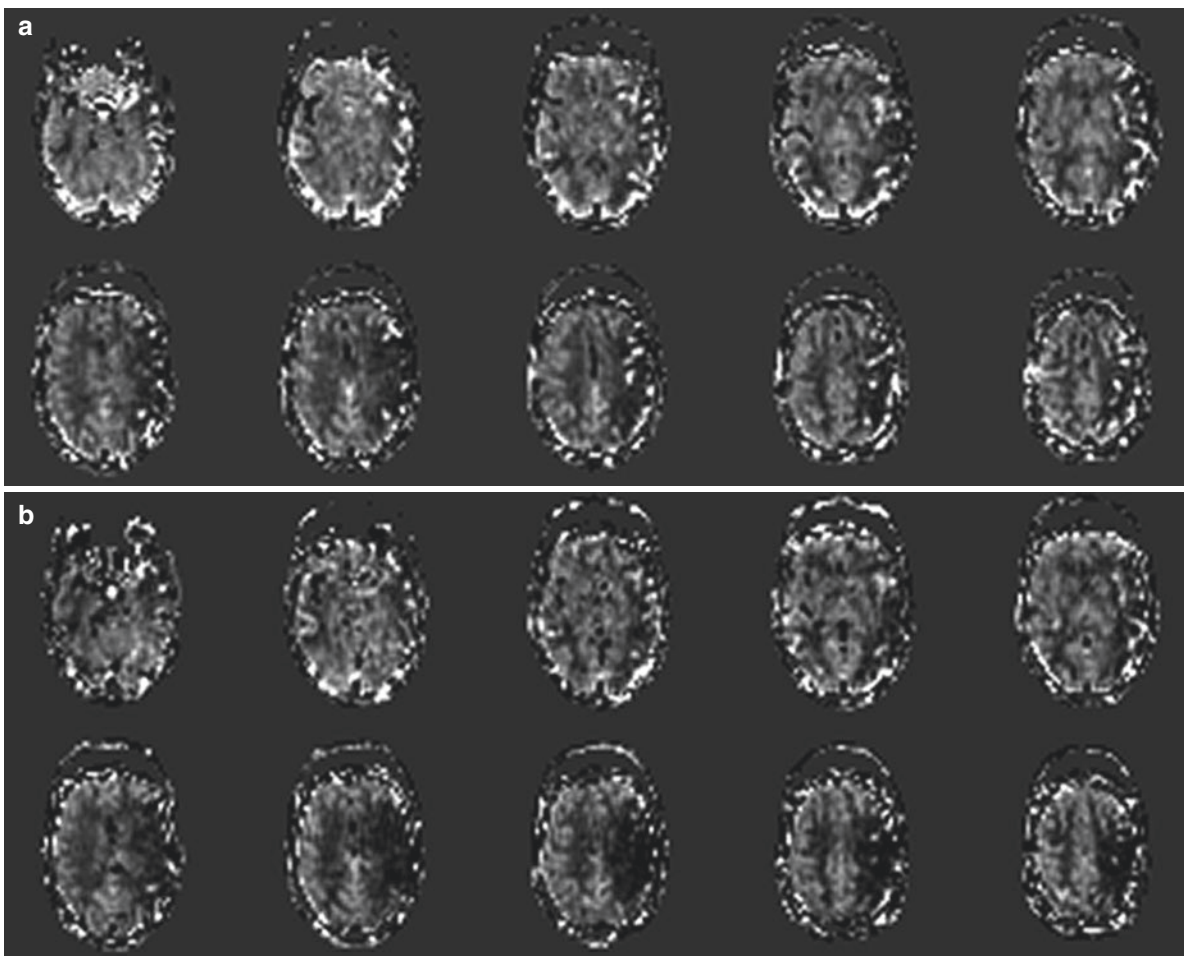


**Fig. 5.4** PASL perfusion MRI before and after acetazolamide for assessing CVR: a 60-year-old with left MCA stenosis, presenting with intermittent right-hand numbness and weakness and expressive aphasia (same patient as in Fig. 5.3). (a) Baseline perfusion images show per-

fusion deficit left MCA territory, with bright signal in large vessels indicating transit delay artifact. (b) Post-acetazolamide perfusion shows increase in extent of perfusion deficit

ments secondary to delayed transit times [107], recent studies focusing on multiple and/or long postlabeling delay ASL imaging to address this limitation. Choi et al. compared ASL imaging with 7 PLDs ranging from 1–3.32 s in 30 patients with unilateral internal carotid artery (ICA) or MCA stenocclusive disease to Tc99m-HMPAO SPECT and demonstrated that transit time-corrected CBF and arterial transit time based on arterial spin-labeling perfusion MRI can predict cerebrovascular reserve impairment [113]. Recently, Fan et al. compared standard, multidelay ASL, and long-label long-delay ASL acquisitions with [<sup>15</sup>O]-PET CBF maps in 15 moyamoya patients and demonstrated that long-label long-delay ASL scans (postlabel delay = 4.0 s) showed the strongest correlation relative to PET [93] (Fig. 5.5).

CVR measured using BOLD techniques has also been described [112, 114–116]. For example, Mandell et al. found reasonable agreement in evaluating CVR with BOLD and ASL methods using a CO<sub>2</sub> challenge [112]. The main limitation of this technique is that it does not provide an absolute measure of CBF; the relationship with CBF is not linear especially at high flow rates [107].

### Territorial Mapping and Collateral Evaluation in Stenotic-Occlusive Disease

Early studies of collateral circulation and its effect in the setting of cerebrovascular stenotic-occlusive disease used a

combination of MRA and bulk macrovascular flow measurements with MR phase contrast techniques [117, 118]. Kluytmans et al. [119] studied the relationship of hemodynamic alterations on DSC perfusion MRI and collateral status as judged by MRA (for circle of Willis) and sonography (for ophthalmic artery) in patients with severe carotid stenosis, unilateral carotid occlusion, or bilateral carotid occlusion, finding that collateral status significantly influenced hemodynamic status. Bokkers et al. [99] used PC MRA or DSA to assess effect of circle of Willis and leptomeningeal collaterals on CBF measured using ASL with multiple delay times, finding hemodynamic impairment in frontal regions when leptomeningeal collaterals were present as compared to when they were not.

ASL methodology provides the ability to separately label individual cerebral arteries and measure the anatomic extent and contribution to CBF in the respective vascular territories on a microvascular scale [120]. This can be done with separate labeling and imaging coils [121], tilted or offset labeling planes or slabs [8, 9, 122–125], or more selective labeling of individual arteries [10, 126]. Examples of clinical applications of selective labeling schemes include studies of the variability of major vascular territories [127], assessment of functional contributions of circle of Willis and leptomeningeal collateral pathways in the setting of ICA or MCA stenosis [128, 129], demonstration of functional contribution of

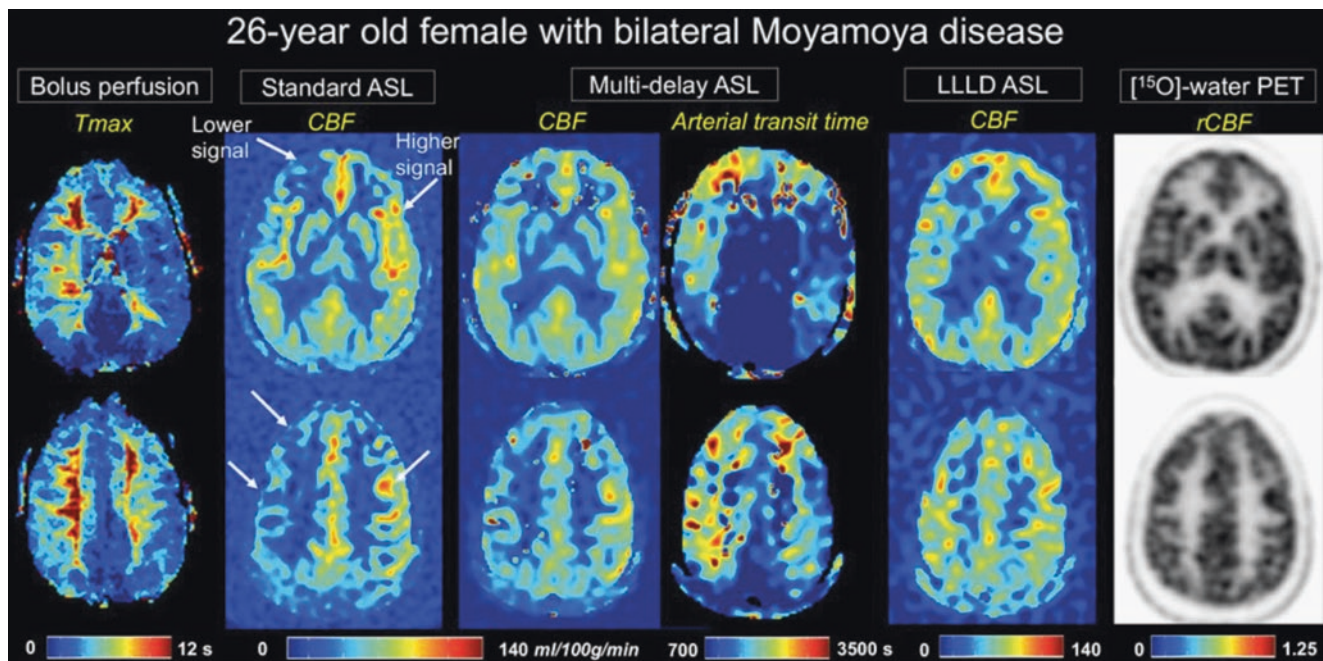


**Fig. 5.5** A 26-year-old female patient with bilateral moyamoya disease. Time-to-maximum (Tmax) images from dynamic susceptibility contrast MRI are shown on the leftmost panel. Cerebral blood flow (CBF) maps (mL/100 g/min) from each of the 3 arterial spin labeling (ASL) acquisitions are depicted at 2 slice locations, as well as arterial transit time from multidelay ASL. Arrows indicate areas of lower and higher signal on standard single-delay ASL relative to the [<sup>15</sup>O]-water positron emission tomography (PET) reference (far right). Improved

cortical CBF measurement compared with PET is seen on multidelay and long-label long-delay (LLL) ASL scans. rCBF indicates relative CBF. Reprinted with permission from Fan AP, Guo J, Khalighi MM, Gulaka PK, Shen B, Park JH, et al. Long-delay arterial spin labeling provides more accurate cerebral blood flow measurements in moyamoya patients: A simultaneous positron emission tomography/MRI study. *Stroke*. 2017;48(9):2441–9

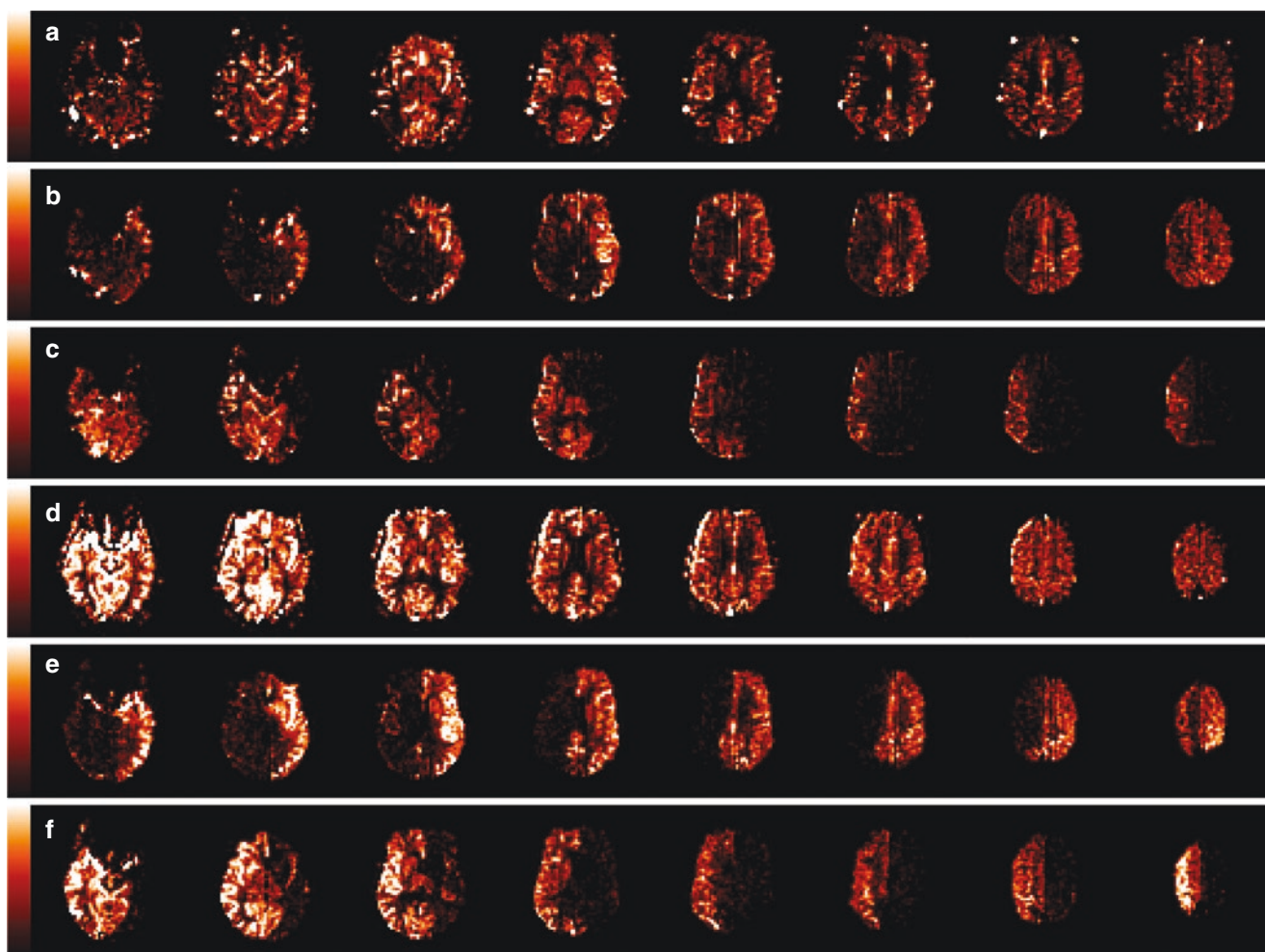


**Fig. 5.6** Selective PASL perfusion MRI before and after CEA: a 67-year-old with asymptomatic right ICA stenosis (70% by area at level of stenosis). Preoperative (a-c) and postoperative (d-f) perfusion studies with bilateral labeling (a, d), left-sided labeling (b, e), and right-sided labeling (c, f) are shown. Before surgery, CBF in MCA territory

measured with label ipsilateral to CEA (c) was 46 ml/100 g/min, and supply from contralateral side (b) was 20 ml/100 g/min. After surgery, CBF in MCA territory measured with label ipsilateral to CEA (f) was 90 ml/100 g/min, and supply from contralateral side (e) was 5 ml/100 g/min

extracranial to intracranial (EC-IC) bypass in patients with occluded carotid arteries [130], assessment of contribution of ECA to cerebral perfusion in the setting of ICA occlusion [120], and evaluating effect of intervention on relative contributions of major cervicocranial arteries to regional cerebral perfusion [123] (Fig. 5.6).

### Moyamoya

Moyamoya disease refers to an occlusive arteriopathy involving proximal anterior circulation (ICA, MCA, and anterior cerebral artery [ACA]), more common in Asian populations. It is slowly progressive, and collateral vessels develop at the base of the brain as occlusive disease increases. It is a noninflammatory, nonatherosclerotic fibrotic process that affects children and young adults, but progressive occlusive arteriopathy in patients with other defined arteriopathies including atherosclerosis who demonstrate similar morphology angio-

graphically are often also referred to with the term moyamoya syndrome [131]. Both DSC and ASL MRI perfusion techniques have been applied in this setting [132–138]. For either MR perfusion approach, marked transit delay and vessel dispersion create problems in implementation. There will be some variability in perfusion pattern depending on severity of disease, but at least for those with bilateral disease the perfusion pattern is generally one of prolonged transit in anterior circulation territories, especially deep watershed, accompanied by relative hyperperfusion in posterior circulation territories and basal ganglia (Fig. 5.7). Schubert et al. [136] used xenon CT and DSC perfusion MRI, finding that TTP > 4s indicated impaired CVR in moyamoya patients. Tanaka et al. [137] compared PET and DSC perfusion MRI, reporting that MTT prolongation greater than 2s compared to cerebellum correlated with abnormally elevated OEF and CBV. MR-derived CBV and MTT correlated with PET mea-

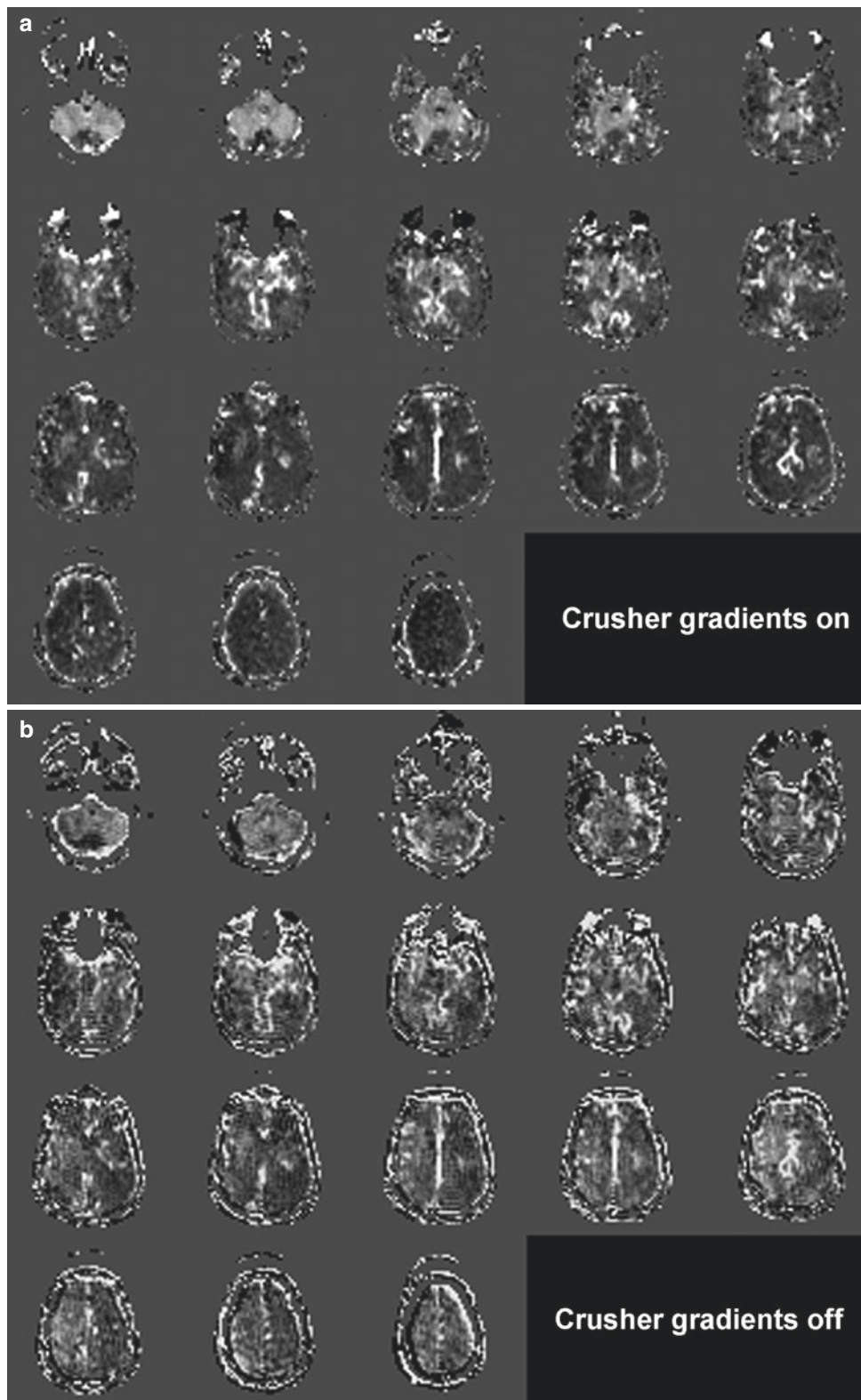


**Fig. 5.7** PASL perfusion MRI with and without vascular crusher gradients: a 45-year-old with moyamoya syndrome. (a) PASL CBF images with vascular crusher gradients on show normal or increased blood flow in posterior circulation and in deep gray matter perforator territories, with nonvisualization of significant label in anterior circulation territories in general. (b) With crusher gradients off, arterial label can be seen in anterior circulation distributions, though still with left greater than

right perfusion deficits, indicating marked transit delay. Stable xenon perfusion CT provides a better evaluation of CBF in this setting, in this case performed (c) before and (d) after acetazolamide challenge and showing augmentation of flow in posterior circulation and deep gray matter perforator territories, poor augmentation on right (CBF in right MCA cortex increased by about 17%) and steal on left (CBF in left MCA cortex decreased by about 12%)

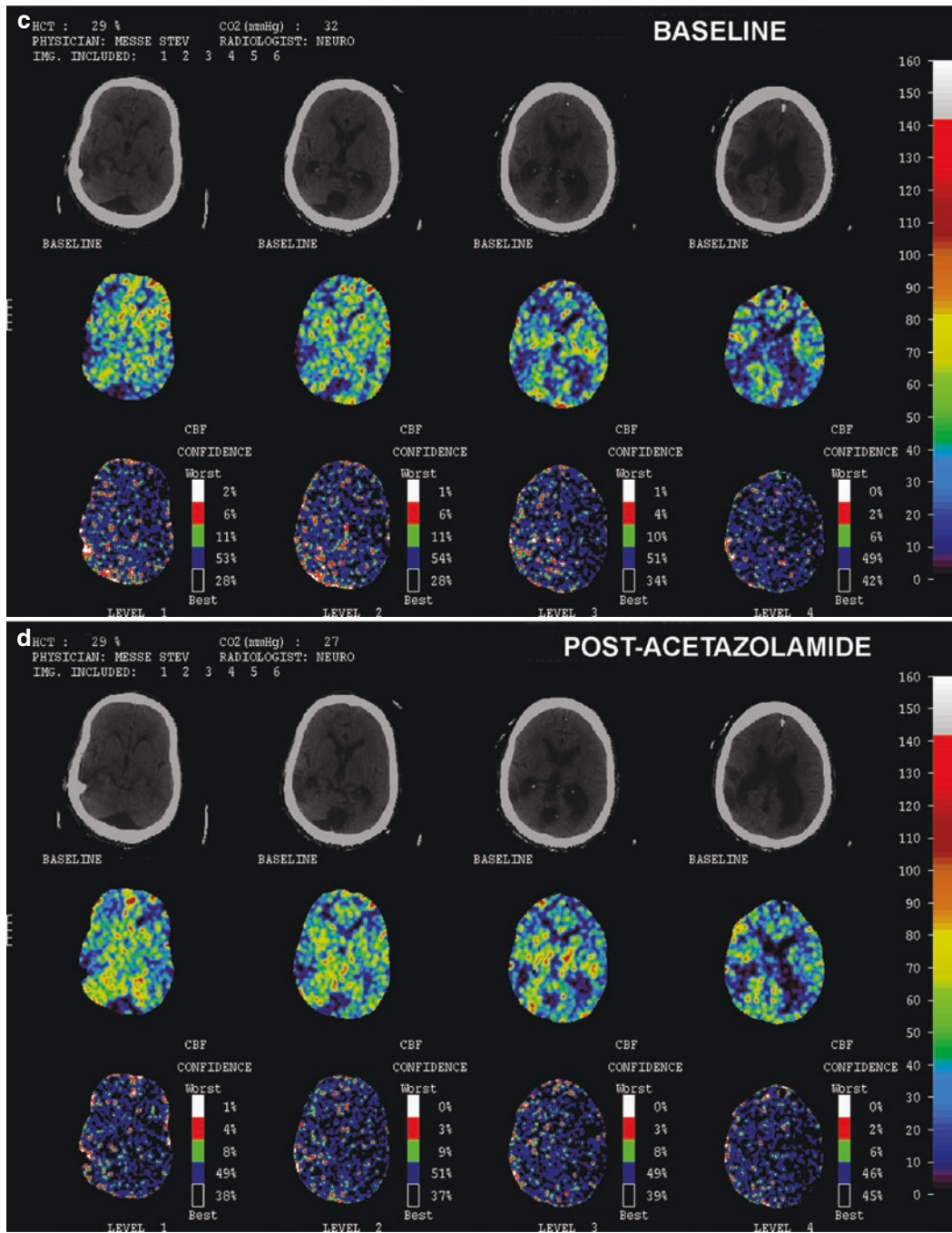
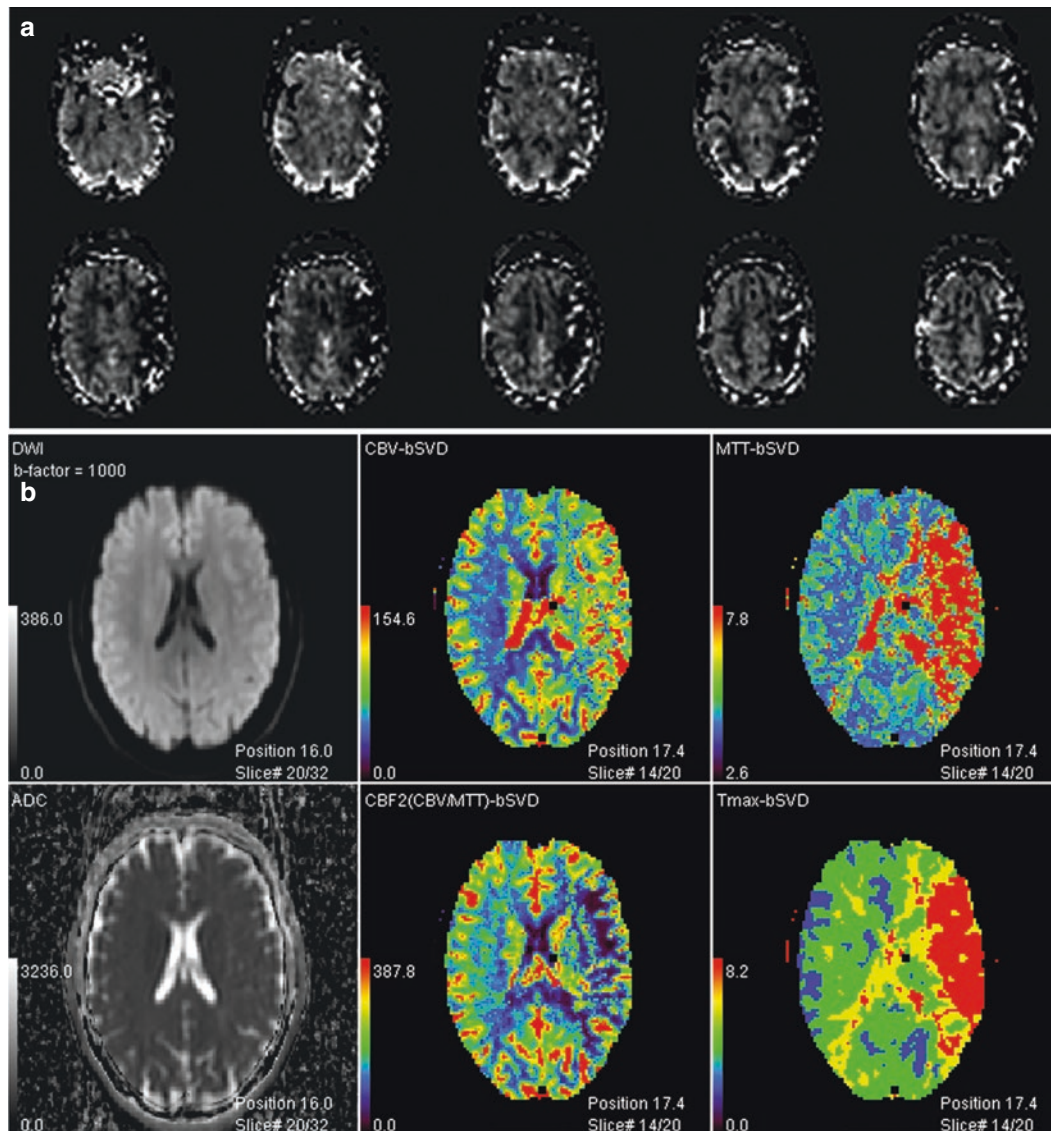


Fig. 5.7 (continued)

surements, but CBF did not. One of the recent solutions to overcome the delayed transit time in ASL imaging is to use multidelay acquisition. Fan et al. studied 15 moyamoya patients and demonstrated that long-label long-delay ASL scans (postlabel delay = 4.0 s) showed the strongest correlation relative to PET [93]. Wang et al. compared four postlabeling delay pCASL with CT perfusion in 17 patients with moyamoya disease and demonstrated improved correlation between perfusion data from ASL and CT perfusion imaging using the multidelay pCASL protocol [139]. Future application of more advanced MR techniques such as ASL MRI fingerprinting can further improve our understanding of cerebral hemodynamics in patients with moyamoya disease [140].

## Interventions

In symptomatic or asymptomatic patients with cerebrovascular disease, the primary goals in evaluating hemodynamic effects of a particular lesion or lesions are to not only assess risk as discussed above, but also to assess the potential for intervention to minimize that risk. Several studies have utilized MR perfusion techniques to assess the effect of different interventions such as carotid endarterectomy (CEA) [71, 114, 141–144], carotid artery stent (CAS) [114, 145], encephalomyosynangiosis or encephaloduroarteriosynangiosis (EDAS) and superficial temporal artery to middle cerebral artery (SMA-MCA) bypass [131, 133, 146, 147] on hemodynamics in this setting (Fig. 5.8). The effects of medical therapy have been less well studied.



**Fig. 5.8** Left MCA stenosis before and after STA-MCA bypass: a 60-year-old initially presenting with intermittent right-hand numbness and weakness and expressive aphasia, resolving after bypass. (a) Preoperative PASL and (b) DSC perfusion MRI show left MCA territory perfusion deficit ( $T_{max} > 8$  s). Postoperative study shows decreased perfusion deficit left MCA territory on PASL images (c), though hyper-

intense vessels indicating transit artifact persist. (d) DSC perfusion MRI likewise shows decrease in perfusion deficit ( $T_{max} < 5$  s corresponding to regions with highest  $T_{max}$  preop), though border zones anterior and posterior still show perfusion abnormality ( $T_{max} = 6-7$  s). \*DSC perfusion using “PMA” image analysis software (copyright owner: Kohsuke Kudo) provided by ASIST-JAPAN

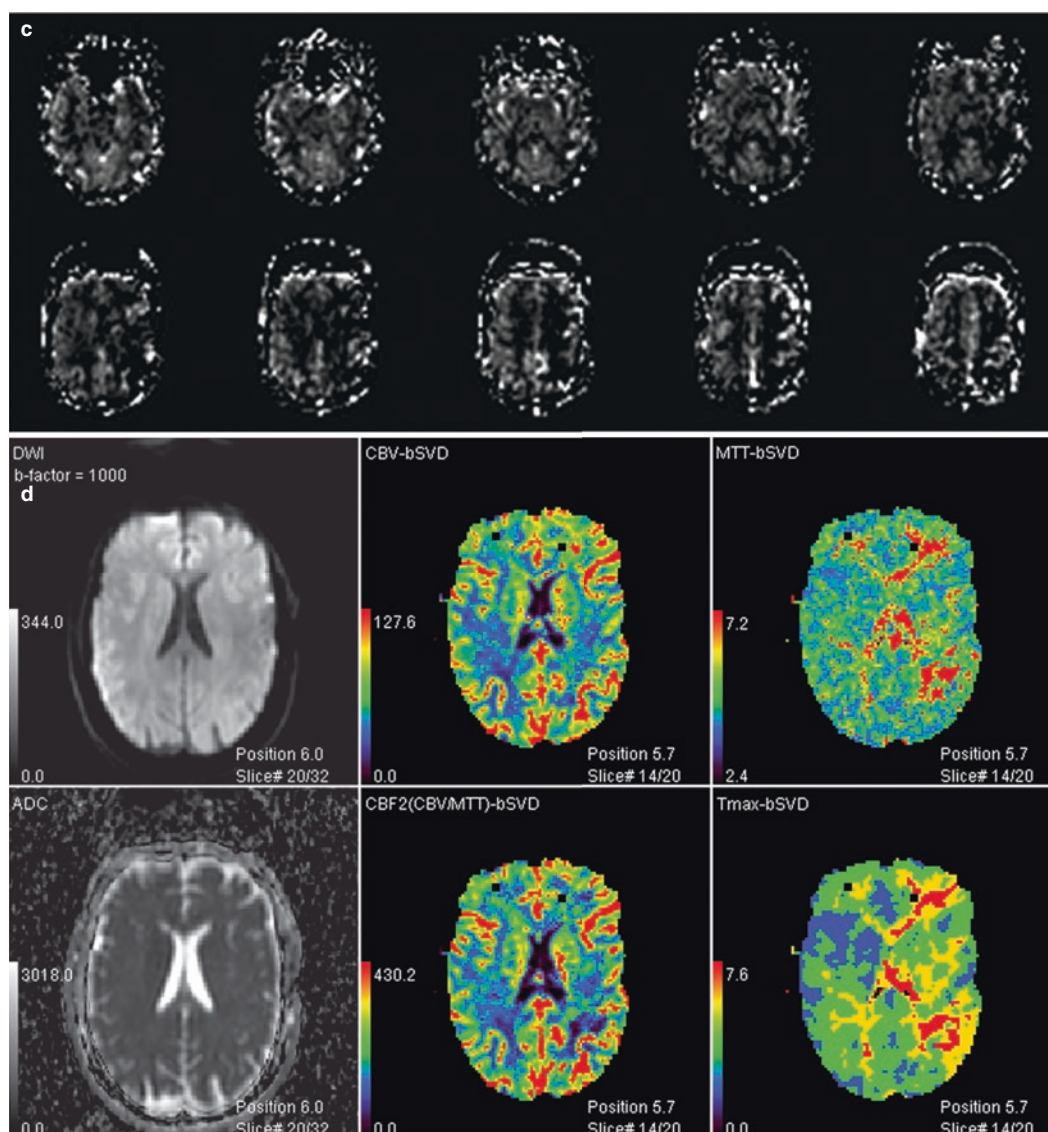


**Fig. 5.8** (continued)

Multiple studies using DSC perfusion MRI techniques were able to show hemodynamic asymmetries that resolved after CEA or CAS [71, 142–144]. Kluytmans et al. [143] found no difference in rCBV or MTT (normalized to cerebellum) ipsilateral to a severe >70% stenosis as compared to controls or contralateral hemisphere; however, if contralateral carotid occlusion was also present rCBV, MTT, and TTP were asymmetrically increased on the occluded side, which normalized after CEA. Doerfler et al. [71] found a delay in normalized first moment and increased rCBV (normalized to contralateral hemisphere) for symptomatic patients with  $\geq 80\%$  ICA stenosis, which normalized after CEA, but did not find a preoperative asymmetry for patients with <80% stenosis. Soenne et al. [144] found greater hemodynamic asymmetries in symptomatic patients compared to asymp-

tomatic patients, with increased MTT and decreased rCBV in the ipsilateral hemisphere, which resolved after CEA. Chang et al. [114] showed CBF increase ipsilateral to CAS was significantly greater in patients with impaired CVR, correlation between CVR impairment (measured with a BOLD technique and breath-holding).

Absolute measures of CBF available with ASL techniques are particularly attractive for longitudinal studies. Ances et al. [141] reported an inverse relationship between preoperative CBF and percent change in CBF in anterior circulation after CEA, with a significant increase in CBF after CEA for patients with preoperative CBF <50 ml/100 g/min. Jones et al. [123] studied symptomatic and asymptomatic patients with carotid stenotic/occlusive disease using a hemispheric labeling strategy, allowing quantitative assessment of CBF

as well as the contribution of flow from cervicocranial vessels on each side to ipsilateral and contralateral hemispheres. CBF supplied by the side ipsilateral to CEA or CAS increased after the procedure and the degree of change was inversely related to the preoperative CBF supplied from that side, while contralateral contributions to the side of CEA or CAS decreased after the procedure.

Improved perfusion metrics after interventions such as EDAS [131, 133, 146] have been reported. For example, Yun et al. [146] showed that relative TTP and CBV (referenced to cerebellum) improved after revascularization surgery (EDAS) and extent of change in TTP correlated with clinical outcome. Hui et al. used DSC perfusion MRI in 33 patients after unilateral STA-MCA bypass and demonstrated that combination of preoperative perfusion weighted imaging and Alberta Stroke Program Early Computerized Tomography Score (PWI-ASPECTS) is a useful predictive index for the long-term prognosis of STA-MCA bypass patients [147]. A recent large study in 145 patients who underwent STA-MCA bypass demonstrated an increase in CBF and normalized CBF in MCA territory using ASL imaging with moderate to good agreement in collateral grading and anastomosis patency when compared to cerebral angiography [148].

### Hyperperfusion

After CEA or CAS, some patients may experience a hyperperfusion syndrome—a substantial increase in CBF exceeding metabolic demand of tissue. Symptoms may include hypertension, headache, seizures, and intracranial hemorrhage (Fig. 5.9). A region of hemodynamic impairment with decreased CVR in the presence of a flow-limiting arterial stenosis lesion (with or without modifying factors such as hypertension, poor collaterals or contralateral disease) is suddenly subjected to a normal CPP after revascularization [149, 150]. Autoregulation is impaired or overwhelmed leading to development of minutes to hours after the procedure, potentially mimicking infarct on clinical exam. Imaging may demonstrate breakdown of the blood–brain barrier, edema, and hemorrhage. Evaluation of cerebral perfusion can help not only with the diagnosis of hyperperfusion but also its anticipation [149]. Fukuda et al. [151] found a significant correlation between CBV measured preoperatively with DSC perfusion MRI and increased CBF after CEA (CBF measured pre- and postoperatively with SPECT). They observed hyperperfusion ( $\geq 100\%$  increase in CBF) in just under half of the patients with elevated preoperative CBV and in none with normal preoperative CBV.

Hyperperfusion has also been described in posterior reversible encephalopathy syndrome (PRES), migraine headaches, status epilepticus, hypercapnea, and hypoxic anoxic injury [152, 153] (Figs. 5.10 and 5.11). Altered perfusion in

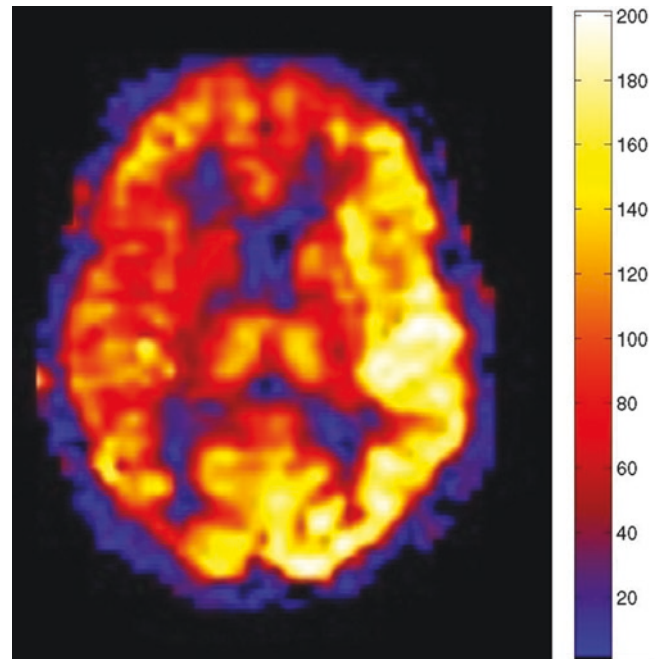


**Fig. 5.9** Hyperperfusion syndrome: status post CEA 2 days prior to imaging with new dizziness and headache. Image courtesy of Jeffrey Pollock, Oregon Health and Science University

many of these entities can also include hypoperfusion, however, depending on etiology and timing of injury [154, 155].

### Spasm

Vasospasm developing after aneurysmal subarachnoid hemorrhage (SAH) is a difficult problem in neuroimaging for multiple reasons. In order to minimize cerebral ischemic injury resulting from vasospasm, the neurointensivist needs a reliable, and optimally a real-time measure of cerebral perfusion. Such a combination does not exist for clinical use as yet. Transcranial Doppler (TCD) measurements can be obtained frequently at bedside, but are not always reliable, are operator dependent, and do not provide a measure of cerebral perfusion. Nuclear medicine techniques such as PET or SPECT have been utilized in this setting, but are not always practical with critically ill intensive care unit (ICU) patients and expose the patient to ionizing radiation. Stable xenon CT perfusion or bolus contrast CT perfusion techniques have been applied in this setting as well and are often combined with CTA. These can even be done at bedside, although with the drawback of additional exposure to ionizing radiation. Since multiple assessments may be required during the course of treatment for vasospasm, this is obviously suboptimal.

MRI is attractive because of the superior sensitivity to ischemia afforded by diffusion weighted imaging and the



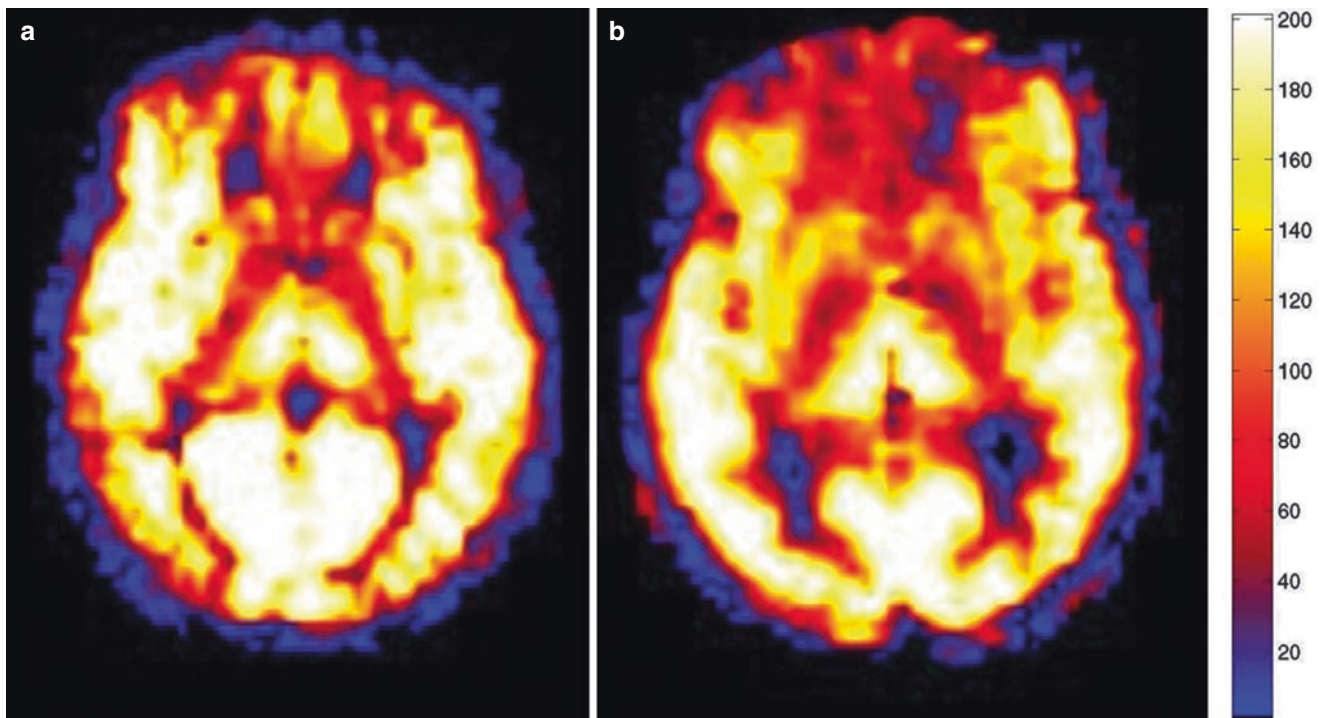


**Fig. 5.10** Hyperperfusion (2 cases) on PASL perfusion MRI: anoxic injury and hypercapnia. (a) An 11-year-old male 9 days after cardiac arrest (mean CBF in gray matter 191 ml/100g/min). (b) A 60-year-old

male with hypercapnea ( $p\text{CO}_2 = 76.6$ , normal 35–45) and hyperperfusion (CBF in gray matter 169 ml/100 g/min). Images courtesy of Jeffrey Pollock, Oregon Health and Science University

ability to assess cerebral perfusion at the same time. This can be done relatively quickly once the patient is on the table, with a complete study of the brain including diffusion, perfusion, and angiographic imaging achievable in less than 15 min. However, transport of a critically ill patient and stability and safety in the MR scanner require more attention and effort than CT or nuclear medicine techniques, and without adequate planning and practice this can create obstacles for routine clinical use in this setting. It remains attractive if it can be efficiently done, and its use has been described [156–160]. Hattingen et al. [157] prospectively studied 51 patients in the first week after SAH, finding vasospasm in just under half. They measured decreased rCBV and rCBF in territories involved by spasm, hypothesizing that this reflects autoregulatory dysfunction in involved regions. Weidauer et al. [161] prospectively studied infarct patterns in patients after SAH, correlating patterns with degree of spasm and cerebral circulation time on DSA as well as delay time on MR perfusion studies (TTP). They studied 117 patients selected at high risk for spasm, finding DSA evidence for spasm in 87.5% in the second week with 52.5% of these showing new ischemic injury, with the majority of infarcts related to severe spasm and perfusion delays (TTP  $6.52 \pm 4.52$  s), and decreasing infarct rates with mild or moderate spasm and shorter perfusion delays. All infarct patterns, especially watershed or territorial, increased

in frequency with increasing degree of spasm, with the exception of laminar cortical patterns, which were seen more with moderate or mild (or no) spasm. Of course, the pattern of infarcts depended also on collateral flow and pattern of involvement of the circle of Willis and intracranial arteries. Perfusion disturbances can also be seen without angiographically significant spasm [157, 161] for many potential reasons, including microvascular spasm, increased intracranial pressure (ICP) related to hydrocephalus or edema, hypotension, etc. Beck et al. [162] used bolus contrast MR perfusion and diffusion in 10 patients to diagnose vasospasm (along with clinical indicators including TCD), confirming with DSA, and then repeating the MR study to assess the effects and outcome of angioplasty. They defined tissue at risk by perfusion delay (TTP), and found that angioplasty resulted in decreased mismatch in perfusion versus diffusion abnormalities, with reductions in TTP preventing or reducing extent of infarction in a given vascular territory compared to territories with delays that did not undergo angioplasty. MR perfusion and diffusion weighted imaging may also be helpful in vasospasm unrelated to subarachnoid hemorrhage [163].

The literature on application of ASL imaging in patients with SAH is sparse. In a small study of 15 patients with SAH and 14 healthy volunteers, Labriffe et al. found global or regional hyperperfusion pattern when SAH was compli-

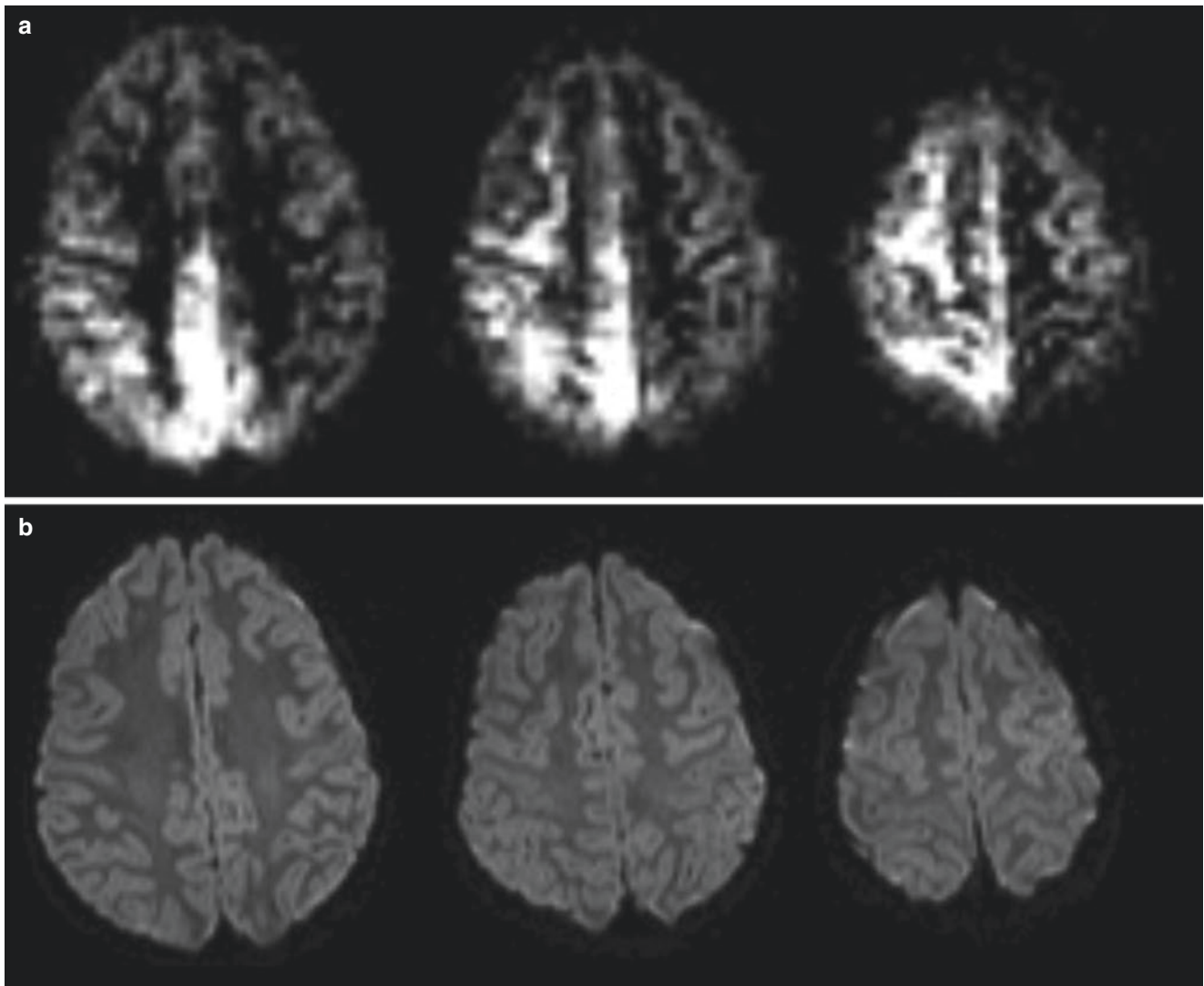


**Fig. 5.11** Complicated migraine headache: an 8-year-old with severe headache and progressive left hemiparesis over a few hours, completely resolving within 2 days. PASL perfusion MRI shows hyperperfusion

right frontal and parietal cortex (a) without abnormality on diffusion-weighted images (b). Images courtesy of Arastoo Vossough, The Children's Hospital of Philadelphia

cated by vasospasm. In addition, they observed serpiginous high signals likely secondary to retention of labeled protons in arteries with vasospasm [164]. Finally, in a recent small prospective study, Russin et al. performed DCE MRI in day 4 after SAH and demonstrated that  $K_{trans}$  was significantly higher in aSAH patients who subsequently developed delayed cerebral ischemia compared to patients with radiographic spasm but no infarct and patients without vasospasm [165].

### AVM

Arteriovenous shunting with arteriovenous malformation (AVM) or arteriovenous fistula (AVF) leads to rapid transit arterial transit, which can also cause artifact on ASL perfusion MRI. In this situation, the assumption that labeled arte-

rial blood is in microvasculature or tissue is violated, with the tracer moving through the AVM behaving as an intravascular as opposed to a diffusible tracer. Just as transit delays can cause artifact with bright signal in arteries and arterioles, rapid transit leads to bright signal in the presence of a shunt. Arterial label traveling normally through tissue with a normal capillary bed will still behave as a diffusible tracer. The feasibility of using this approach to detect the presence of a shunt and potentially evaluate effects on perfusion distant from and in proximity to AVM was shown by Wolf et al. in a pilot study of seven patients with AVM [166] (Fig. 5.12). Le et al. subsequently demonstrated that identification of venous ASL signal intensity improved detection of dural arteriovenous fistulas and small AVMs [167]. Studies using a combination of ASL and susceptibility-weighted imaging

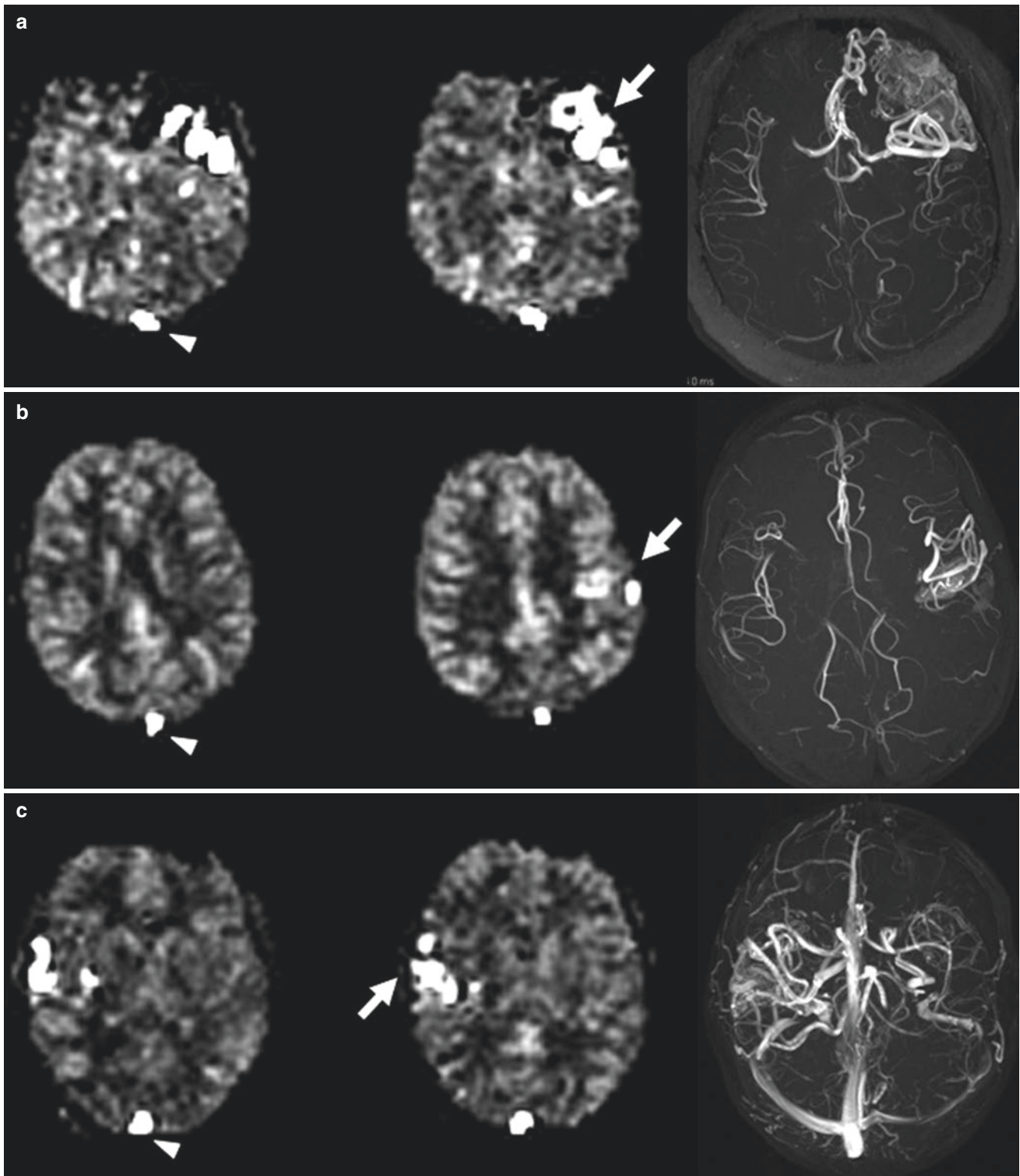


**Fig. 5.12** Shunt visualization in AVM using CASL perfusion MRI: 3 different patients with AVM in left frontal lobe (**a**), along left central sulcus (**b**), and in right frontal lobe (**c**). For each patient, 2 of 12 CASL imaging locations are shown on the left and slab maximum intensity projections from 3D time of flight MRA through the AVM on the right.

AVM nidus and draining vessels (arrows) are clearly seen on CASL CBF maps, as is labeling in cortical veins and sagittal sinus (arrowhead) indicating rapid transit or AV shunting. Reprinted with permission from Wolf RL, Detre JA. Clinical neuroimaging using arterial spin-labeled perfusion MRI. *Neurotherapeutics* 2007;4(3):346–59

demonstrated increasing sensitivity and specificity comparable to contrast-enhanced MRA, but still lower than catheter angiography [168, 169]. DSC perfusion MRI has also been used to evaluate AVM effects on perfusion and effects of treatment such as stereotactic radiosurgery on AVM hemodynamics [170, 171].

## Neoplastic Disorders

The primary target of perfusion MRI methodology is neoplastic vasculature. Neoplasm vascularity and angiogenesis can be assessed using estimates of blood volume, and integrity of the blood–brain barrier or the “leakiness” of neoplastic vessels can be assessed with measurements of endothelial permeability. Methods based on first pass T2\*-weighted (DSC MRI) and steady state T1-weighted (DCE MRI) acquisitions have been applied to this end [20, 172–174], though routine clinical work tends to rely more on DSC perfusion MRI to date. The majority of studies employ a T2\*-weighted approach, although some have used a T2-weighted [175–177] or combined T2\*/T2-weighted approach [178, 179]. The advantage of dual-echo, combined T2\*/T2-weighted approach is the ability to measure to the vessel size, which has been used to evaluate vascular normalization in the context of antiangiogenic treatments [180, 181]. ASL techniques have been increasingly utilized in this setting as well [12, 182, 183]. In this section, blood flow or volume in neoplasms (more broadly termed tumors) will be referred to as TBF and TBV (tumor blood flow and volume, as opposed to cerebral blood flow and volume). While the focus here is on perfusion imaging of neoplasms, it is important to note that perfusion imaging should be interpreted in the context of clinical findings and other conventional and advanced imaging techniques including diffusion and spectroscopic imaging [173, 184, 185].

## Diagnosis and Grading

### Differentiation of Neoplastic from Non-neoplastic Lesions

Inflammatory lesions such as tumefactive demyelinating lesions (TDLs) show decreased rCBV compared to neoplasms. For example, Cha et al. [186] evaluated 10 patients with suspected TDLs and compared blood volume measures in these lesions as compared to a selection of neoplasms (6 high-grade gliomas, 1 low-grade glioma, and 4 lymphomas) in 11 patients, finding mean rCBV of 0.88 (range: 0.22–1.79) in TDLs compared to mean rTBV of 6.47 (range: 1.55–19.2) in neoplasms (Fig. 5.13). Other reports regarding inflammatory lesions are concordant [187, 188]. However, inflammatory lesions may show increased rCBV [189], though marked hypervascularity or elevations in rCBV are uncommon. While the increase may be mild, there can still be enough overlap with rTBV from some brain neoplasms that the distinction between non-neoplastic and neoplastic processes is blurred. Infectious lesions also typically show decreased blood volume [190–194]; however, elevated rCBV can be seen, for example, in fungal infections and tuberculomas secondary to reactive neovascularization [195, 196]. Review of clinical findings with conventional imaging results and other advanced imaging studies such as diffusion and spectroscopic imaging remains necessary [197, 198]. A recent study using ASL perfusion imaging in 60 subjects with intra-axial brain masses demonstrated higher rCBF in neoplastic compared to non-neoplastic lesions with rCBF of higher than 1.89 to have 90% sensitivity and 73% specificity for differentiation [199].

### Intra-Axial Neoplasms

**DSC and DCE Imaging** Blood volume of gliomas has been shown to correlate with grade in many studies implementing DSC perfusion MRI [175, 198, 200–202]. Vascular

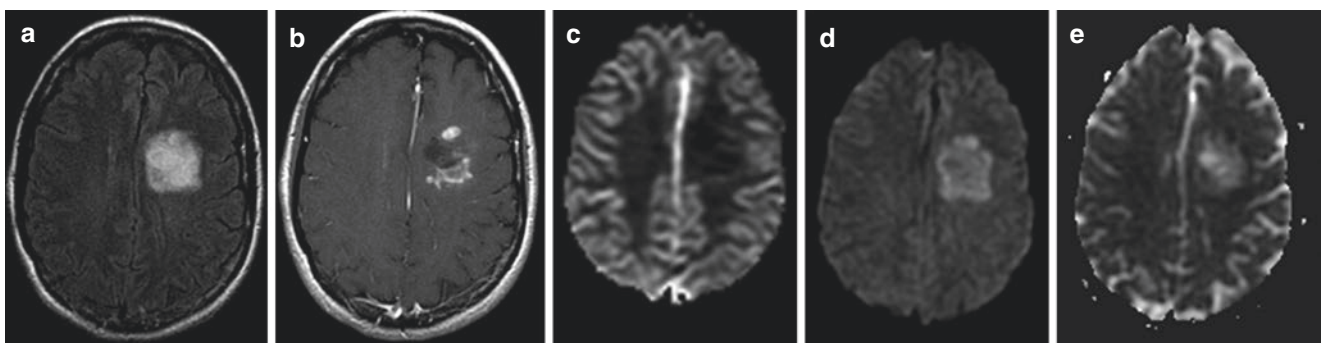


**Fig. 5.13** Lack of increased blood volume in non-neoplastic disease: a 38-year-old with tumefactive demyelinating lesion (TDL). (a) FLAIR and (b) post contrast T1-weighted images show mass with incomplete enhancement at margins. (c) Relative blood volume was low, and there

was facilitated diffusion except for margin of lesion where diffusion was decreased on (d) diffusion-weighted and (e) ADC maps. The constellation of findings is most consistent with TDL, with the lesion decreasing in size and enhancement resolving within 6 months

morphology has also been evaluated with studies of vascular tortuosity [203, 204] and size [179, 180, 205, 206]. Permeability measured using T2\* or T1-based approaches also correlates with grade [201, 207–210]. In general, the more aggressive a neoplasm the more abnormal the vasculature with greater vascular density and tortuosity (higher TBV) and greater permeability. There are exceptions, however, the most troublesome of which are gliomas with oligodendroglial components, which may show increased TBV (or TBF) [177, 211–213]. Hemangioblastoma, ganglioglioma, and pilocytic astrocytoma may show increased TBV as well [214, 215].

Despite the demonstrated correlation of blood volume with grade, there is a fair amount of overlap between grades, and this complicates interpretation. Some authors have found that using a T2\*-weighted approach (gradient echo EPI) provides better discrimination between low- and high-grade gliomas [178, 179, 205], while others have suggested T2-weighted (spin echo EPI) approach is superior for at least some applications. For example, Young et al. proposed that the decreased sensitivity to larger vessels associated with T2-weighted DSC MRI may improve distinction between glioblastoma and metastasis [206]. A combination of these can also be used, where  $\Delta R2^*/\Delta R2$  ratio can be used as an index of vessel diameter [178, 179].

A commonly used interpretation strategy for clinical evaluation of TBV is to obtain a maximum relative TBV in the neoplasm by manually placing regions of interest (ROIs) and normalizing to contralateral white matter, which has been demonstrated to be reproducible [216, 217]. A large study in 160 patients with glioma demonstrated that the rCBV threshold of 1.75 provided a sensitivity of 95% and specificity of 57.5% in differentiation of high-grade and low-grade gliomas [218]. Histogram analysis has also been proposed to address heterogeneity in neoplasms and to improve reliability for such measurements [204, 216, 219, 220] and has been shown to be as effective as rCBVmax analysis in the correlation with glioma grade [216]. Evaluation of peritumoral tissue outside of enhancing margins with histogram analysis has been found to be helpful in reproducible grading of gliomas, even when no ROI is placed and analysis is performed on the entire imaging sections covering the neoplasm [220].

More recently investigators used DCE imaging for glioma grading. Jia et al. showed significantly higher  $K^{\text{trans}}$  and  $V_e$  values in high-grade compared to low-grade gliomas [221]. Jung et al. performed histogram analysis of pharmacokinetic parameters and demonstrated that the 98th percentile of  $K^{\text{trans}}$  could best differentiate high-grade from low-grade gliomas [222]. A recent multicenter study of DSC perfusion and DCE MRI in 94 patients demonstrated that both techniques have a comparable, high diagnostic accuracy for grading gliomas. Among DCE-derived param-

eters,  $V_p$  and  $V_e$  had the highest accuracy, and rTBV had the highest accuracy in DSC imaging [223]. Multiparametric evaluations have also been employed to improve diagnostic accuracy [210, 218, 224, 225].

### ASL Perfusion Imaging

The first studies evaluating brain tumors using ASL implemented pulsed ASL (PASL) methodology [226, 227]; and while contrast-enhanced methods are more commonly used clinically, experience with ASL perfusion methodology is increasing given improved image quality and more widespread availability on clinical MRI scanners in the last several years. Potential advantages of ASL perfusion MRI include complete noninvasiveness, diffusible tracer with improved quantitation capability, and decreased sensitivity to errors from altered permeability [12, 213]. Relative insensitivity to permeability may be viewed as a drawback, although preliminary work has shown that it is possible to address this [228]. Other disadvantages include low SNR, although this is improving with advances in software and hardware. Several studies demonstrated correlation of blood flow with blood volume and also with neoplastic vascularity as measured by histopathologic assessment of vascular density [210, 215, 227]. Though absolute measures of CBF and TBF can be obtained with ASL techniques, relative or normalized measures may be more useful in this setting [213, 227]. In general, ASL measures of TBF correlate with DSC and DCE measures of TBF and permeability, TBF increasing with increasing grade and aggressiveness for intra-axial brain neoplasms [210] (Fig. 5.14). Oligodendroglial neoplasms create difficulties for this approach as well [213]. In a recent study of 34 patients with glioma, Arsawa et al. used histogram analysis of cerebral blood flow and demonstrated a strong correlation between the ASL and DSC in the 75th percentile, mean, median, and standard deviation values; however, the area under the curve values was greater for DSC compared to ASL technique, DSC-MRI superior to ASL for glioma grading in this study [229].

### Extent of Infiltration: Glioma Versus Metastasis Versus Lymphoma

High-grade gliomas, lymphomas, and metastases can look very similar on conventional imaging, and all can be solitary or multifocal. Although lymphomas almost always enhance, they tend not to develop the neovascularization typical of other aggressive neoplasms. Vascular abnormalities are present, however, including angiocentric growth pattern, extension into perivascular spaces, disturbance of blood–brain barrier, and potentially angioinvasion [198, 230]. Lymphomas tend to show less striking changes in TBV as compared to glioblastoma or metastases, usually with rTBV less than 2.5 compared to contralateral white matter and often ranging close to 1 [198, 231–233]; however, some lymphomas do

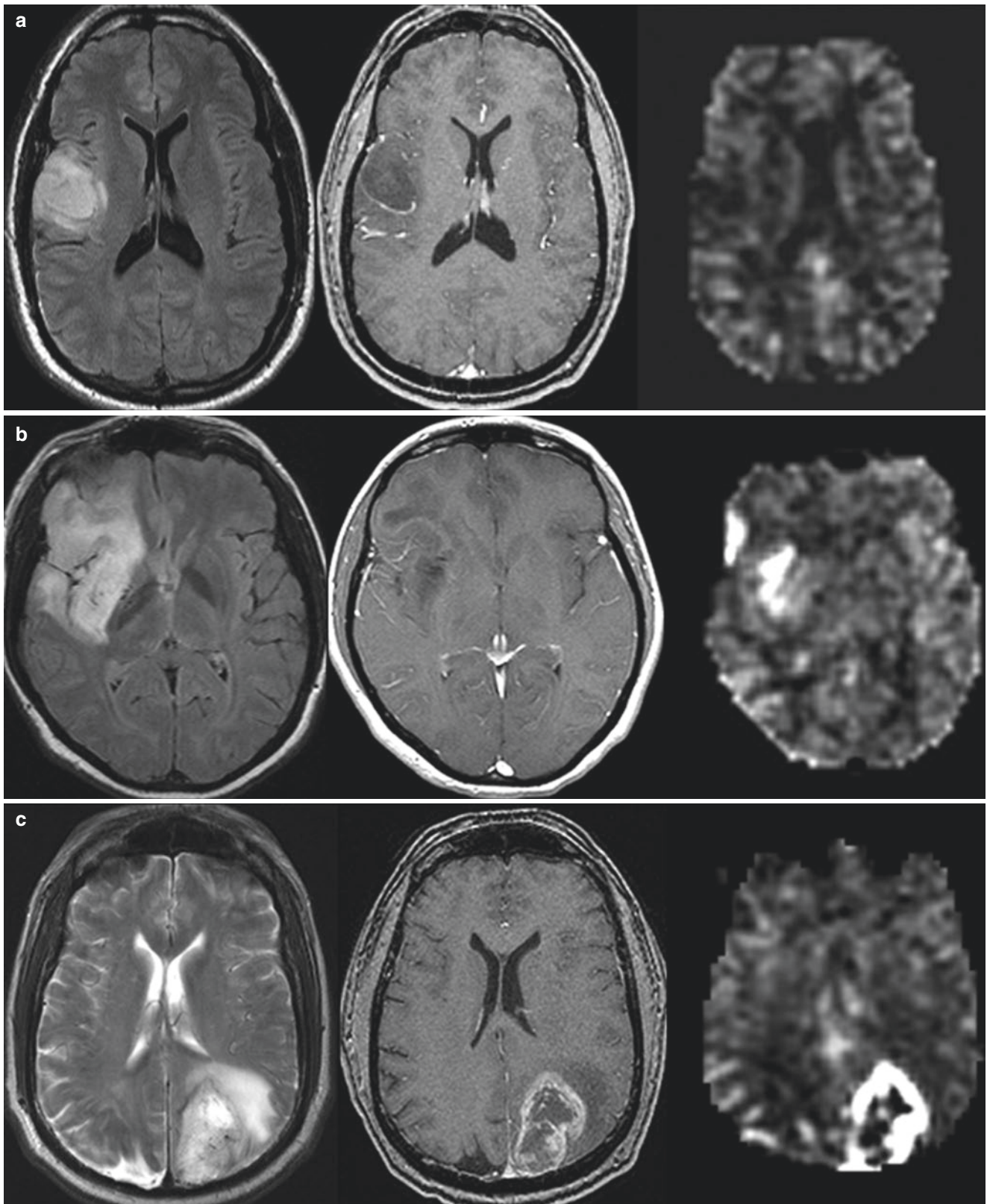


**Fig. 5.14** CASL perfusion MRI: 3 cases showing increasing CBF with increasing glioma grade. From *left to right*, FLAIR or T2-weighted, post-contrast T1, and CASL perfusion MRI are shown. Examples of (a) oligodendroglioma (WHO grade II), (b) anaplastic oligoastrocytoma

(grade III), and (c) glioblastoma (grade IV) are shown. Reprinted with permission from Wolf RL, Detre JA. Clinical neuroimaging using arterial spin-labeled perfusion MRI. *Neurotherapeutics*. 2007;4(3):346-59

show markedly elevated TBV (i.e., greater than 5) [234]. Metastases do develop neovascularity and thus also show increased permeability and blood volume.

Blood volume and permeability measures show sufficient overlap that differentiation of the lesions in an individual is problematic; however, attempts at evaluating the tissue outside of the enhancing mass have shown promise. For example, Law et al. [235] reported elevated relative blood volume (ratio greater than 1 compared to contralateral white matter) in the peritumoral region of high-grade gliomas just outside of the enhancing component, where metastases showed ratios less than 1 (Fig. 5.15).

Another approach that has been shown to be helpful in differentiating of high-grade glioma, metastasis, and lymphoma is analysis of time intensity curve of DSC perfusion images. In lymphoma, percentage of signal recovery (PSR) is higher compared to glioblastoma and metastasis secondary to contrast extravasation with a resultant T1 effect and can even overshoot over the baseline signal intensity [236, 237]. Cha et al. demonstrated that the percentage of signal intensity recovery is reduced in both enhancing and peritumoral region in metastasis compared to glioblastoma, likely due to leakier vessels in metastasis [238].

Multiparametric studies have also proven to be useful in differentiation of glioblastoma from lymphoma. In one such study of 28 patients with glioblastoma and 19 patients with lymphoma, Kickingereder et al. demonstrated that combined multiparametric assessment of mean ADC, mean rCBV, and presence of ITSS (intratumoral susceptibility signal) significantly improved the differentiation between lymphoma and glioblastoma when compared to 1 or 2 imaging parameters [239]. In another study, of 42 patients with glioblastoma and 18 patients with lymphoma, significantly higher  $K^{\text{trans}}$  and  $V_e$  were found in lymphoma compared to GBM; however, the combination of rADC and  $K^{\text{trans}}$  significantly improved the diagnostic accuracy for discriminating between the lesions [240].

### Extra-Axial Neoplasms

Multiple studies have evaluated extra-axial masses using perfusion MRI, in general describing high relative TBV [198, 232, 241] or TBF [215, 226, 242]. Conventional imaging techniques are usually adequate for the evaluation of straightforward extra-axial masses; however, there are some cases where conventional imaging fails to determine whether a mass is intra-axial or extra-axial. The surgical approach may not be substantially altered in this case, but the surgeon would prefer to know in advance what is expected so that plans can be made to resect the dura with an appropriate margin if the lesion is likely a meningioma. Other helpful information may include a determination of whether a meningioma is likely typical versus atypical. Dural-based metastases or non-neoplastic disease may have an imaging appearance

similar to meningioma, and this potential would be important for the surgeon to know as well. Perfusion MRI techniques have been applied to the evaluation of extra-axial neoplasms in this light [198, 241–245].

One of the problems with meningiomas illustrated in the studies above is that they are quite hypervascular, and lack of a BBB leads to immediate contrast agent leakage such that the intravascular compartmentalization of the contrast agent needed for first-pass DSC perfusion MRI analysis is not present. Another problem is the common presence of mineral in meningiomas. This can be extensive and leads to susceptibility artifact that further limits accuracy. Mineral can also be a problem for ASL techniques especially with echoplanar readouts, but they are less sensitive to the problem of high permeability. Estimates of tumor blood volume may be unreliable as a result, even with correction schemes, but small series have suggested elevated TBV in meningiomas and other extra-axial neoplasms versus intra-axial neoplasms [198, 245]. Other series have described meningiomas tending to show higher TBV than other extra-axial neoplasms such as metastases [246] and schwannomas [244]. The shape of the time intensity curve in DSC MRI experiments may provide an additional clue that a mass is extra-axial, where the signal drop does not return to baseline or does so more slowly as compared to intra-axial masses [198, 241].

Uematsu et al. [244] used a double echo dynamic MRI perfusion method to estimate tumor vascularity and permeability in meningioma as compared to vestibular schwannoma, finding substantial overlap in TBV but good separation based on a leakage index derived from the difference between  $\Delta R2^*$  values with and without T1 correction measured after the first pass. Meningiomas had higher vascularity, while schwannomas had higher leakage or permeability. Yang et al. [245] found that calculation of permeability was helpful in grading meningioma, with  $K^{\text{trans}} = 0.0016 \text{ s}^{-1} \pm 0.0012$  in typical meningioma (mean and SD) and  $K^{\text{trans}} = 0.0066 \text{ s}^{-1} \pm 0.0026$  in atypical meningiomas, a statistically significant difference, where tumor blood volume showed substantial overlap in values and was not helpful.

Kimura et al. [242] used CASL perfusion MRI measures of blood flow and DSC MRI measures TBF, TBV, and MTT to study meningiomas, correlating findings with measures of vessel density (microvessel area or MVA). They found that TBF derived from ASL or DSC methods was significantly correlated, and that CASL-derived TBF was correlated with MVA. They found differences in TBF between meningioma subtypes, with highest TBF in angiomatous subtypes and lowest TBF in fibrous subtypes, though atypical meningiomas were excluded in this analysis. Qiao et al. studied 54 patients with meningioma using pCASL and described three patterns: homogeneous hyper-perfusion (pattern 1), heterogeneous hyper-perfusion (pattern 2), and no substantial hyper-perfusion (pattern 3). They demonstrated that patterns

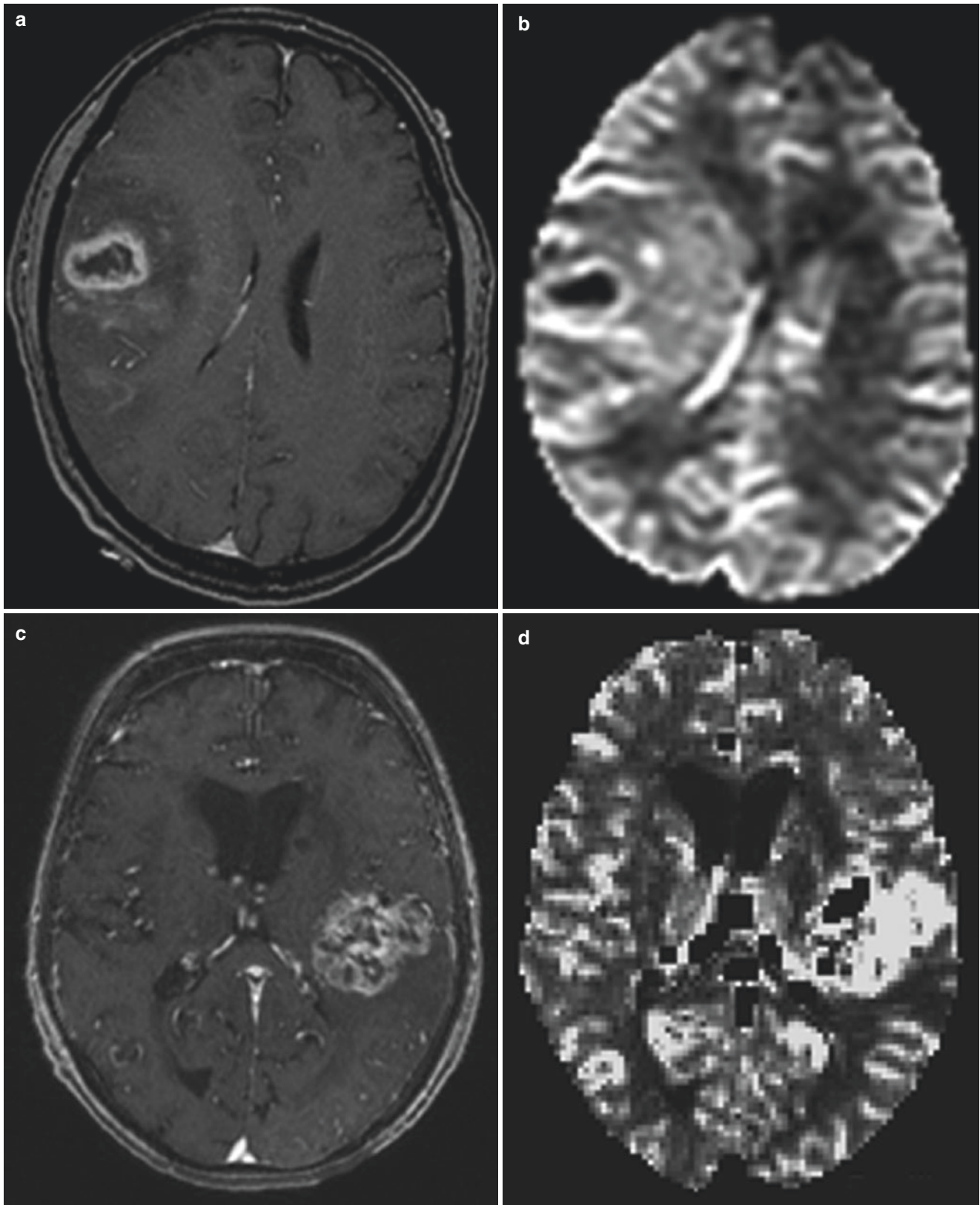


**Fig. 5.15** DSC perfusion MRI, infiltration and grade (2 cases): glioblastoma (a, b) and metastatic melanoma (c, d). Aggressive enhancement pattern is seen on T1-weighted post contrast image (a) in the patient with glioblastoma, with elevated rTBV on T2-weighted DSC perfusion MRI (b) well away from enhancing margins suggesting

extensive infiltrating component. Aggressive enhancement is also seen for the melanoma metastasis (c), but edges appear better defined and T2\*-weighted DSC perfusion MRI confirms defined edges arguing against infiltrative component



2 and 3 were predictive of World Health Organization (WHO) Grade II and III meningioma [247]. In a study of 34 patients with parasellar extra-axial lesion, Xiao et al. showed that nCBF was significantly higher in meningioma than cavernous hemangioma [248]. Finally, territorial ASL imaging has been used to determine the vascular supply of meningiomas. Lu et al. demonstrated that territorial ASL can complement 3D-TOF-MRA and increase the accuracy for determining the supplying arteries of meningiomas [249].

## Pre-treatment Planning

### Biopsy Guidance

Brain neoplasms can be quite heterogeneous, and this becomes critical when complete resection of an enhancing mass is impossible, such as with unacceptable risk related to location and when neoplastic etiology is uncertain such as with suspected TDL. Though higher grade components of neoplasms tend to show greater enhancement, which can be targeted in biopsies, the relationship is not adequate for assessing grade and therefore is not optimal for determining biopsy sites. Many low-grade neoplasms enhance, some intensely, and not all high-grade neoplasms enhance. Since perfusion and permeability metrics better correlate with grade and apparently with angiogenesis, it is logical to target the most abnormal regions of a mass on these types of studies to maximize likelihood of sampling the highest grade portions of the mass and thus decrease risk of sampling error [200, 250–252] (Fig. 5.16).

Maia et al. [252] used a T2-weighted DSC MRI technique to generate rTBV measurements and used these to target areas of increased blood volume for stereotactic biopsy prior to resection in nonenhancing supratentorial gliomas. In six cases where heterogeneous blood volume was demonstrated in the glioma, biopsies from higher rTBV foci yielded diagnoses of oligoastrocytoma and anaplastic astrocytoma, while completely resected specimens were primarily diffuse low-grade astrocytoma on histology. Chaskis et al. [251] also reported added value of biopsy guided by rTBV values, with areas of high rTBV showing histological features of endothelial proliferation, increased vascularity and cellularity, and enhancing areas corresponding more to necrosis with or without pseudopalisading. Ningning et al. used ASL perfusion imaging to target biopsies in 47 patients with treatment-naive brain gliomas and demonstrated a statistically significant correlation between CBF and microvascular density of biopsied specimens [253]. Finally, in a study of 22 patients with glioma, combined MR spectroscopy and ASL improved the accuracy of target selection for the stereotactic biopsy of intracranial tumors [254].

### Prognosis

Multiple studies have shown the potential for perfusion MRI to predict outcome for primary [177, 184, 255–257] and

secondary [258] CNS neoplasms. In general, lesions with lower rTBV have a longer time to progression compared to those with higher rTBV. For example, Law et al. [256] found that low-grade gliomas with maximum rTBV less than 1.75 on preoperative imaging had a median time to progression of 4620 days  $\pm$  433, while maximum rTBV greater than 1.75 had median time to progression of 245  $\pm$  62 days. Bisdas et al. [259] studied patients with low- and high-grade gliomas, excluding gliomas with oligodendroglial components. They found maximum rTBV values predictive of outcome, with values less than or equal to 3.8 a significant predictor of 1-year survival and values greater than 4.2 at 11 times greater risk for shorter progression-free survival. Studies in high-grade gliomas [260–262] also have reported that maximum rTBV measured prior to initiation of chemotherapy and radiation can be useful as a prognostic biomarker. In a study of 135 patients with newly diagnosed glioblastoma, Paik et al. demonstrated that higher skewness and kurtosis of rCBV histogram were associated with longer progression-free survival after partial tumor resection [263]. In a study of 58 patients with glioblastoma, Coban et al. found that maximum rCBV was significantly higher in patients with short survival compared to those with longer survival. They demonstrated that a maximum rCBV cutoff value of 5.79 can differentiate patients with low and high survival with an area under the curve of 0.93 [264]. Maralani et al. evaluated the prognostic value of DSC perfusion in elderly patients with glioblastomas and demonstrated that rCBV parameters were higher in elderly compared to younger patients. They also showed that high rCBV in elderly patients was independently associated with shorter survival [265]. The result of this study can be explained by the fact that the vast majority of GBMs in elderly patients develop de novo, without a preexisting lesion (primary glioblastomas), while in younger patients secondary GBMs progress from lower-grade diffuse astrocytoma [266]. Permeability metrics have been evaluated along these lines as well, also showing predictive value with regard to survival and time to progression [267]. An association between increased rTBV and 1p or 1p19q deletions has also been described, the deletions associated with improved survival [212, 268].

### Radiogenomics

Radiogenomics is a recently established field that extracts information from different imaging features to predict genetics and molecular characteristics of tumors. The ultimate goal of radiogenomics approach is to longitudinally follow the clonal evolution of glioma cells without the need for repeated biopsies, which are invasive and frequently associated with sampling error. In recent years, multiple studies investigated the relationship of MR perfusion metrics with genomic features of glioma. In a study of 106 patients with glioblastoma, Gupta et al. demonstrated that higher median

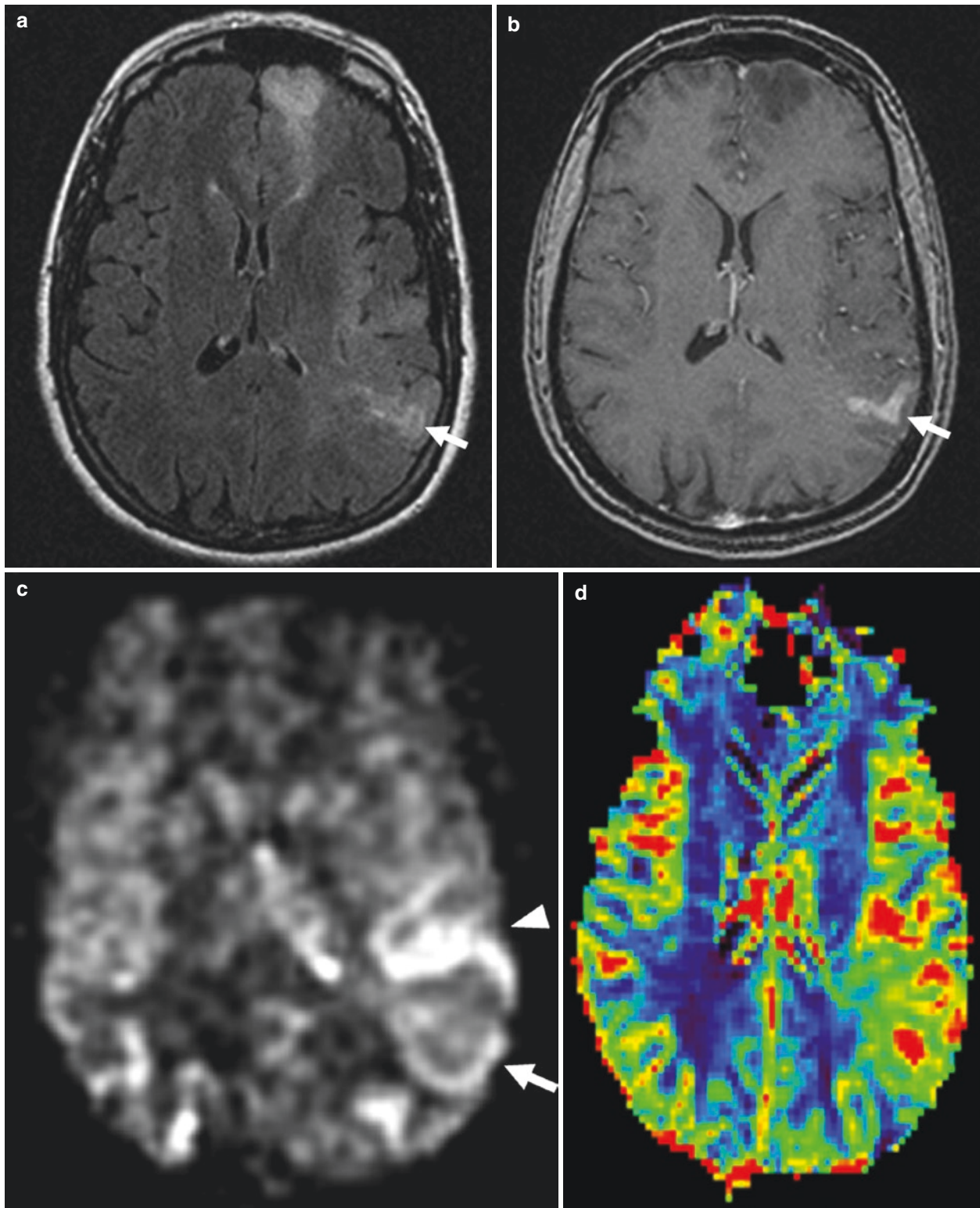


**Fig. 5.16** Sampling error and potential value of perfusion weighted imaging: a 47-year-old with multicentric infiltrating glioma, preoperative study. (a) FLAIR and (b) postcontrast T1-weighted images show nonenhancing mass left frontal and left temporal parietal regions with enhancing component left temporal parietal region. (c) Calculated tumor blood flow (TBF) using CASL perfusion MRI and (d) relative tumor blood volume (rTBV) using DSC perfusion MRI are increased in

not only enhancing component of mass (*arrows*) but in nonenhancing portions anterior to this as well (*arrowhead*). Left frontal mass would have been preferred for biopsy but did not show enhancement, elevated TBF, or elevated rTBV. Biopsy revealed grade III astrocytoma, but abnormal perfusion anterior to enhancing component may have indicated higher grade. Proximity to language areas precluded more extensive resection

rCBV and lower percent signal recovery were associated with high levels of EGFR amplification [269]. Ryoo et al. studied 25 patients with glioblastoma and demonstrated that tumors with aggressive genetic alterations had higher rCBV [270]. Tan et al. studied 91 patients with grade 2–4 gliomas and demonstrated that the rCBV was higher in the IDH wild type compared to IDH mutants for all grades [271]. Similarly, Xing et al. demonstrated that a combination of conventional MR, DWI, and DSC-perfusion imaging features has high accuracy for predicting IDH mutations in grade II and III astrocytomas [272]. In a study of 33 patients with IDH-mutated and 1p/19q co-deleted oligodendrogliomas, Lin et al. found that rCBV and rCBF from DSC perfusion imaging were significantly different between grades 2 and 3 and the combination of SWI and DSC-PWI provided the highest accuracy for the differentiation [273]. Additionally, Bakas et al. studied the peritumoral region in 64 patients with glioblastoma and validated the findings in 78 cohorts and demonstrated that a peritumoral heterogeneity index derived from DSC perfusion imaging is highly accurate to predict EGFRvIII status [274].

## Post-Treatment Planning

### Response to Therapy and Recurrence/Progression

MR perfusion techniques have shown promise as a quantitative measure of response to treatment as well as predictor of outcome [180, 227, 260, 275–278]. Early studies showed that MR perfusion measures of blood volume could be used to evaluate response to radiation in low-grade gliomas and normal brain [276, 278]. ASL perfusion imaging has also been applied in this setting. For example, using PASL and DSC perfusion MRI to evaluate metastases before and after radiation, Weber et al. [277] found that a drop in the ratio of rTBF to gray matter from pre-treatment study to 6 weeks after stereotactic radiosurgery using either approach was predictive of outcome, and a decrease in rTBF to gray matter ratio predicted ultimate treatment response.

Multiple investigators applied DSC perfusion imaging as a predictive marker in the setting of treatment with antiangiogenic agents and demonstrated that baseline rCBV correlates with overall survival in patients with high-grade glioma [279, 280]. Schmainda et al. studied 36 subjects with high-grade glioma who underwent bevacizumab treatment and demonstrated that the overall survival was significantly longer if either the pre- or post-treatment standardized rCBV was <4400 [281]. This finding was corroborated in a subsequent study, which demonstrated that patients with at least 1 year of overall survival had large decreases in normalized rCBV at week 2 and week 16 [282].

Multimodality MRI with longitudinal assessment of treatment with a vascular endothelial growth factor (VEGF)

inhibitor illustrated normalization of tumor vasculature as measured by rTBF, permeability ( $K^{trans}$ ), and relative vessel size [180]. A recent meta-analysis of 13 DSC and DCE perfusion studies in patients with recurrent glioma treated with bevacizumab-based regimens demonstrated the usefulness of rCBV in predicting tumor progression and eventual outcome after treatment. This meta-analysis also showed that rCBV,  $K^{trans}$ , CBVmax, Vp, Ve, and Kep demonstrated a consistent decrease on the follow-up MRI after treatment [283]. Perfusion MR techniques have also been used to study effects of corticosteroids on brain neoplasms and associated edema [284–287].

### Post-Treatment Imaging of Brain Tumors: Tumor Recurrence, Pseudoprogression and Radiation Necrosis

Immediately after radiotherapy, especially when combined with chemotherapy, a treated brain neoplasm may initially show apparent progression with increased edema and contrast enhancement but with subsequent stabilization or improvement (pseudoprogression). The timing of pseudoprogression is different than classic radiation necrosis, which usually occurs 9–12 months or even years following radiation [288, 289]. In addition, classic radiation necrosis tends to stabilize or worsen over time in contrary to spontaneous resolution in pseudoprogression. Neurooncologists have been familiar with the concept of pseudoprogression for some time and tend to delay postradiation MRI for several weeks to better assess true treatment response; however, pseudoprogression remains an issue, typically seen within the first several months after completion of radiotherapy [290, 291]. With standard of care radiation and concurrent temozolomide (chemoradiation) for glioblastoma, this is commonly seen and rates of pseudoprogression as high as 64% have been reported [292, 293]. Two basic problems arise as a result: (1) pseudoprogression could be mistaken for progression of disease and a potentially beneficial treatment could be stopped or altered, and (2) improvement after initial pseudoprogression could be mistaken for actual response to a given treatment strategy [290] (Fig. 5.17). MR techniques evaluating diffusion, perfusion, and metabolic characteristics of these lesions have shown improved differentiation between recurrence and post-treatment changes. For perfusion MRI imaging, DSC MRI techniques have been the primary focus [176, 258, 294–296] (Fig. 5.18).

Gasparetto et al. used a T2-weighted DSC perfusion MR technique to assess the fraction of malignant histologic features in enhancing masses appearing after treatment [176]. They found that a rCBV threshold relative to normal-appearing white matter of 1.8 was an efficient and accurate cutoff for a fraction of 20% malignant histological features.

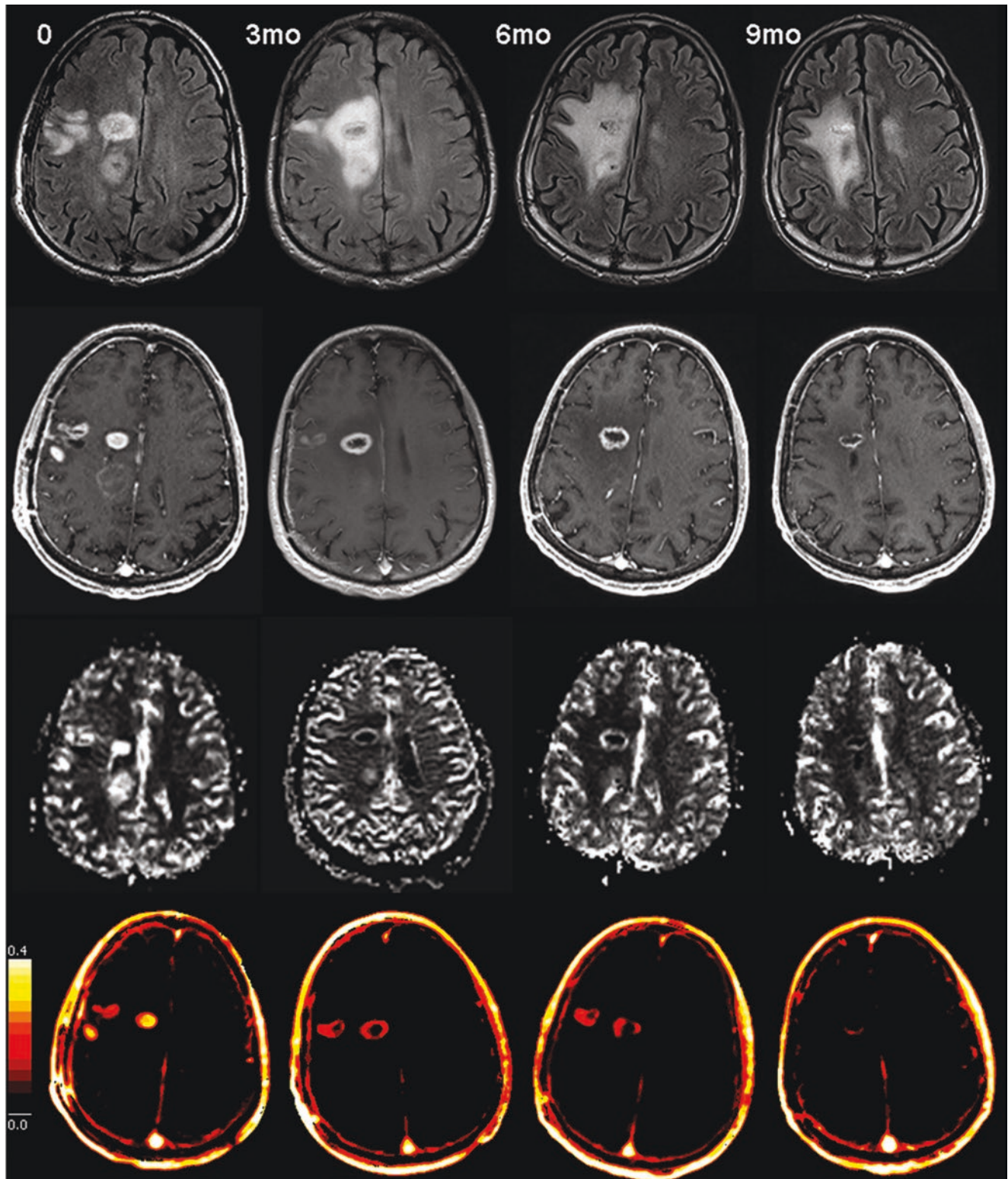


**Fig. 5.17** Response to therapy monitored with conventional MRI, T2\*-weighted DSC perfusion MRI, and T1-weighted DCE permeability MRI: a 48-year-old with glioblastoma. From *top to bottom*, FLAIR, post-contrast T1-weighted spin echo or gradient echo, relative tumor blood volume (rTBV), and permeability ( $K^{\text{trans}}$ , *bottom*) are shown. Time point 0 indicates post-resection, pre-chemoradiation exam, followed by 3-month interval follow-up studies. Chemoradiation was

given between 0- and 3-month time points, with pseudoprogession in callosal mass anteriorly on FLAIR and post-contrast imaging and improvement in other enhancing lesions, but apparent response on rTBV and  $K^{\text{trans}}$  maps at 3- and 6-month time points, and with improvement on all sequences by 9-month time point. Image locations are not perfectly registered between studies

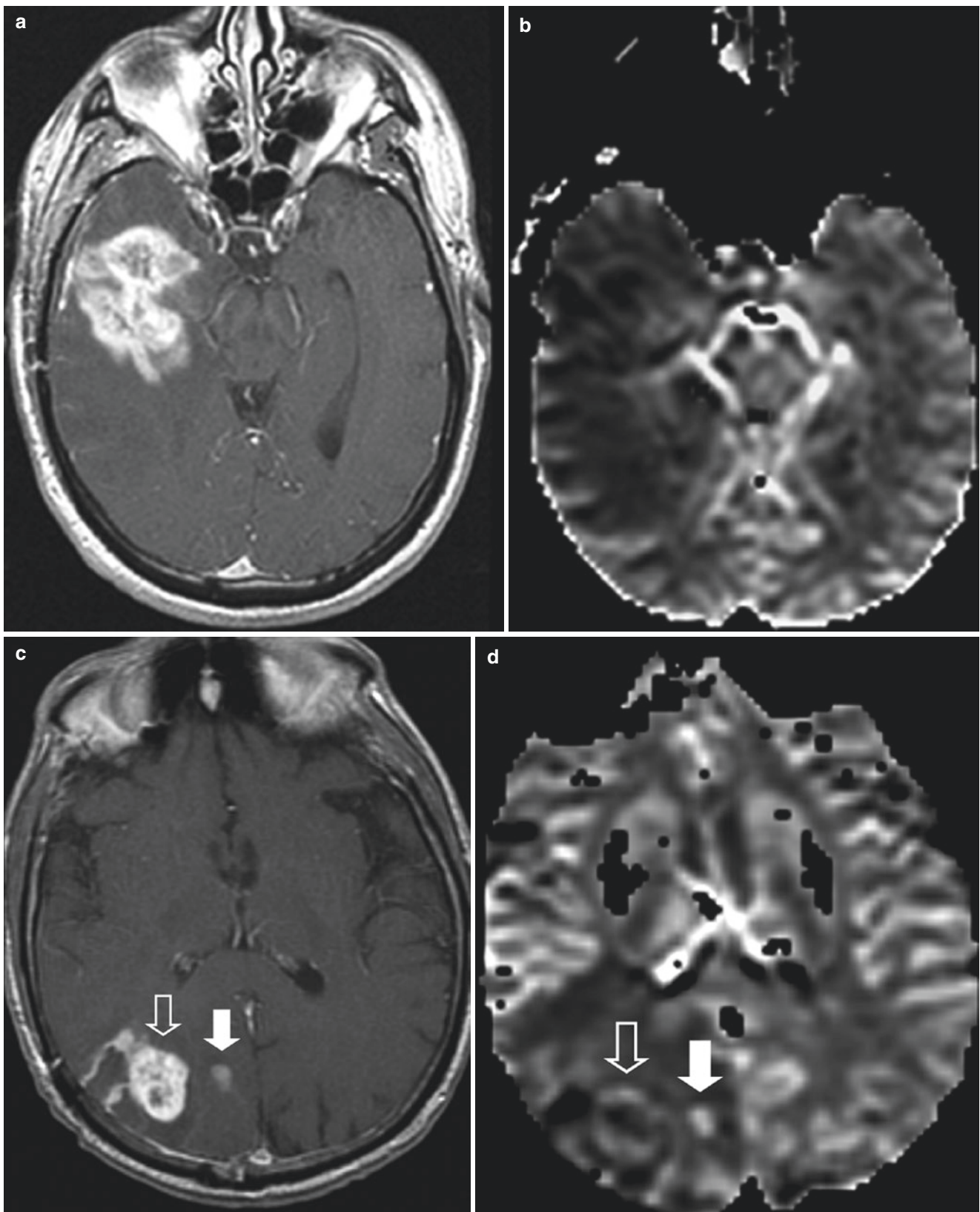


**Fig. 5.18** Treatment related necrosis (TRN) versus progression: 2 glioblastoma cases status post-surgery and chemoradiation. Despite aggressive enhancement and mass effect (a), rTBV was low for TRN

(b). Enhancing masses are also seen for the case of progression (c), while rTBV is increased in this case (arrows), especially for smaller focus (closed arrow) (d)

Wang et al. demonstrated that using a cutoff value of  $rCBV_{max} = 2.77$  provides 82% sensitivity and 63% specificity to differentiate pseudoprogression from true progression and mixed tissue [297]. In a recent study in 19 patients with GBM with progressive enhancement on postchemoradiation MRI, Boxerman et al. demonstrated that the initial  $rCBV$  was not significantly different in between pseudoprogression and the true progression group on initial MRI; however, there was a significant difference in the overall linear trend in  $rCBV$  on follow-up MRIs between the two groups [298] (Fig. 5.19).

Hoefnagels et al. [258] studied metastases treated with stereotactic radiosurgery using a  $T2^*$ -weighted DSC MRI technique, reporting an optimal cutoff for maximum  $rCBV$  of 2.0 relative to white matter for sensitivity and specificity of 85 and 71.4%, respectively; although survival after time of suspected recurrence (defined as time of the perfusion MRI) was only minimally and not significantly increased for the radiation necrosis group compared to the recurrence group ( $13.4 \pm 8.6$  months vs.  $8.4 \pm 7.1$  months). Barajas et al. [294] studied brain metastases after gamma knife radiosurgery, using DSC perfusion MRI and evaluating perfusion metrics  $rCBV$ ,  $rPH$  (relative peak height), and  $PSR$  (percent signal recovery) in this setting. They found that measures of  $PSR$  were best in making this distinction, with  $PSR$  lower in cases of recurrent metastatic disease (cutoff of  $PSR = 76.3\%$  gave sensitivity = 95.65% and specificity of 100%). However,  $rCBV$  and  $rPH$  measures were also significantly different between these groups, showing higher values in cases of recurrent metastatic disease but with more overlap between groups as compared with  $PSR$ .

In recent years, multiple investigators used DCE MRI to differentiate true progression from pseudoprogression. Thomas et al. studied 37 patients with glioblastoma treated with radiation and temozolomide after surgical resection and demonstrated lower plasma volume and  $K_{trans}$  values in pseudoprogression compared to tumor progression [299].

Bisdas et al. prospectively studied 18 patients with high-grade glioma, analyzing DCE data with both pharmacokinetic modeling and model free analyses. They demonstrated that both the initial area under the signal intensity curve ( $iAUC$ ) and  $K_{trans}$  were significantly higher in the recurrent glioma compared to radiation necrosis group [300]. In another study, Chung et al. applied a bimodal histogram analysis of  $AUC$  using DCE MRI and demonstrated that ratio of the initial area under the time signal intensity curve ( $IAUC$ ) to the final  $AUC$  was the best indicator to differentiate recurrent GBM from radiation necrosis with a sensitivity of 93.8% and a specificity of 88.0% [301].

ASL imaging has also been used in post-treatment evaluation of brain tumors. Ye et al. studied 16 cases of recurrent glioma and 5 cases of radiation necrosis using both DSC and ASL perfusion. They demonstrated that both normalized  $CBF$  and  $rCBV$  ratio were significantly higher in patients with tumor recurrence compared to radiation necrosis [302]. In a retrospective study, Choi et al. included 117 patients with GBM following resection and chemoradiation to investigate the added value of ASL compared to DSC perfusion alone. They used a semiquantitative grading system for ASL imaging based on comparing tumor perfusion signal intensity to the white matter (grade I), gray matter (grade II), and blood vessels (grade III). They found that adjunctive ASL improved the diagnostic accuracy of DSC perfusion in differentiating pseudoprogression from early tumor progression [303]. It should be noted that pseudoprogression may also occur with immunotherapy. Though experience with assessing response to these agents is evolving, the understanding of the application of perfusion techniques in this setting is incomplete. Alternative approaches such as those employing ferumoxytol are of particular interest and may become more relevant in assessing immune response and inflammation in this setting, but these are beyond the scope of this chapter [304].

### Pseudoresponse

An additional consideration is that radiographic response based on conventional or advanced imaging techniques, including perfusion and permeability imaging, may be misleading; specifically, an apparent improvement may not truly indicate tumor response (*pseudoresponse*) [290, 305]. This is also increasingly seen, primarily with antiangiogenic therapies such as with bevacizumab. Briefly, a dramatic response to antiangiogenic therapy may be seen [180], but viable neoplasm persists such that removal of the drug may reverse the effect with resurgence of disease. The radiographic response with “normalization” of vessels and the resulting decrease in abnormal permeability with restoration of the BBB does not necessarily translate to tumor response. In fact, antiangiogenic agents may promote progression of invasive nonenhancing tumor by selecting tumor cells and/or growth patterns that are not relying on angiogenesis [306]. Progression in nonenhancing neoplasm can occur by co-opting normal vessels and without angiogenesis or increased tumor vascularity, such that progressive neoplasm is better seen on conventional imaging sequences such as FLAIR, while maps of tumor blood volume and permeability underestimate extent of disease [290, 305] (Fig. 5.20). Nevertheless, the patient may still benefit from antiangiogenic treatment by reducing symptoms and steroid dependence.

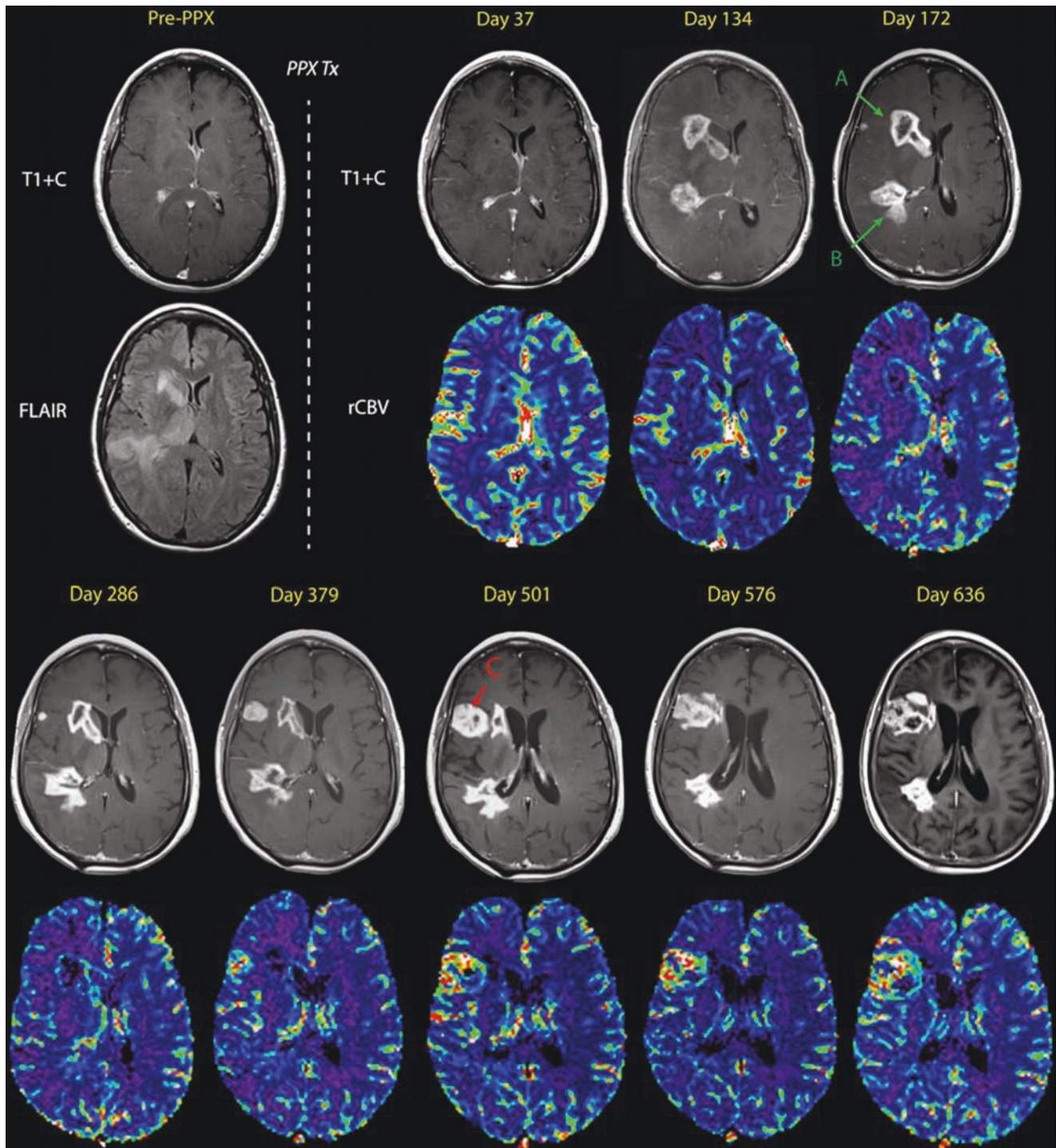


**Fig. 5.19** PPX, TMZ, and radiation-treated anaplastic astrocytoma (WHO III). The radiation field included all pretreatment regions of FLAIR hyperintensity, including the right frontal opercular source of lesion C. Longitudinal postcontrast T1-weighted MRI and corresponding rCBV maps demonstrate concomitant PsP (lesions A, B) and PD (lesion C). Pseudoproggressive enhancement peaked 172 days after PPX +TMZ with decreasing rCBV after appearance of enhancement. Progressive tumor enhancement appeared later and monotonically grew with increasing rCBV. Note the prolonged course of pseudoproggressive

enhancement characteristic of PPX +TMZ therapy. *MRI* magnetic resonance imaging, *PD* progressive disease, *PPX* paclitaxel poliglumex, *PsP* pseudoprogression, *rCBV* relative cerebral blood volume, *TMZ* temozolomide. Reprinted with permission from Boxerman JL, Ellingson BM, Jeyapalan S, Elinzano H, Harris RJ, Rogg JM, et al. Longitudinal DSC-MRI for distinguishing tumor recurrence from pseudoprogression in patients with a high-grade glioma. *Am J Clin Oncol.* 2017;40(3):228–34

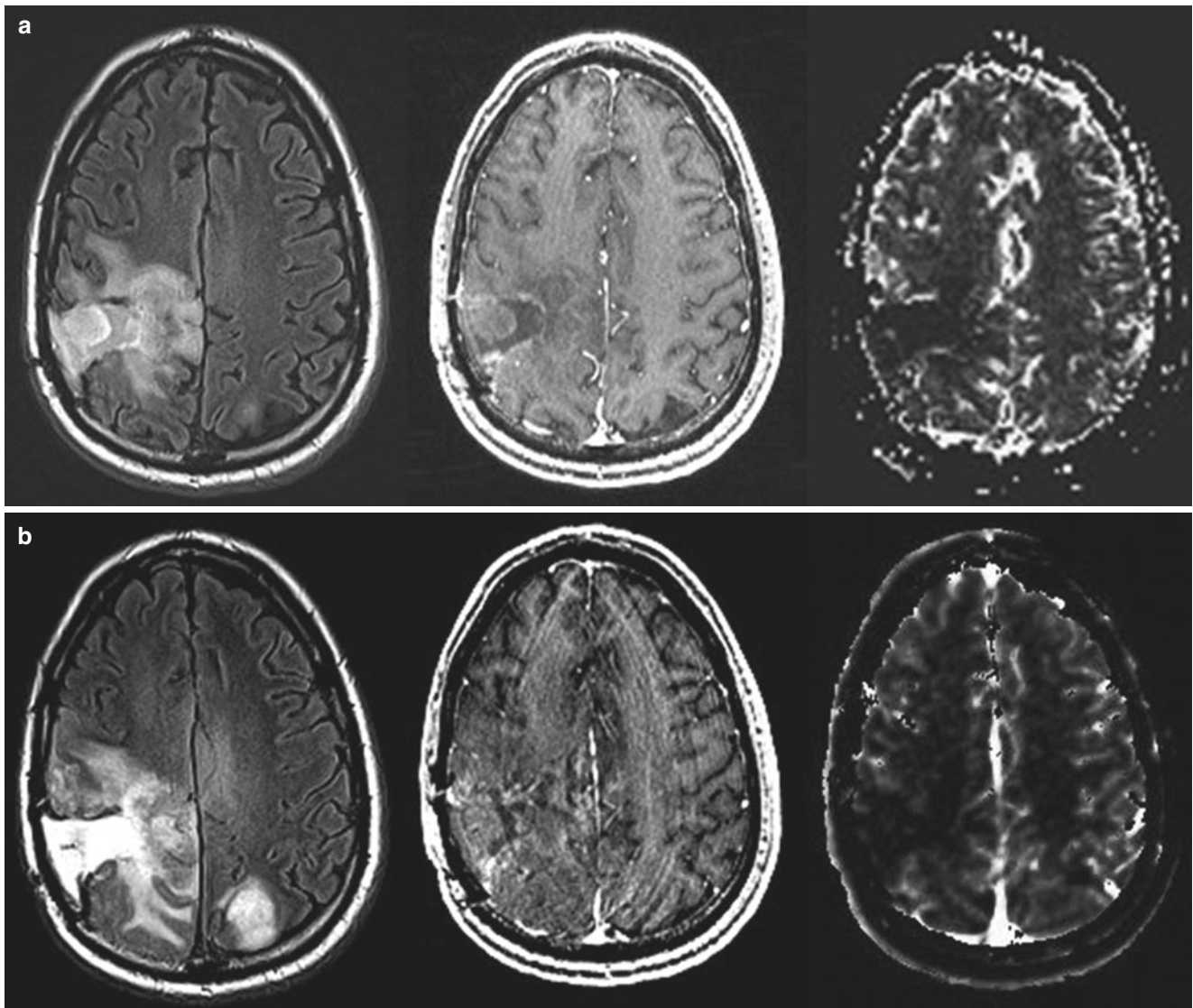


**Fig. 5.20** Pseudoresponse: patient with glioblastoma on bevacizumab. Two different time points are shown: (a) 6 weeks before (b) with resection cavity and surrounding mixed neoplasm and treatment effect on right showing relatively little change compared to increase in infiltrat-

ing nonenhancing neoplasm medial left frontal lobe and more focally in left parietal lobe. Blood volume maps calculated with different techniques—(a) DSC T2\*-weighted and (b) DCE T1-weighted approach—showed no striking increase in blood volume

## Conclusion

DSC, DCE, and ASL perfusion MRI approaches have been discussed in multiple clinical settings, focusing on cerebrovascular disease (especially in subacute and chronic settings) and intracranial neoplasms. Most of the literature to date has employed contrast-enhanced perfusion methodology, especially DSC perfusion MRI, but use of DCE and ASL perfu-

sion techniques is increasing (Table 5.1). Each technique has advantages and disadvantages, discussed briefly herein but also in greater depth in chapters elsewhere in this book. Improvements in acquisition and postprocessing strategies over the last several years have made efficient implementation of both approaches a reality not only in clinical trials but also in routine daily clinical practice.



**Table 5.1** Summary of key articles discussing perfusion

Authors	Topic, type of study	Perfusion technique	Summary
Tofts et al. (1999) [21]	Dynamic contrast enhanced imaging principles, theory	DCE	Discussion of DCE principles along with useful references, addresses standardization of parameter names and symbols
Alsop et al. (2015) [94]	ASL perfusion MRI, recommended implementation and consensus statement	ASL	Consensus statement of ISMRM perfusion study group and the European consortium for ASL in dementia, provides summary of recommended implementations of ASL for clinical work
Haller et al. (2016) [41]	ASL clinical applications, review		Review of primary clinical applications for the main ASL perfusion implementations: pulsed and pseudocontinuous labeling techniques. Applications in stroke, vascular malformations, dementia, epilepsy, neoplasia, and neuropsychiatric disorders including TBI and PTSD are discussed as well as future directions and implementations
Lanzman and Heit (2017) [307]	MR perfusion techniques and clinical applications, technical review	ASL, DSC, DCE, IVIM	Succinct overview of cerebral hemodynamic assessment techniques and primary clinical applications
Fan et al. (2017) [93]	Cerebrovascular occlusive disease and long transit times, optimization and validation of ASL, controlled crossover study	ASL, DSC, PET	Utilization of longer post-labeling delays for ASL perfusion MRI evaluation of patients with prolonged transit times, validated with [ <sup>15</sup> O]-PET CBF
Dehkharghani and Andre (2017) [27]	Acute Ischemic Syndrome (AIS), review	DSC, CTP, ASL	Review of imaging approaches in AIS including perfusion imaging
Ellingson et al. (2017) [304]	Glioblastoma and post-treatment evaluation, review	DSC	Review discussing imaging approaches in post-treatment glioblastoma including immunotherapy effects, perfusion imaging focusing on DSC perfusion MRI
Fisher et al. (2018) [107]	Chronic cerebrovascular disease and cerebrovascular reactivity, review		Review of pathophysiology and methods in measuring CVR, with focus on implementation and standardization for clinical application in cerebrovascular stenotic occlusive disease
Albers et al. (2018) [35]	Acute Ischemic Syndrome (AIS) and intervention, multicenter, randomized, open-label trial	DSC, CTP	Trial with randomization of large vessel occlusion in 6 to 16 hours window to endovascular plus medical therapy or medical therapy alone, showing better functional outcome with addition of endovascular intervention
Anzalone et al. (2018) [223]	DSC and DCE MRI metrics for grading glioma, prospective multicenter study	DSC, DCE	Standardized multicenter acquisition and analysis protocol studied showing good accuracy and reproducibility for routine clinical application

*DCE* dynamic contrast enhanced, *DSC* dynamic susceptibility contrast, *ASL* arterial spin labeled, *IVIM* intravoxel incoherent motion, *CVR* cerebral vascular reactivity, *CTP* CT perfusion

## References

- Wintermark M, Sesay M, Barbier E, Borbely K, Dillon WP, Eastwood JD, et al. Comparative overview of brain perfusion imaging techniques. *Stroke*. 2005;36(9):83–99.
- Calamante F, Thomas DL, Pell GS, Wiersma J, Turner R. Measuring cerebral blood flow using magnetic resonance imaging techniques. *J Cereb Blood Flow Metab*. 1999;19(7):701–35.
- Petersen ET, Lim T, Golay X. Model-free arterial spin labeling quantification approach for perfusion MRI. *Magn Reson Med*. 2006;55(2):219–32.
- Wang J, Alsop DC, Song HK, Maldjian JA, Tang K, Salvucci AE, et al. Arterial transit time imaging with flow encoding arterial spin tagging (feast). *Magn Reson Med*. 2003;50(3):599–607.
- Aguirre GK, Detre JA, Zarahn E, Alsop DC. Experimental design and the relative sensitivity of bold and perfusion fMRI. *NeuroImage*. 2002;15(3):488–500.
- Wang J, Aguirre GK, Kimberg DY, Roc AC, Li L, Detre JA. Arterial spin labeling perfusion fMRI with very low task frequency. *Magn Reson Med*. 2003;49(5):796–802.
- Wong EC, Buxton RB, Frank LR. Implementation of quantitative perfusion imaging techniques for functional brain mapping using pulsed arterial spin labeling. *NMR Biomed*. 1997;10(4-5):237–49.
- Golay X, Petersen ET, Hui F. Pulsed star labeling of arterial regions (pulsar): a robust regional perfusion technique for high field imaging. *Magn Reson Med*. 2005;53(1):15–21.
- Hendrikse J, van der Grond J, Lu H, van Zijl PC, Golay X. Flow territory mapping of the cerebral arteries with regional perfusion MRI. *Stroke*. 2004;35(4):882–7.
- Werner R, Norris DG, Alfke K, Mehdorn HM, Jansen O. Continuous artery-selective spin labeling (cassl). *Magn Reson Med*. 2005;53(5):1006–12.
- Latchaw RE, Yonas H, Hunter GJ, Yuh WT, Ueda T, Sorensen AG, et al. Guidelines and recommendations for perfusion imaging in cerebral ischemia: a scientific statement for healthcare professionals by the writing group on perfusion imaging, from the council on cardiovascular radiology of the American Heart Association. *Stroke*. 2003;34(4):1084–104.
- Wolf RL, Detre JA. Clinical neuroimaging using arterial spin-labeled perfusion magnetic resonance imaging. *Neurotherapeutics*. 2007;4(3):346–59.

13. Ostergaard L. Principles of cerebral perfusion imaging by bolus tracking. *J Magn Reson Imaging*. 2005;22(6):710–7.
14. Boxerman JL, Prah DE, Paulson ES, Machan JT, Bedekar D, Schmainda KM. The role of preload and leakage correction in gadolinium-based cerebral blood volume estimation determined by comparison with mion as a criterion standard. *AJNR Am J Neuroradiol*. 2012;33(6):1081–7.
15. Paulson ES, Schmainda KM. Comparison of dynamic susceptibility-weighted contrast-enhanced MR methods: recommendations for measuring relative cerebral blood volume in brain tumors. *Radiology*. 2008;249(2):601–13.
16. Gahramanov S, Muldoon LL, Li X, Neuwelt EA. Improved perfusion MR imaging assessment of intracerebral tumor blood volume and antiangiogenic therapy efficacy in a rat model with ferumoxytol. *Radiology*. 2011;261(3):796–804.
17. Gahramanov S, Raslan AM, Muldoon LL, Hamilton BE, Rooney WD, Varallyay CG, et al. Potential for differentiation of pseudoprogression from true tumor progression with dynamic susceptibility-weighted contrast-enhanced magnetic resonance imaging using ferumoxytol vs. Gadoteridol: a pilot study. *Int J Radiat Oncol Biol Phys*. 2011;79(2):514–23.
18. Maralani PJ, Das S, Mainprize T, Phan N, Bharatha A, Keith J, et al. Hypoxia detection in infiltrative astrocytoma: ferumoxytol-based quantitative bold MRI with intraoperative and histologic validation. *Radiology*. 2018;288(3):821–9.
19. Lu M, Cohen MH, Rieves D, Pazdur R. FDA report: ferumoxytol for intravenous iron therapy in adult patients with chronic kidney disease. *Am J Hematol*. 2010;85(5):315–9.
20. Choyke PL, Dwyer AJ, Knopp MV. Functional tumor imaging with dynamic contrast-enhanced magnetic resonance imaging. *J Magn Reson Imaging*. 2003;17(5):509–20.
21. Tofts PS, Brix G, Buckley DL, Evelhoch JL, Henderson E, Knopp MV, et al. Estimating kinetic parameters from dynamic contrast-enhanced  $t_1$ -weighted MRI of a diffusible tracer: standardized quantities and symbols. *J Magn Reson Imaging*. 1999;10(3):223–32.
22. Alsop DC. Perfusion MR imaging. In: Atlas SW, editor. *Magnetic resonance imaging of the brain and spine*. 3rd ed. Philadelphia: Lippincott Williams and Wilkins; 2002. p. 215–38.
23. Wong EC. Quantifying CBF with pulsed ASL: technical and pulse sequence factors. *J Magn Reson Imaging*. 2005;22(6):727–31.
24. Nael K, Khan R, Choudhary G, Meshksar A, Villablanca P, Tay J, et al. Six-minute magnetic resonance imaging protocol for evaluation of acute ischemic stroke: pushing the boundaries. *Stroke*. 2014;45(7):1985–91.
25. Grobner T. Gadolinium—a specific trigger for the development of nephrogenic fibrosing dermopathy and nephrogenic systemic fibrosis? *Nephrol Dial Transplant*. 2006;21(4):1104–8.
26. Ramalho J, Semelka RC, Ramalho M, Nunes RH, AIObaidy M, Castillo M. Gadolinium-based contrast agent accumulation and toxicity: an update. *AJNR Am J Neuroradiol*. 2016;37(7):1192–8.
27. Dehkharghani S, Andre J. Imaging approaches to stroke and neurovascular disease. *Neurosurgery*. 2017;80(5):681–700.
28. Krieger DA, Dehkharghani S. Magnetic resonance imaging in ischemic stroke and cerebral venous thrombosis. *Top Magn Reson Imaging*. 2015;24(6):331–52.
29. Latchaw RE, Alberts MJ, Lev MH, Connors JJ, Harbaugh RE, Higashida RT, et al. Recommendations for imaging of acute ischemic stroke: a scientific statement from the American Heart Association. *Stroke*. 2009;40(11):3646–78.
30. Lansberg MG, Straka M, Kemp S, Mlynash M, Wechsler LR, Jovin TG, et al. MRI profile and response to endovascular reperfusion after stroke (defuse 2): a prospective cohort study. *Lancet Neurol*. 2012;11(10):860–7.
31. Davis SM, Donnan GA, Parsons MW, Levi C, Butcher KS, Peeters A, et al. Effects of alteplase beyond 3 h after stroke in the echoplanar imaging thrombolytic evaluation trial (epithet): a placebo-controlled randomised trial. *Lancet Neurol*. 2008;7(4):299–309.
32. Albers GW, Thijs VN, Wechsler L, Kemp S, Schlaug G, Skalabrini E, et al. Magnetic resonance imaging profiles predict clinical response to early reperfusion: the diffusion and perfusion imaging evaluation for understanding stroke evolution (defuse) study. *Ann Neurol*. 2006;60(5):508–17.
33. Olivot JM, Mlynash M, Thijs VN, Kemp S, Lansberg MG, Wechsler L, et al. Optimal tmax threshold for predicting penumbra tissue in acute stroke. *Stroke*. 2009;40(2):469–75.
34. Campbell BC, Mitchell PJ, Yan B, Parsons MW, Christensen S, Churilov L, et al. A multicenter, randomized, controlled study to investigate extending the time for thrombolysis in emergency neurological deficits with intra-arterial therapy (extend-ia). *Int J Stroke*. 2014;9(1):126–32.
35. Albers GW, Marks MP, Kemp S, Christensen S, Tsai JP, Ortega-Gutierrez S, et al. Thrombectomy for stroke at 6 to 16 hours with selection by perfusion imaging. *N Engl J Med*. 2018;378(8):708–18.
36. Wang DJ, Alger JR, Qiao JX, Hao Q, Hou S, Fiaz R, et al. The value of arterial spin-labeled perfusion imaging in acute ischemic stroke: comparison with dynamic susceptibility contrast-enhanced MRI. *Stroke*. 2012;43(4):1018–24.
37. Wang DJ, Alger JR, Qiao JX, Gunther M, Pope WB, Saver JL, et al. Multi-delay multi-parametric arterial spin-labeled perfusion MRI in acute ischemic stroke - comparison with dynamic susceptibility contrast enhanced perfusion imaging. *NeuroImage Clin*. 2013;3:1–7.
38. Bivard A, Krishnamurthy V, Stanwell P, Levi C, Spratt NJ, Davis S, et al. Arterial spin labeling versus bolus-tracking perfusion in hyperacute stroke. *Stroke*. 2014;45(1):127–33.
39. Tada Y, Satomi J, Abe T, Kuwayama K, Sogabe S, Fujita K, et al. Intra-arterial signal on arterial spin labeling perfusion MRI to identify the presence of acute middle cerebral artery occlusion. *Cerebrovasc Dis*. 2014;38(3):191–6.
40. Majer M, Mejdoubi M, Schertz M, Colombani S, Arrigo A. Raw arterial spin labeling data can help identify arterial occlusion in acute ischemic stroke. *Stroke*. 2015;46(6):e141–4.
41. Haller S, Zaharchuk G, Thomas DL, Lovblad KO, Barkhof F, Golay X. Arterial spin labeling perfusion of the brain: emerging clinical applications. *Radiology*. 2016;281(2):337–56.
42. Olivot JM, Mlynash M, Inoue M, Marks MP, Wheeler HM, Kemp S, et al. Hypoperfusion intensity ratio predicts infarct progression and functional outcome in the defuse 2 cohort. *Stroke*. 2014;45(4):1018–23.
43. Lee MJ, Son JP, Kim SJ, Ryoo S, Woo SY, Cha J, et al. Predicting collateral status with magnetic resonance perfusion parameters: Probabilistic approach with a tmax-derived prediction model. *Stroke*. 2015;46(10):2800–7.
44. Nael K, Doshi A, De Leacy R, Puig J, Castellanos M, Bederson J, et al. MR perfusion to determine the status of collaterals in patients with acute ischemic stroke: a look beyond time maps. *AJNR Am J Neuroradiol*. 2018;39(2):219–25.
45. de Havenon A, Haynor DR, Tirschwell DL, Majersik JJ, Smith G, Cohen W, et al. Association of collateral blood vessels detected by arterial spin labeling magnetic resonance imaging with neurological outcome after ischemic stroke. *JAMA Neurol*. 2017;74(4):453–8.
46. Lyu J, Ma N, Liebeskind DS, Wang DJ, Ma L, Xu Y, et al. Arterial spin labeling magnetic resonance imaging estimation of antegrade and collateral flow in unilateral middle cerebral artery stenosis. *Stroke*. 2016;47(2):428–33.
47. Lou X, Yu S, Scalzo F, Starkman S, Ali LK, Kim D, et al. Multi-delay asl can identify leptomeningeal collateral perfusion in endovascular therapy of ischemic stroke. *Oncotarget*. 2017;8(2):2437–43.

48. Schaller B, Graf R. Cerebral ischemia and reperfusion: the pathophysiologic concept as a basis for clinical therapy. *J Cereb Blood Flow Metab.* 2004;24(4):351–71.
49. Larrue V, von Kummer RR, Muller A, Bluhmki E. Risk factors for severe hemorrhagic transformation in ischemic stroke patients treated with recombinant tissue plasminogen activator: a secondary analysis of the European-Australasian Acute Stroke Study (ECASS II). *Stroke.* 2001;32(2):438–41.
50. Alsop DC, Makovetskaya E, Kumar S, Selim M, Schlaug G. Markedly reduced apparent blood volume on bolus contrast magnetic resonance imaging as a predictor of hemorrhage after thrombolytic therapy for acute ischemic stroke. *Stroke.* 2005;36(4):746–50.
51. Fiehler J, Remmele C, Kucinski T, Rosenkranz M, Thomalla G, Weiller C, et al. Reperfusion after severe local perfusion deficit precedes hemorrhagic transformation: an MRI study in acute stroke patients. *Cerebrovasc Dis.* 2005;19(2):117–24.
52. Kidwell CS, Villablanca JP, Saver JL. Advances in neuroimaging of acute stroke. *Curr Atheroscler Rep.* 2000;2(2):126–35.
53. Selim M, Fink JN, Kumar S, Caplan LR, Horkan C, Chen Y, et al. Predictors of hemorrhagic transformation after intravenous recombinant tissue plasminogen activator: prognostic value of the initial apparent diffusion coefficient and diffusion-weighted lesion volume. *Stroke.* 2002;33(8):2047–52.
54. Firlik AD, Yonas H, Kaufmann AM, Wechsler LR, Jungreis CA, Fukui MB, et al. Relationship between cerebral blood flow and the development of swelling and life-threatening herniation in acute ischemic stroke. *J Neurosurg.* 1998;89(2):243–9.
55. Bang OY, Saver JL, Alger JR, Shah SH, Buck BH, Starkman S, et al. Patterns and predictors of blood-brain barrier permeability derangements in acute ischemic stroke. *Stroke.* 2009;40(2):454–61.
56. Kassner A, Roberts T, Taylor K, Silver F, Mikulis D. Prediction of hemorrhage in acute ischemic stroke using permeability MR imaging. *AJNR Am J Neuroradiol.* 2005;26(9):2213–7.
57. Kassner A, Roberts TP, Moran B, Silver FL, Mikulis DJ. Recombinant tissue plasminogen activator increases blood-brain barrier disruption in acute ischemic stroke: an MR imaging permeability study. *AJNR Am J Neuroradiol.* 2009;30(10):1864–9.
58. Wu S, Thornhill RE, Chen S, Rammo W, Mikulis DJ, Kassner A. Relative recirculation: a fast, model-free surrogate for the measurement of blood-brain barrier permeability and the prediction of hemorrhagic transformation in acute ischemic stroke. *Investig Radiol.* 2009;44(10):662–8.
59. Yu S, Liebeskind DS, Dua S, Wilhalme H, Elashoff D, Qiao XJ, et al. Posts ischemic hyperperfusion on arterial spin labeled perfusion MRI is linked to hemorrhagic transformation in stroke. *J Cereb Blood Flow Metab.* 2015;35(4):630–7.
60. Caplan LR, Hennerici M. Impaired clearance of emboli (washout) is an important link between hypoperfusion, embolism, and ischemic stroke. *Arch Neurol.* 1998;55(11):1475–82.
61. Derdeyn CP, Grubb RL Jr, Powers WJ. Cerebral hemodynamic impairment: methods of measurement and association with stroke risk. *Neurology.* 1999;53(2):251–9.
62. Powers WJ. Cerebral hemodynamics in ischemic cerebrovascular disease. *Ann Neurol.* 1991;29(3):231–40.
63. Derdeyn CP, Videen TO, Yundt KD, Fritsch SM, Carpenter DA, Grubb RL, et al. Variability of cerebral blood volume and oxygen extraction: stages of cerebral haemodynamic impairment revisited. *Brain.* 2002;125(Pt 3):595–607.
64. Vagal AS, Leach JL, Fernandez-Ulloa M, Zuccarello M. The acetazolamide challenge: techniques and applications in the evaluation of chronic cerebral ischemia. *AJNR Am J Neuroradiol.* 2009;30(5):876–84.
65. Ginsberg MD. The new language of cerebral ischemia. *AJNR Am J Neuroradiol.* 1997;18(8):1435–45.
66. Lu H, Ge Y. Quantitative evaluation of oxygenation in venous vessels using t2-relaxation-under-spin-tagging MRI. *Magn Reson Med.* 2008;60(2):357–63.
67. Barhoum S, Rodgers ZB, Langham M, Magland JF, Li C, Wehrli FW. Comparison of MRI methods for measuring whole-brain venous oxygen saturation. *Magn Reson Med.* 2015;73(6):2122–8.
68. Rodgers ZB, Englund EK, Langham MC, Magland JF, Wehrli FW. Rapid t2- and susceptometry-based cmro2 quantification with interleaved trust (itrust). *NeuroImage.* 2015;106:441–50.
69. Kim JH, Lee SJ, Shin T, Kang KH, Choi PY, Kim JH, et al. Correlative assessment of hemodynamic parameters obtained with t2\*-weighted perfusion MR imaging and spect in symptomatic carotid artery occlusion. *AJNR Am J Neuroradiol.* 2000;21(8):1450–6.
70. Bozzao A, Floris R, Gaudiello F, Finocchi V, Fantozzi LM, Simonetti G. Hemodynamic modifications in patients with symptomatic unilateral stenosis of the internal carotid artery: evaluation with MR imaging perfusion sequences. *AJNR Am J Neuroradiol.* 2002;23(8):1342–5.
71. Doerfler A, Eckstein HH, Eichbaum M, Heiland S, Benner T, Allenberg JR, et al. Perfusion-weighted magnetic resonance imaging in patients with carotid artery disease before and after carotid endarterectomy. *J Vasc Surg.* 2001;34(4):587–93.
72. Kajimoto K, Moriwaki H, Yamada N, Hayashida K, Kobayashi J, Miyashita K, et al. Cerebral hemodynamic evaluation using perfusion-weighted magnetic resonance imaging: comparison with positron emission tomography values in chronic occlusive carotid disease. *Stroke.* 2003;34(7):1662–6.
73. Kluytmans M, van der Grond J, Folkers PJ, Mali WP, Viergever MA. Differentiation of gray matter and white matter perfusion in patients with unilateral internal carotid artery occlusion. *J Magn Reson Imaging.* 1998;8(4):767–74.
74. Kluytmans M, van der Grond J, Viergever MA. Gray matter and white matter perfusion imaging in patients with severe carotid artery lesions. *Radiology.* 1998;209(3):675–82.
75. Maeda M, Yuh WT, Ueda T, Maley JE, Crosby DL, Zhu MW, et al. Severe occlusive carotid artery disease: hemodynamic assessment by MR perfusion imaging in symptomatic patients. *AJNR Am J Neuroradiol.* 1999;20(1):43–51.
76. Nasel C, Azizi A, Wilfort A, Mallek R, Schindler E. Measurement of time-to-peak parameter by use of a new standardization method in patients with stenotic or occlusive disease of the carotid artery. *AJNR Am J Neuroradiol.* 2001;22(6):1056–61.
77. Nasel C, Kronsteiner N, Schindler E, Kreuzer S, Gentsch S. Standardized time to peak in ischemic and regular cerebral tissue measured with perfusion MR imaging. *AJNR Am J Neuroradiol.* 2004;25(6):945–50.
78. Nighoghossian N, Berthezene Y, Philippon B, Adeleine P, Froment JC, Trouillas P. Hemodynamic parameter assessment with dynamic susceptibility contrast magnetic resonance imaging in unilateral symptomatic internal carotid artery occlusion. *Stroke.* 1996;27(3):474–9.
79. van Osch MJ, Rutgers DR, Voncken EP, van Huffelen AC, Klijn CJ, Bakker CJ, et al. Quantitative cerebral perfusion MRI and co2 reactivity measurements in patients with symptomatic internal carotid artery occlusion. *NeuroImage.* 2002;17(1):469–78.
80. Zaharchuk G. Theoretical basis of hemodynamic MR imaging techniques to measure cerebral blood volume, cerebral blood flow, and permeability. *AJNR Am J Neuroradiol.* 2007;28(10):1850–8.
81. Thulborn KR, Atkinson IC, Alexander A, Singal M, Amin-Hanjani S, Du X, et al. Comparison of blood oxygenation level-dependent fMRI and provocative DSC perfusion MR imaging for monitoring cerebrovascular reserve in intracranial chronic cerebrovascular disease. *AJNR Am J Neuroradiol.* 2018;39(3):448–53.
82. Kudo K, Sasaki M, Yamada K, Momoshima S, Utsunomiya H, Shirato H, et al. Differences in ct perfusion maps gener-

- ated by different commercial software: quantitative analysis by using identical source data of acute stroke patients. *Radiology*. 2010;254(1):200–9.
83. Wu O, Ostergaard L, Weisskoff RM, Benner T, Rosen BR, Sorensen AG. Tracer arrival timing-insensitive technique for estimating flow in MR perfusion-weighted imaging using singular value decomposition with a block-circulant deconvolution matrix. *Magn Reson Med*. 2003;50(1):164–74.
  84. Olivot JM, Mlynash M, Zaharchuk G, Straka M, Bammer R, Schwartz N, et al. Perfusion MRI (tmax and MTT) correlation with xenon ct cerebral blood flow in stroke patients. *Neurology*. 2009;72(13):1140–5.
  85. Chalela JA, Alsop DC, Gonzalez-Atavales JB, Maldjian JA, Kasner SE, Detre JA. Magnetic resonance perfusion imaging in acute ischemic stroke using continuous arterial spin labeling. *Stroke*. 2000;31(3):680–7.
  86. Detre JA, Alsop DC, Vives LR, Maccotta L, Teener JW, Raps EC. Noninvasive MRI evaluation of cerebral blood flow in cerebrovascular disease. *Neurology*. 1998;50(3):633–41.
  87. Siewert B, Schlaug G, Edelman RR, Warach S. Comparison of epistar and t2\*-weighted gadolinium-enhanced perfusion imaging in patients with acute cerebral ischemia. *Neurology*. 1997;48(3):673–9.
  88. Hunsche S, Sauner D, Schreiber WG, Oelkers P, Stoeter P. Fair and dynamic susceptibility contrast-enhanced perfusion imaging in healthy subjects and stroke patients. *J Magn Reson Imaging*. 2002;16(2):137–46.
  89. Kimura H, Kado H, Koshimoto Y, Tsuchida T, Yonekura Y, Itoh H. Multislice continuous arterial spin-labeled perfusion MRI in patients with chronic occlusive cerebrovascular disease: a correlative study with co2 pet validation. *J Magn Reson Imaging*. 2005;22(2):189–98.
  90. Wolf RL, Alsop DC, McGarvey ML, Maldjian JA, Wang J, Detre JA. Susceptibility contrast and arterial spin labeled perfusion MRI in cerebrovascular disease. *J Neuroimaging*. 2003;13(1):17–27.
  91. Yoneda K, Harada M, Morita N, Nishitani H, Uno M, Matsuda T. Comparison of fair technique with different inversion times and post contrast dynamic perfusion MRI in chronic occlusive cerebrovascular disease. *Magn Reson Imaging*. 2003;21(7):701–5.
  92. Alsop DC, Detre JA. Reduced transit-time sensitivity in noninvasive magnetic resonance imaging of human cerebral blood flow. *J Cereb Blood Flow Metab*. 1996;16(6):1236–49.
  93. Fan AP, Guo J, Khalighi MM, Gulaka PK, Shen B, Park JH, et al. Long-delay arterial spin labeling provides more accurate cerebral blood flow measurements in moyamoya patients: a simultaneous positron emission tomography/MRI study. *Stroke*. 2017;48(9):2441–9.
  94. Alsop DC, Detre JA, Golay X, Gunther M, Hendrikse J, Hernandez-Garcia L, et al. Recommended implementation of arterial spin-labeled perfusion MRI for clinical applications: a consensus of the ismrm perfusion study group and the European consortium for asl in dementia. *Magn Reson Med*. 2015;73(1):102–16.
  95. Gunther M, Bock M, Schad LR. Arterial spin labeling in combination with a look-locker sampling strategy: Inflow turbo-sampling epi-fair (its-fair). *Magn Reson Med*. 2001;46(5):974–84.
  96. Hendrikse J, van Osch MJ, Rutgers DR, Bakker CJ, Kappelle LJ, Golay X, et al. Internal carotid artery occlusion assessed at pulsed arterial spin-labeling perfusion MR imaging at multiple delay times. *Radiology*. 2004;233(3):899–904.
  97. Hendrikse J, Petersen ET, van Laar PJ, Golay X. Cerebral border zones between distal end branches of intracranial arteries: MR imaging. *Radiology*. 2008;246(2):572–80.
  98. Bokkers RP, van der Worp HB, Mali WP, Hendrikse J. Noninvasive MR imaging of cerebral perfusion in patients with a carotid artery stenosis. *Neurology*. 2009;73(11):869–75.
  99. Bokkers RP, van Laar PJ, van de Ven KC, Kapelle LJ, Klijn CJ, Hendrikse J. Arterial spin-labeling MR imaging measurements of timing parameters in patients with a carotid artery occlusion. *AJNR Am J Neuroradiol*. 2008;29(9):1698–703.
  100. Mull M, Schwarz M, Thron A. Cerebral hemispheric low-flow infarcts in arterial occlusive disease. Lesion patterns and angiomorphological conditions. *Stroke*. 1997;28(1):118–23.
  101. Markus HS, Lythgoe DJ, Ostergaard L, O'Sullivan M, Williams SC. Reduced cerebral blood flow in white matter in ischaemic leukoaraiosis demonstrated using quantitative exogenous contrast based perfusion MRI. *J Neurol Neurosurg Psychiatry*. 2000;69(1):48–53.
  102. O'Sullivan M, Lythgoe DJ, Pereira AC, Summers PE, Jarosz JM, Williams SC, et al. Patterns of cerebral blood flow reduction in patients with ischemic leukoaraiosis. *Neurology*. 2002;59(3):321–6.
  103. Markus H, Cullinane M. Severely impaired cerebrovascular reactivity predicts stroke and tia risk in patients with carotid artery stenosis and occlusion. *Brain*. 2001;124(Pt 3):457–67.
  104. Vernieri F, Pasqualetti P, Passarelli F, Rossini PM, Silvestrini M. Outcome of carotid artery occlusion is predicted by cerebrovascular reactivity. *Stroke*. 1999;30(3):593–8.
  105. Webster MW, Makaroun MS, Steed DL, Smith HA, Johnson DW, Yonas H. Compromised cerebral blood flow reactivity is a predictor of stroke in patients with symptomatic carotid artery occlusive disease. *J Vasc Surg*. 1995;21(2):338–44.
  106. Fierstra J, Sobczyk O, Battisti-Charbonney A, Mandell DM, Poublanc J, Crawley AP, et al. Measuring cerebrovascular reactivity: what stimulus to use? *J Physiol*. 2013;591(23):5809–21.
  107. Fisher JA, Venkatraghavan L, Mikulis DJ. Magnetic resonance imaging-based cerebrovascular reactivity and hemodynamic reserve. *Stroke*. 2018;49(8):2011–8.
  108. Fisher JA. The CO<sub>2</sub> stimulus for cerebrovascular reactivity: fixing inspired concentrations vs. targeting end-tidal partial pressures. *J Cereb Blood Flow Metab*. 2016;36(6):1004–11.
  109. Berthezene Y, Nighoghossian N, Meyer R, Damien J, Cinotti L, Adeleine P, et al. Can cerebrovascular reactivity be assessed by dynamic susceptibility contrast-enhanced MRI? *Neuroradiology*. 1998;40(1):1–5.
  110. Nighoghossian N, Berthezene Y, Meyer R, Cinotti L, Adeleine P, Philippon B, et al. Assessment of cerebrovascular reactivity by dynamic susceptibility contrast-enhanced MR imaging. *J Neurol Sci*. 1997;149(2):171–6.
  111. Detre JA, Samuels OB, Alsop DC, Gonzalez-At JB, Kasner SE, Raps EC. Noninvasive magnetic resonance imaging evaluation of cerebral blood flow with acetazolamide challenge in patients with cerebrovascular stenosis. *J Magn Reson Imaging*. 1999;10(5):870–5.
  112. Mandell DM, Han JS, Poublanc J, Crawley AP, Stainsby JA, Fisher JA, et al. Mapping cerebrovascular reactivity using blood oxygen level-dependent MRI in patients with arterial steno-occlusive disease: comparison with arterial spin labeling MRI. *Stroke*. 2008;39(7):2021–8.
  113. Choi HJ, Sohn CH, You SH, Yoo RE, Kang KM, Yun TJ, et al. Can arterial spin-labeling with multiple postlabeling delays predict cerebrovascular reserve? *AJNR Am J Neuroradiol*. 2018;39(1):84–90.
  114. Chang TY, Liu HL, Lee TH, Kuan WC, Chang CH, Wu HC, et al. Change in cerebral perfusion after carotid angioplasty with stenting is related to cerebral vasoreactivity: a study using dynamic susceptibility-weighted contrast-enhanced MR imaging and functional MR imaging with a breath-holding paradigm. *AJNR Am J Neuroradiol*. 2009;30(7):1330–6.
  115. Goode SD, Krishan S, Alexakis C, Mahajan R, Auer DP. Precision of cerebrovascular reactivity assessment with use of different

- quantification methods for hypercapnia functional MR imaging. *AJNR Am J Neuroradiol.* 2009;30(5):972–7.
116. Lythgoe DJ, Williams SC, Cullinane M, Markus HS. Mapping of cerebrovascular reactivity using bold magnetic resonance imaging. *Magn Reson Imaging.* 1999;17(4):495–502.
  117. Rutgers DR, Klijn CJ, Kappelle LJ, van der Grond J. Recurrent stroke in patients with symptomatic carotid artery occlusion is associated with high-volume flow to the brain and increased collateral circulation. *Stroke.* 2004;35(6):1345–9.
  118. Rutgers DR, Klijn CJ, Kappelle LJ, van Huffelen AC, van der Grond J. A longitudinal study of collateral flow patterns in the circle of willis and the ophthalmic artery in patients with a symptomatic internal carotid artery occlusion. *Stroke.* 2000;31(8):1913–20.
  119. Kluytmans M, van der Grond J, van Everdingen KJ, Klijn CJ, Kappelle LJ, Viergever MA. Cerebral hemodynamics in relation to patterns of collateral flow. *Stroke.* 1999;30(7):1432–9.
  120. van Laar PJ, van der Grond J, Bremmer JP, Klijn CJ, Hendrikse J. Assessment of the contribution of the external carotid artery to brain perfusion in patients with internal carotid artery occlusion. *Stroke.* 2008;39(11):3003–8.
  121. Zaharchuk G, Ledden PJ, Kwong KK, Reese TG, Rosen BR, Wald LL. Multislice perfusion and perfusion territory imaging in humans with separate label and image coils. *Magn Reson Med.* 1999;41(6):1093–8.
  122. Gunther M. Efficient visualization of vascular territories in the human brain by cycled arterial spin labeling MRI. *Magn Reson Med.* 2006;56(3):671–5.
  123. Jones CE, Wolf RL, Detre JA, Das B, Saha PK, Wang J, et al. Structural MRI of carotid artery atherosclerotic lesion burden and characterization of hemispheric cerebral blood flow before and after carotid endarterectomy. *NMR Biomed.* 2006;19(2):198–208.
  124. Werner R, Alfke K, Schaeffter T, Nabavi A, Mehdorn HM, Jansen O. Brain perfusion territory imaging applying oblique-plane arterial spin labeling with a standard send/receive head coil. *Magn Reson Med.* 2004;52(6):1443–7.
  125. Wong EC. Vessel-encoded arterial spin-labeling using pseudocontinuous tagging. *Magn Reson Med.* 2007;58(6):1086–91.
  126. Davies NP, Jezard P. Selective arterial spin labeling (sas): perfusion territory mapping of selected feeding arteries tagged using two-dimensional radiofrequency pulses. *Magn Reson Med.* 2003;49(6):1133–42.
  127. van Laar PJ, van der Grond J, Mali WP, Hendrikse J. Magnetic resonance evaluation of the cerebral circulation in obstructive arterial disease. *Cerebrovasc Dis.* 2006;21(5-6):297–306.
  128. Wu B, Wang X, Guo J, Xie S, Wong EC, Zhang J, et al. Collateral circulation imaging: MR perfusion territory arterial spin-labeling at 3t. *AJNR Am J Neuroradiol.* 2008;29(10):1855–60.
  129. Chng SM, Petersen ET, Zimine I, Sitoh YY, Lim CC, Golay X. Territorial arterial spin labeling in the assessment of collateral circulation: comparison with digital subtraction angiography. *Stroke.* 2008;39(12):3248–54.
  130. Hendrikse J, van der Zwan A, Ramos LM, van Osch MJ, Golay X, Tulleken CA, et al. Altered flow territories after extracranial-intracranial bypass surgery. *Neurosurgery.* 2005;57(3):486–94.
  131. Wityk RJ, Hillis A, Beauchamp N, Barker PB, Rigamonti D. Perfusion-weighted magnetic resonance imaging in adult moyamoya syndrome: characteristic patterns and change after surgical intervention: case report. *Neurosurgery.* 2002;51(6):1499–505.
  132. Calamante F, Ganesan V, Kirkham FJ, Jan W, Chong WK, Gadian DG, et al. MR perfusion imaging in moyamoya syndrome: potential implications for clinical evaluation of occlusive cerebrovascular disease. *Stroke.* 2001;32(12):2810–6.
  133. Jefferson AL, Glosser G, Detre JA, Sinson G, Liebeskind DS. Neuropsychological and perfusion MR imaging correlates of revascularization in a case of moyamoya syndrome. *AJNR Am J Neuroradiol.* 2006;27(1):98–100.
  134. Kim SK, Wang KC, Oh CW, Kim IO, Lee DS, Song IC, et al. Evaluation of cerebral hemodynamics with perfusion MRI in childhood moyamoya disease. *Pediatr Neurosurg.* 2003;38(2):68–75.
  135. Lee M, Zaharchuk G, Guzman R, Achrol A, Bell-Stephens T, Steinberg GK. Quantitative hemodynamic studies in moyamoya disease: a review. *Neurosurg Focus.* 2009;26(4):5.
  136. Schubert GA, Weinmann C, Seiz M, Gerigk L, Weiss C, Horn P, et al. Cerebrovascular insufficiency as the criterion for revascularization procedures in selected patients: a correlation study of xenon contrast-enhanced ct and pwi. *Neurosurg Rev.* 2009;32(1):29–35.
  137. Tanaka Y, Nariai T, Nagaoka T, Akimoto H, Ishiwata K, Ishii K, et al. Quantitative evaluation of cerebral hemodynamics in patients with moyamoya disease by dynamic susceptibility contrast magnetic resonance imaging—comparison with positron emission tomography. *J Cereb Blood Flow Metab.* 2006;26(2):291–300.
  138. Togao O, Mihara F, Yoshiura T, Tanaka A, Noguchi T, Kuwabara Y, et al. Cerebral hemodynamics in moyamoya disease: correlation between perfusion-weighted MR imaging and cerebral angiography. *AJNR Am J Neuroradiol.* 2006;27(2):391–7.
  139. Wang R, Yu S, Alger JR, Zuo Z, Chen J, Wang R, et al. Multidelay arterial spin labeling perfusion MRI in moyamoya disease—comparison with ct perfusion imaging. *Eur Radiol.* 2014;24(5):1135–44.
  140. Su P, Mao D, Liu P, Li Y, Pinho MC, Welch BG, et al. Multiparametric estimation of brain hemodynamics with MR fingerprinting asl. *Magn Reson Med.* 2017;78(5):1812–23.
  141. Anceas BM, McGarvey ML, Abrahams JM, Maldjian JA, Alsop DC, Zager EL, et al. Continuous arterial spin labeled perfusion magnetic resonance imaging in patients before and after carotid endarterectomy. *J Neuroimaging.* 2004;14(2):133–8.
  142. Gillard JH, Hardingham CR, Antoun NM, Freer CE, Kirkpatrick PJ. Evaluation of carotid endarterectomy with sequential MR perfusion imaging: a preliminary 12-month follow up. *Clin Radiol.* 1999;54(12):798–803.
  143. Kluytmans M, van der Grond J, Eikelboom BC, Viergever MA. Long-term hemodynamic effects of carotid endarterectomy. *Stroke.* 1998;29(8):1567–72.
  144. Soenne L, Helenius J, Tatlisumak T, Saimanen E, Salonen O, Lindsberg PJ, et al. Cerebral hemodynamics in asymptomatic and symptomatic patients with high-grade carotid stenosis undergoing carotid endarterectomy. *Stroke.* 2003;34(7):1655–61.
  145. Wilkinson ID, Griffiths PD, Hoggard N, Cleveland TJ, Gaines PA, Macdonald S, et al. Short-term changes in cerebral microhemodynamics after carotid stenting. *AJNR Am J Neuroradiol.* 2003;24(8):1501–7.
  146. Yun TJ, Cheon JE, Na DG, Kim WS, Kim IO, Chang KH, et al. Childhood moyamoya disease: quantitative evaluation of perfusion MR imaging—correlation with clinical outcome after revascularization surgery. *Radiology.* 2009;251(1):216–23.
  147. Hui L, Tong H. Prediction of the long-term efficacy of STA-MCA bypass by DSC-PI. *Transl Neurosci.* 2016;7(1):110–5.
  148. Lee S, Yun TJ, Yoo RE, Yoon BW, Kang KM, Choi SH, et al. Monitoring cerebral perfusion changes after revascularization in patients with moyamoya disease by using arterial spin-labeling MR imaging. *Radiology.* 2018;288(2):565–72.
  149. Hosoda K, Kawaguchi T, Shibata Y, Kamei M, Kidoguchi K, Koyama J, et al. Cerebral vasoreactivity and internal carotid artery flow help to identify patients at risk for hyperperfusion after carotid endarterectomy. *Stroke.* 2001;32(7):1567–73.
  150. Reigel MM, Hollier LH, Sundt TM Jr, Piepgras DG, Sharbrough FW, Cherry KJ. Cerebral hyperperfusion syndrome: a cause of neurologic dysfunction after carotid endarterectomy. *J Vasc Surg.* 1987;5(4):628–34.
  151. Fukuda T, Ogasawara K, Kobayashi M, Komoribayashi N, Endo H, Inoue T, et al. Prediction of cerebral hyperperfusion after carotid endarterectomy using cerebral blood volume measured

- by perfusion-weighted MR imaging compared with single-photon emission CT. *AJNR Am J Neuroradiol.* 2007;28(4):737–42.
152. Deibler AR, Pollock JM, Kraft RA, Tan H, Burdette JH, Maldjian JA. Arterial spin-labeling in routine clinical practice, part 3: hyperperfusion patterns. *AJNR Am J Neuroradiol.* 2008;29(8):1428–35.
  153. Pollock JM, Deibler AR, Whitlow CT, Tan H, Kraft RA, Burdette JH, et al. Hypercapnia-induced cerebral hyperperfusion: an underrecognized clinical entity. *AJNR Am J Neuroradiol.* 2009;30(2):378–85.
  154. Bartynski WS. Posterior reversible encephalopathy syndrome, part 2: Controversies surrounding pathophysiology of vasogenic edema. *AJNR Am J Neuroradiol.* 2008;29(6):1043–9.
  155. Bartynski WS. Posterior reversible encephalopathy syndrome, part 1: fundamental imaging and clinical features. *AJNR Am J Neuroradiol.* 2008;29(6):1036–42.
  156. Bracard S, Anxionnat R, Auliac S, Melo Neto J, Lebendinsky A, Audibert G, et al. Relevance of diffusion and perfusion weighted MRI for endovascular treatment of vasospasm in subarachnoid hemorrhage. *J Neuroradiol.* 2001;28(1):27–32.
  157. Hattingen E, Blasel S, Dettmann E, Vatter H, Pilatus U, Seifert V, et al. Perfusion-weighted MRI to evaluate cerebral autoregulation in aneurysmal subarachnoid haemorrhage. *Neuroradiology.* 2008;50(11):929–38.
  158. Hertel F, Walter C, Bettag M, Morsdorf M. Perfusion-weighted magnetic resonance imaging in patients with vasospasm: a useful new tool in the management of patients with subarachnoid hemorrhage. *Neurosurgery.* 2005;56(1):28–35.
  159. Ohtonari T, Kakinuma K, Kito T, Ezuka I, Kanazawa T. Diffusion-perfusion mismatch in symptomatic vasospasm after subarachnoid hemorrhage. *Neurol Med Chir.* 2008;48(8):331–6.
  160. Rordorf G, Koroshetz WJ, Copen WA, Gonzalez G, Yamada K, Schaefer PW, et al. Diffusion- and perfusion-weighted imaging in vasospasm after subarachnoid hemorrhage. *Stroke.* 1999;30(3):599–605.
  161. Weidauer S, Lanfermann H, Raabe A, Zanella F, Seifert V, Beck J. Impairment of cerebral perfusion and infarct patterns attributable to vasospasm after aneurysmal subarachnoid hemorrhage: a prospective MRI and DSA study. *Stroke.* 2007;38(6):1831–6.
  162. Beck J, Raabe A, Lanfermann H, Berkefeld J, De Rochemont RM, Zanella F, et al. Effects of balloon angioplasty on perfusion- and diffusion-weighted magnetic resonance imaging results and outcome in patients with cerebral vasospasm. *J Neurosurg.* 2006;105(2):220–7.
  163. Nিকে C, Muro K, Getch CC, Walker MT, Bernstein RA. Severe reversible cerebral vasoconstriction syndrome mimicking aneurysmal rupture and vasospasm. *Neurocrit Care.* 2007;7(1):81–5.
  164. Labriffe M, Ter Minassian A, Pasco-Papon A, N'Guyen S, Aube C. Feasibility and validity of monitoring subarachnoid hemorrhage by a noninvasive MRI imaging perfusion technique: pulsed arterial spin labeling (PASL). *J Neuroradiol.* 2015;42(6):358–67.
  165. Russin JJ, Montagne A, D'Amore F, He S, Shiroishi MS, Rennett RC, et al. Permeability imaging as a predictor of delayed cerebral ischemia after aneurysmal subarachnoid hemorrhage. *J Cereb Blood Flow Metab.* 2018;38(6):973–9.
  166. Wolf RL, Wang J, Detre JA, Zager EL, Hurst RW. Arteriovenous shunt visualization in arteriovenous malformations with arterial spin-labeling MR imaging. *AJNR Am J Neuroradiol.* 2008;29(4):681–7.
  167. Le TT, Fischbein NJ, Andre JB, Wijman C, Rosenberg J, Zaharchuk G. Identification of venous signal on arterial spin labeling improves diagnosis of dural arteriovenous fistulas and small arteriovenous malformations. *AJNR Am J Neuroradiol.* 2012;33(1):61–8.
  168. Hodel J, Leclerc X, Kalsoum E, Zuber M, Tamazyan R, Benadjouad MA, et al. Intracranial arteriovenous shunting: detection with arterial spin-labeling and susceptibility-weighted imaging combined. *AJNR Am J Neuroradiol.* 2017;38(1):71–6.
  169. Nabavizadeh SA, Edgar JC, Vossough A. Utility of susceptibility-weighted imaging and arterial spin perfusion imaging in pediatric brain arteriovenous shunting. *Neuroradiology.* 2014;56(10):877–84.
  170. Guo WY, Wu YT, Wu HM, Chung WY, Kao YH, Yeh TC, et al. Toward normal perfusion after radiosurgery: perfusion MR imaging with independent component analysis of brain arteriovenous malformations. *AJNR Am J Neuroradiol.* 2004;25(10):1636–44.
  171. Ducreux D, Buvat I, Meder JF, Mikulis D, Crawley A, Fredy D, et al. Perfusion-weighted MR imaging studies in brain hypervascular diseases: comparison of arterial input function extractions for perfusion measurement. *AJNR Am J Neuroradiol.* 2006;27(5):1059–69.
  172. Aronen HJ, Perkiö J. Dynamic susceptibility contrast MRI of gliomas. *Neuroimaging Clin N Am.* 2002;12(4):501–23.
  173. Cha S. Update on brain tumor imaging: from anatomy to physiology. *AJNR Am J Neuroradiol.* 2006;27(3):475–87.
  174. Provenzale JM, Mukundan S, Dewhurst M. The role of blood-brain barrier permeability in brain tumor imaging and therapeutics. *AJR Am J Roentgenol.* 2005;185(3):763–7.
  175. Aronen HJ, Gazit IE, Louis DN, Buchbinder BR, Pardo FS, Weisskoff RM, et al. Cerebral blood volume maps of gliomas: comparison with tumor grade and histologic findings. *Radiology.* 1994;191(1):41–51.
  176. Gasparetto EL, Pawlak MA, Patel SH, Huse J, Woo JH, Krejza J, et al. Posttreatment recurrence of malignant brain neoplasm: accuracy of relative cerebral blood volume fraction in discriminating low from high malignant histologic volume fraction. *Radiology.* 2009;250(3):887–96.
  177. Lev MH, Ozsunar Y, Henson JW, Rasheed AA, Barest GD, et al. Glial tumor grading and outcome prediction using dynamic spin-echo MR susceptibility mapping compared with conventional contrast-enhanced MR: confounding effect of elevated rcbv of oligodendrogliomas. *AJNR Am J Neuroradiol.* 2004;25(2):214–21.
  178. Donahue KM, Krouwer HG, Rand SD, Pathak AP, Marszalkowski CS, Censky SC, et al. Utility of simultaneously acquired gradient-echo and spin-echo cerebral blood volume and morphology maps in brain tumor patients. *Magn Reson Med.* 2000;43(6):845–53.
  179. Schmainda KM, Rand SD, Joseph AM, Lund R, Ward BD, Pathak AP, et al. Characterization of a first-pass gradient-echo spin-echo method to predict brain tumor grade and angiogenesis. *AJNR Am J Neuroradiol.* 2004;25(9):1524–32.
  180. Batchelor TT, Sorensen AG, di Tomaso E, Zhang WT, Duda DG, Cohen KS, et al. AZD2171, a pan-VEGF receptor tyrosine kinase inhibitor, normalizes tumor vasculature and alleviates edema in glioblastoma patients. *Cancer Cell.* 2007;11(1):83–95.
  181. Emblem KE, Mouridsen K, Bjornerud A, Farrar CT, Jennings D, Borra RJ, et al. Vessel architectural imaging identifies cancer patient responders to anti-angiogenic therapy. *Nat Med.* 2013;19(9):1178–83.
  182. Tourdias T, Rodrigo S, Oppenheim C, Naggara O, Varlet P, Amoussa S, et al. Pulsed arterial spin labeling applications in brain tumors: practical review. *J Neuroradiol.* 2008;35(2):79–89.
  183. Kong L, Chen H, Yang Y, Chen L. A meta-analysis of arterial spin labelling perfusion values for the prediction of glioma grade. *Clin Radiol.* 2017;72(3):255–61.
  184. Cao Y, Sundgren PC, Tsien CI, Chenevert TT, Junck L. Physiologic and metabolic magnetic resonance imaging in gliomas. *J Clin Oncol.* 2006;24(8):1228–35.
  185. Cha S. Neuroimaging in neuro-oncology. *Neurotherapeutics.* 2009;6(3):465–77.
  186. Cha S, Pierce S, Knopp EA, Johnson G, Yang C, Ton A, et al. Dynamic contrast-enhanced T2\*-weighted MR imaging of

- tumefactive demyelinating lesions. *AJNR Am J Neuroradiol.* 2001;22(6):1109–16.
187. Bernarding J, Braun J, Koennecke HC. Diffusion- and perfusion-weighted MR imaging in a patient with acute demyelinating encephalomyelitis (adem). *J Magn Reson Imaging.* 2002;15(1):96–100.
  188. Pivawer G, Law M, Zagzag D. Perfusion MR imaging and proton MR spectroscopic imaging in differentiating necrotizing cerebritis from glioblastoma multiforme. *Magn Reson Imaging.* 2007;25(2):238–43.
  189. Ge Y, Law M, Johnson G, Herbert J, Babb JS, Mannon LJ, et al. Dynamic susceptibility contrast perfusion MR imaging of multiple sclerosis lesions: characterizing hemodynamic impairment and inflammatory activity. *AJNR Am J Neuroradiol.* 2005;26(6):1539–47.
  190. Chan JH, Tsui EY, Chau LF, Chow KY, Chan MS, Yuen MK, et al. Discrimination of an infected brain tumor from a cerebral abscess by combined MR perfusion and diffusion imaging. *Comput Med Imaging Graph.* 2002;26(1):19–23.
  191. Erdogan C, Hakyemez B, Yildirim N, Parlak M. Brain abscess and cystic brain tumor: discrimination with dynamic susceptibility contrast perfusion-weighted MRI. *J Comput Assist Tomogr.* 2005;29(5):663–7.
  192. Ernst TM, Chang L, Witt MD, Aronow HA, Cornford ME, Walot I, et al. Cerebral toxoplasmosis and lymphoma in aids: perfusion MR imaging experience in 13 patients. *Radiology.* 1998;208(3):663–9.
  193. Holmes TM, Petrella JR, Provenzale JM. Distinction between cerebral abscesses and high-grade neoplasms by dynamic susceptibility contrast perfusion MRI. *AJR Am J Roentgenol.* 2004;183(5):1247–52.
  194. Muccio CF, Esposito G, Bartolini A, Cerase A. Cerebral abscesses and necrotic cerebral tumours: Differential diagnosis by perfusion-weighted magnetic resonance imaging. *Radiol Med.* 2008;113(5):747–57.
  195. Floriano VH, Torres US, Spotti AR, Ferraz-Filho JR, Tognola WA. The role of dynamic susceptibility contrast-enhanced perfusion MR imaging in differentiating between infectious and neoplastic focal brain lesions: results from a cohort of 100 consecutive patients. *PLoS One.* 2013;8(12):e81509.
  196. Chawla S, Wang S, Mohan S, Nasrallah M, Verma G, Brem S, et al. Differentiation of brain infection from necrotic glioblastoma using combined analysis of diffusion and perfusion MRI. *J Magn Reson Imaging.* 2018;49(1):184–94.
  197. Al-Okaili RN, Krejza J, Woo JH, Wolf RL, O'Rourke DM, Judy KD, et al. Intraaxial brain masses: MR imaging-based diagnostic strategy—initial experience. *Radiology.* 2007;243(2):539–50.
  198. Cha S, Knopp EA, Johnson G, Wetzel SG, Litt AW, Zagzag D. Intracranial mass lesions: dynamic contrast-enhanced susceptibility-weighted echo-planar perfusion MR imaging. *Radiology.* 2002;223(1):11–29.
  199. Soni N, Srindharan K, Kumar S, Mishra P, Bathla G, Kalita J, et al. Arterial spin labeling perfusion: Prospective MR imaging in differentiating neoplastic from non-neoplastic intra-axial brain lesions. *Neuroradiol J.* 2018;2018:1971400918783058.
  200. Knopp EA, Cha S, Johnson G, Mazumdar A, Golfinos JG, Zagzag D, et al. Glial neoplasms: dynamic contrast-enhanced t2\*-weighted MR imaging. *Radiology.* 1999;211(3):791–8.
  201. Ludemann L, Grieger W, Wurm R, Budzisch M, Hamm B, Zimmer C. Comparison of dynamic contrast-enhanced MRI with who tumor grading for gliomas. *Eur Radiol.* 2001;11(7):1231–41.
  202. Maeda M, Itoh S, Kimura H, Iwasaki T, Hayashi N, Yamamoto K, et al. Tumor vascularity in the brain: evaluation with dynamic susceptibility-contrast MR imaging. *Radiology.* 1993;189(1):233–8.
  203. Jackson A, Kassner A, Annesley-Williams D, Reid H, Zhu XP, Li KL. Abnormalities in the recirculation phase of contrast agent bolus passage in cerebral gliomas: comparison with relative blood volume and tumor grade. *AJNR Am J Neuroradiol.* 2002;23(1):7–14.
  204. Lupo JM, Cha S, Chang SM, Nelson SJ. Dynamic susceptibility-weighted perfusion imaging of high-grade gliomas: characterization of spatial heterogeneity. *AJNR Am J Neuroradiol.* 2005;26(6):1446–54.
  205. Sugahara T, Korogi Y, Kochi M, Ushio Y, Takahashi M. Perfusion-sensitive MR imaging of gliomas: comparison between gradient-echo and spin-echo echo-planar imaging techniques. *AJNR Am J Neuroradiol.* 2001;22(7):1306–15.
  206. Young GS, Setayesh K. Spin-echo echo-planar perfusion MR imaging in the differential diagnosis of solitary enhancing brain lesions: distinguishing solitary metastases from primary glioma. *AJNR Am J Neuroradiol.* 2009;30(3):575–7.
  207. Law M, Yang S, Babb JS, Knopp EA, Golfinos JG, Zagzag D, et al. Comparison of cerebral blood volume and vascular permeability from dynamic susceptibility contrast-enhanced perfusion MR imaging with glioma grade. *AJNR Am J Neuroradiol.* 2004;25(5):746–55.
  208. Provenzale JM, Wang GR, Brenner T, Petrella JR, Sorensen AG. Comparison of permeability in high-grade and low-grade brain tumors using dynamic susceptibility contrast MR imaging. *AJR Am J Roentgenol.* 2002;178(3):711–6.
  209. Roberts HC, Roberts TP, Brasch RC, Dillon WP. Quantitative measurement of microvascular permeability in human brain tumors achieved using dynamic contrast-enhanced MR imaging: correlation with histologic grade. *AJNR Am J Neuroradiol.* 2000;21(5):891–9.
  210. Weber MA, Zoubaa S, Schlieter M, Juttler E, Huttner HB, Geletneky K, et al. Diagnostic performance of spectroscopic and perfusion MRI for distinction of brain tumors. *Neurology.* 2006;66(12):1899–906.
  211. Maia AC Jr, Malheiros SM, da Rocha AJ, da Silva CJ, Gabbai AA, Ferraz FA, et al. MR cerebral blood volume maps correlated with vascular endothelial growth factor expression and tumor grade in nonenhancing gliomas. *AJNR Am J Neuroradiol.* 2005;26(4):777–83.
  212. Whitmore RG, Krejza J, Kapoor GS, Huse J, Woo JH, Bloom S, et al. Prediction of oligodendroglial tumor subtype and grade using perfusion weighted magnetic resonance imaging. *J Neurosurg.* 2007;107(3):600–9.
  213. Wolf RL, Wang J, Wang S, Melhem ER, O'Rourke DM, Judy KD, et al. Grading of CNS neoplasms using continuous arterial spin labeled perfusion MR imaging at 3 tesla. *J Magn Reson Imaging.* 2005;22(4):475–82.
  214. Law M, Meltzer DE, Wetzel SG, Yang S, Knopp EA, Golfinos J, et al. Conventional MR imaging with simultaneous measurements of cerebral blood volume and vascular permeability in ganglioglioma. *Magn Reson Imaging.* 2004;22(5):599–606.
  215. Noguchi T, Yoshiura T, Hiwatashi A, Togao O, Yamashita K, Nagao E, et al. Perfusion imaging of brain tumors using arterial spin-labeling: correlation with histopathologic vascular density. *AJNR Am J Neuroradiol.* 2008;29(4):688–93.
  216. Law M, Young R, Babb J, Pollack E, Johnson G. Histogram analysis versus region of interest analysis of dynamic susceptibility contrast perfusion MR imaging data in the grading of cerebral gliomas. *AJNR Am J Neuroradiol.* 2007;28(4):761–6.
  217. Wetzel SG, Cha S, Law M, Johnson G, Golfinos J, Lee P, et al. Preoperative assessment of intracranial tumors with perfusion MR and a volumetric interpolated examination: a comparative study with DSA. *AJNR Am J Neuroradiol.* 2002;23(10):1767–74.

218. Law M, Yang S, Wang H, Babb JS, Johnson G, Cha S, et al. Glioma grading: sensitivity, specificity, and predictive values of perfusion MR imaging and proton MR spectroscopic imaging compared with conventional MR imaging. *AJNR Am J Neuroradiol.* 2003;24(10):1989–98.
219. Emblem KE, Nedregard B, Nome T, Due-Tonnessen P, Hald JK, Scheie D, et al. Glioma grading by using histogram analysis of blood volume heterogeneity from mr-derived cerebral blood volume maps. *Radiology.* 2008;247(3):808–17.
220. Young R, Babb J, Law M, Pollack E, Johnson G. Comparison of region-of-interest analysis with three different histogram analysis methods in the determination of perfusion metrics in patients with brain gliomas. *J Magn Reson Imaging.* 2007;26(4):1053–63.
221. Jia Z, Geng D, Xie T, Zhang J, Liu Y. Quantitative analysis of neovascular permeability in glioma by dynamic contrast-enhanced MR imaging. *J Clin Neurosci.* 2012;19(6):820–3.
222. Jung SC, Yeom JA, Kim JH, Ryoo I, Kim SC, Shin H, et al. Glioma: application of histogram analysis of pharmacokinetic parameters from t1-weighted dynamic contrast-enhanced MR imaging to tumor grading. *AJNR Am J Neuroradiol.* 2014;35(6):1103–10.
223. Anzalone N, Castellano A, Cadioli M, Conte GM, Cuccarini V, Bizzi A, et al. Brain gliomas: multicenter standardized assessment of dynamic contrast-enhanced and dynamic susceptibility contrast MR images. *Radiology.* 2018;287(3):933–43.
224. Chawla S, Wang S, Wolf RL, Woo JH, Wang J, O'Rourke DM, et al. Arterial spin-labeling and MR spectroscopy in the differentiation of gliomas. *AJNR Am J Neuroradiol.* 2007;28(9):1683–9.
225. Verma R, Zacharaki EI, Ou Y, Cai H, Chawla S, Lee SK, et al. Multiparametric tissue characterization of brain neoplasms and their recurrence using pattern classification of MR images. *Acad Radiol.* 2008;15(8):966–77.
226. Gaa J, Warach S, Wen P, Thangaraj V, Wielopolski P, Edelman RR. Noninvasive perfusion imaging of human brain tumors with epistar. *Eur Radiol.* 1996;6(4):518–22.
227. Warmuth C, Gunther M, Zimmer C. Quantification of blood flow in brain tumors: comparison of arterial spin labeling and dynamic susceptibility-weighted contrast-enhanced MR imaging. *Radiology.* 2003;228(2):523–32.
228. Wang J, Fernandez-Seara MA, Wang S, St Lawrence KS. When perfusion meets diffusion: in vivo measurement of water permeability in human brain. *J Cereb Blood Flow Metab.* 2006;13:13.
229. Arisawa A, Watanabe Y, Tanaka H, Takahashi H, Matsuo C, Fujiwara T, et al. Comparative study of pulsed-continuous arterial spin labeling and dynamic susceptibility contrast imaging by histogram analysis in evaluation of glial tumors. *Neuroradiology.* 2018;60(6):599–608.
230. Sugahara T, Korogi Y, Kochi M, Ikushima I, Hirai T, Okuda T, et al. Correlation of MR imaging-determined cerebral blood volume maps with histologic and angiographic determination of vascularity of gliomas. *AJR Am J Roentgenol.* 1998;171(6):1479–86.
231. Calli C, Kitis O, Yuntun N, Yurtseven T, Islekel S, Akalin T. Perfusion and diffusion MR imaging in enhancing malignant cerebral tumors. *Eur J Radiol.* 2006;58(3):394–403.
232. Hakyemez B, Erdogan C, Bolca N, Yildirim N, Gokalp G, Parlak M. Evaluation of different cerebral mass lesions by perfusion-weighted MR imaging. *J Magn Reson Imaging.* 2006;24(4):817–24.
233. Liao W, Liu Y, Wang X, Jiang X, Tang B, Fang J, et al. Differentiation of primary central nervous system lymphoma and high-grade glioma with dynamic susceptibility contrast-enhanced perfusion magnetic resonance imaging. *Acta Radiol.* 2009;50(2):217–25.
234. Sugahara T, Korogi Y, Shigematsu Y, Hirai T, Ikushima I, Liang L, et al. Perfusion-sensitive MRI of cerebral lymphomas: a preliminary report. *J Comput Assist Tomogr.* 1999;23(2):232–7.
235. Law M, Cha S, Knopp EA, Johnson G, Arnett J, Litt AW. High-grade gliomas and solitary metastases: differentiation by using perfusion and proton spectroscopic MR imaging. *Radiology.* 2002;222(3):715–21.
236. Mangla R, Kolar B, Zhu T, Zhong J, Almast J, Ekholm S. Percentage signal recovery derived from MR dynamic susceptibility contrast imaging is useful to differentiate common enhancing malignant lesions of the brain. *AJNR Am J Neuroradiol.* 2011;32(6):1004–10.
237. Xing Z, You RX, Li J, Liu Y, Cao DR. Differentiation of primary central nervous system lymphomas from high-grade gliomas by rcbv and percentage of signal intensity recovery derived from dynamic susceptibility-weighted contrast-enhanced perfusion MR imaging. *Clin Neuroradiol.* 2014;24(4):329–36.
238. Cha S, Lupo JM, Chen MH, Lamborn KR, McDermott MW, Berger MS, et al. Differentiation of glioblastoma multiforme and single brain metastasis by peak height and percentage of signal intensity recovery derived from dynamic susceptibility-weighted contrast-enhanced perfusion MR imaging. *AJNR Am J Neuroradiol.* 2007;28(6):1078–84.
239. Kickingeder P, Wiestler B, Sahn F, Heiland S, Roethke M, Schlemmer HP, et al. Primary central nervous system lymphoma and atypical glioblastoma: multiparametric differentiation by using diffusion-, perfusion-, and susceptibility-weighted MR imaging. *Radiology.* 2014;272(3):843–50.
240. Lu S, Wang S, Gao Q, Zhou M, Li Y, Cao P, et al. Quantitative evaluation of diffusion and dynamic contrast-enhanced magnetic resonance imaging for differentiation between primary central nervous system lymphoma and glioblastoma. *J Comput Assist Tomogr.* 2017;41(6):898–903.
241. Hakyemez B, Yildirim N, Erdogan C, Kocaeli H, Korfali E, Parlak M. Meningiomas with conventional MRI findings resembling intraaxial tumors: can perfusion-weighted MRI be helpful in differentiation? *Neuroradiology.* 2006;48(10):695–702.
242. Kimura H, Takeuchi H, Koshimoto Y, Arishima H, Uematsu H, Kawamura Y, et al. Perfusion imaging of meningioma by using continuous arterial spin-labeling: comparison with dynamic susceptibility-weighted contrast-enhanced MR images and histopathologic features. *AJNR Am J Neuroradiol.* 2006;27(1):85–93.
243. Ludemann L, Grieger W, Wurm R, Wust P, Zimmer C. Quantitative measurement of leakage volume and permeability in gliomas, meningiomas and brain metastases with dynamic contrast-enhanced MRI. *Magn Reson Imaging.* 2005;23(8):833–41.
244. Uematsu H, Maeda M, Sadato N, Matsuda T, Ishimori Y, Koshimoto Y, et al. Vascular permeability: Quantitative measurement with double-echo dynamic MR imaging—theory and clinical application. *Radiology.* 2000;214(3):912–7.
245. Yang S, Law M, Zagzag D, Wu HH, Cha S, Golfinos JG, et al. Dynamic contrast-enhanced perfusion MR imaging measurements of endothelial permeability: differentiation between atypical and typical meningiomas. *AJNR Am J Neuroradiol.* 2003;24(8):1554–9.
246. Kremer S, Grand S, Remy C, Pasquier B, Benabid AL, Bracard S, et al. Contribution of dynamic contrast MR imaging to the differentiation between dural metastasis and meningioma. *Neuroradiology.* 2004;46(8):642–8.
247. Qiao XJ, Kim HG, Wang DJJ, Salamon N, Linetsky M, Sepahdari A, et al. Application of arterial spin labeling perfusion MRI to differentiate benign from malignant intracranial meningiomas. *Eur J Radiol.* 2017;97:31–6.
248. Xiao HF, Lou X, Liu MY, Wang YL, Wang Y, Chen ZY, et al. The role of magnetic resonance diffusion-weighted imaging and three-dimensional arterial spin labelling perfusion imaging in the differentiation of parasellar meningioma and cavernous haemangioma. *J Int Med Res.* 2014;42(4):915–25.



249. Lu Y, Luan S, Liu L, Xiong J, Wen J, Qu J, et al. Evaluation of the applicability of territorial arterial spin labeling in meningiomas for presurgical assessments compared with 3-dimensional time-of-flight magnetic resonance angiography. *Eur Radiol*. 2017;27(10):4072–81.
250. Callot V, Galanaud D, Figarella-Branger D, Lefur Y, Metellus P, Nicoli F, et al. Correlations between MR and endothelial hyperplasia in low-grade gliomas. *J Magn Reson Imaging*. 2007;26(1):52–60.
251. Chaskis C, Stadnik T, Michotte A, Van Rompaey K, D'Haens J. Prognostic value of perfusion-weighted imaging in brain glioma: a prospective study. *Acta Neurochir*. 2006;148(3):277–85. discussion 85
252. Maia AC Jr, Malheiros SM, da Rocha AJ, Stavale JN, Guimaraes IF, Borges LR, et al. Stereotactic biopsy guidance in adults with supratentorial nonenhancing gliomas: role of perfusion-weighted magnetic resonance imaging. *J Neurosurg*. 2004;101(6):970–6.
253. Ningning D, Haopeng P, Xuefei D, Wenna C, Yan R, Jingsong W, et al. Perfusion imaging of brain gliomas using arterial spin labeling: correlation with histopathological vascular density in MRI-guided biopsies. *Neuroradiology*. 2017;59(1):51–9.
254. Jin T, Ren Y, Zhang H, Xie Q, Yao Z, Feng X. Application of MRS- and ASL-guided navigation for biopsy of intracranial tumors. *Acta Radiol*. 2018;2018:284185118780906.
255. Law M, Oh S, Babb JS, Wang E, Inglese M, Zagzag D, et al. Low-grade gliomas: dynamic susceptibility-weighted contrast-enhanced perfusion MR imaging—prediction of patient clinical response. *Radiology*. 2006;238(2):658–67. Epub 2006 Jan 5
256. Law M, Oh S, Johnson G, Babb JS, Zagzag D, Golfinos J, et al. Perfusion magnetic resonance imaging predicts patient outcome as an adjunct to histopathology: a second reference standard in the surgical and nonsurgical treatment of low-grade gliomas. *Neurosurgery*. 2006;58(6):1099–107. discussion -107
257. Law M, Young RJ, Babb JS, Peccerelli N, Chheang S, Gruber ML, et al. Gliomas: predicting time to progression or survival with cerebral blood volume measurements at dynamic susceptibility-weighted contrast-enhanced perfusion MR imaging. *Radiology*. 2008;247(2):490–8.
258. Hoefnagels FW, Lagerwaard FJ, Sanchez E, Haasbeek CJ, Knol DL, Slotman BJ, et al. Radiological progression of cerebral metastases after radiosurgery: Assessment of perfusion MRI for differentiating between necrosis and recurrence. *J Neurol*. 2009;256(6):878–87.
259. Bisdas S, Kirkpatrick M, Giglio P, Welsh C, Spampinato MV, Rumboldt Z. Cerebral blood volume measurements by perfusion-weighted MR imaging in gliomas: ready for prime time in predicting short-term outcome and recurrent disease? *AJNR Am J Neuroradiol*. 2009;30(4):681–8.
260. Cao Y, Tsien CI, Nagesh V, Junck L, Ten Haken R, Ross BD, et al. Survival prediction in high-grade gliomas by MRI perfusion before and during early stage of RT [corrected]. *Int J Radiat Oncol Biol Phys*. 2006;64(3):876–85.
261. Hirai T, Murakami R, Nakamura H, Kitajima M, Fukuoka H, Sasao A, et al. Prognostic value of perfusion MR imaging of high-grade astrocytomas: long-term follow-up study. *AJNR Am J Neuroradiol*. 2008;29(8):1505–10.
262. Saraswathy S, Crawford FW, Lamborn KR, Pirzkall A, Chang S, Cha S, et al. Evaluation of MR markers that predict survival in patients with newly diagnosed gbm prior to adjuvant therapy. *J Neuro-Oncol*. 2009;91(1):69–81.
263. Paik W, Kim HS, Choi CG, Kim SJ. Pre-operative perfusion skewness and kurtosis are potential predictors of progression-free survival after partial resection of newly diagnosed glioblastoma. *Korean J Radiol*. 2016;17(1):117–26.
264. Coban G, Mohan S, Kural F, Wang S, O'Rourke DM, Poptani H. Prognostic value of dynamic susceptibility contrast-enhanced and diffusion-weighted MR imaging in patients with glioblastomas. *AJNR Am J Neuroradiol*. 2015;36(7):1247–52.
265. Jabehdar Maralani P, Melhem ER, Wang S, Herskovits EH, Voluck MR, Kim SJ, et al. Association of dynamic susceptibility contrast enhanced MR perfusion parameters with prognosis in elderly patients with glioblastomas. *Eur Radiol*. 2015;25(9):2738–44.
266. Ohgaki H, Kleihues P. The definition of primary and secondary glioblastoma. *Clin Cancer Res*. 2013;19(4):764–72.
267. Cao Y, Nagesh V, Hamstra D, Tsien CI, Ross BD, Chenevert TL, et al. The extent and severity of vascular leakage as evidence of tumor aggressiveness in high-grade gliomas. *Cancer Res*. 2006;66(17):8912–7.
268. Law M, Brodsky JE, Babb J, Rosenblum M, Miller DC, Zagzag D, et al. High cerebral blood volume in human gliomas predicts deletion of chromosome 1p: preliminary results of molecular studies in gliomas with elevated perfusion. *J Magn Reson Imaging*. 2007;25(6):1113–9.
269. Gupta A, Young RJ, Shah AD, Schweitzer AD, Graber JJ, Shi W, et al. Pretreatment dynamic susceptibility contrast MRI perfusion in glioblastoma: prediction of egfr gene amplification. *Clin Neuroradiol*. 2015;25(2):143–50.
270. Ryoo I, Choi SH, Kim JH, Sohn CH, Kim SC, Shin HS, et al. Cerebral blood volume calculated by dynamic susceptibility contrast-enhanced perfusion MR imaging: preliminary correlation study with glioblastoma genetic profiles. *PLoS One*. 2013;8(8):e71704.
271. Tan W, Xiong J, Huang W, Wu J, Zhan S, Geng D. Noninvasively detecting isocitrate dehydrogenase 1 gene status in astrocytoma by dynamic susceptibility contrast MRI. *J Magn Reson Imaging*. 2017;45(2):492–9.
272. Xing Z, Yang X, She D, Lin Y, Zhang Y, Cao D. Noninvasive assessment of idh mutational status in world health organization grade ii and iii astrocytomas using dwi and DSC-PWI combined with conventional MR imaging. *AJNR Am J Neuroradiol*. 2017;38(6):1138–44.
273. Lin Y, Xing Z, She D, Yang X, Zheng Y, Xiao Z, et al. Idh mutant and 1p/19q co-deleted oligodendrogliomas: tumor grade stratification using diffusion-, susceptibility-, and perfusion-weighted MRI. *Neuroradiology*. 2017;59(6):555–62.
274. Bakas S, Akbari H, Pisapia J, Martinez-Lage M, Rozycki M, Rathore S, et al. In vivo detection of egfrviii in glioblastoma via perfusion magnetic resonance imaging signature consistent with deep peritumoral infiltration: the phi-index. *Clin Cancer Res*. 2017;23(16):4724–34.
275. Cha S, Knopp EA, Johnson G, Litt A, Glass J, Gruber ML, et al. Dynamic contrast-enhanced t2-weighted MR imaging of recurrent malignant gliomas treated with thalidomide and carboplatin. *AJNR Am J Neuroradiol*. 2000;21(5):881–90.
276. Fuss M, Wenz F, Scholdei R, Essig M, Debus J, Knopp MV, et al. Radiation-induced regional cerebral blood volume (rcbv) changes in normal brain and low-grade astrocytomas: quantification and time and dose-dependent occurrence. *Int J Radiat Oncol Biol Phys*. 2000;48(1):53–8.
277. Weber MA, Thilmann C, Lichy MP, Gunther M, Delorme S, Zuna I, et al. Assessment of irradiated brain metastases by means of arterial spin-labeling and dynamic susceptibility-weighted contrast-enhanced perfusion MRI: initial results. *Investig Radiol*. 2004;39(5):277–87.
278. Wenz F, Rempp K, Hess T, Debus J, Brix G, Engenhart R, et al. Effect of radiation on blood volume in low-grade astrocytomas and normal brain tissue: quantification with dynamic susceptibility contrast MR imaging. *AJR Am J Roentgenol*. 1996;166(1):187–93.

279. Kickingereder P, Wiestler B, Burth S, Wick A, Nowosielski M, Heiland S, et al. Relative cerebral blood volume is a potential predictive imaging biomarker of bevacizumab efficacy in recurrent glioblastoma. *Neuro-Oncology*. 2015;17(8):1139–47.
280. Verhoeff JJ, Lavini C, van Linde ME, Stalpers LJ, Majoie CB, Reijneveld JC, et al. Bevacizumab and dose-intense temozolomide in recurrent high-grade glioma. *Ann Oncol*. 2010;21(8):1723–7.
281. Schmainda KM, Prah M, Connelly J, Rand SD, Hoffman RG, Mueller W, et al. Dynamic-susceptibility contrast agent MRI measures of relative cerebral blood volume predict response to bevacizumab in recurrent high-grade glioma. *Neuro-Oncology*. 2014;16(6):880–8.
282. Schmainda KM, Zhang Z, Prah M, Snyder BS, Gilbert MR, Sorensen AG, et al. Dynamic susceptibility contrast MRI measures of relative cerebral blood volume as a prognostic marker for overall survival in recurrent glioblastoma: results from the acrin 6677/rtog 0625 multicenter trial. *Neuro-Oncology*. 2015;17(8):1148–56.
283. Choi SH, Jung SC, Kim KW, Lee JY, Choi Y, Park SH, et al. Perfusion MRI as the predictive/prognostic and pharmacodynamic biomarkers in recurrent malignant glioma treated with bevacizumab: a systematic review and a time-to-event meta-analysis. *J Neuro-Oncol*. 2016;128(2):185–94.
284. Andersen C, Jensen FT. Differences in blood-tumour-barrier leakage of human intracranial tumours: quantitative monitoring of vasogenic oedema and its response to glucocorticoid treatment. *Acta Neurochir*. 1998;140(9):919–24.
285. Armitage PA, Schwindack C, Bastin ME, Whittle IR. Quantitative assessment of intracranial tumor response to dexamethasone using diffusion, perfusion and permeability magnetic resonance imaging. *Magn Reson Imaging*. 2007;25(3):303–10.
286. Bastin ME, Carpenter TK, Armitage PA, Sinha S, Wardlaw JM, Whittle IR. Effects of dexamethasone on cerebral perfusion and water diffusion in patients with high-grade glioma. *AJNR Am J Neuroradiol*. 2006;27(2):402–8.
287. Wilkinson ID, Jellineck DA, Levy D, Giesel FL, Romanowski CA, Miller BA, et al. Dexamethasone and enhancing solitary cerebral mass lesions: alterations in perfusion and blood-tumor barrier kinetics shown by magnetic resonance imaging. *Neurosurgery*. 2006;58(4):640–6. discussion –6
288. Kumar AJ, Leeds NE, Fuller GN, Van Tassel P, Maor MH, Sawaya RE, et al. Malignant gliomas: MR imaging spectrum of radiation therapy- and chemotherapy-induced necrosis of the brain after treatment. *Radiology*. 2000;217(2):377–84.
289. Giglio P, Gilbert MR. Cerebral radiation necrosis. *Neurologist*. 2003;9(4):180–8.
290. Clarke JL, Chang S. Pseudoprogression and pseudoresponse: challenges in brain tumor imaging. *Curr Neurol Neurosci Rep*. 2009;9(3):241–6.
291. Robins HL, Lassman AB, Khuntia D. Therapeutic advances in malignant glioma: current status and future prospects. *Neuroimaging Clin N Am*. 2009;19(4):647–56.
292. Brandes AA, Franceschi E, Tosoni A, Blatt V, Pession A, Tallini G, et al. Mgmt promoter methylation status can predict the incidence and outcome of pseudoprogression after concomitant radiochemotherapy in newly diagnosed glioblastoma patients. *J Clin Oncol*. 2008;26(13):2192–7.
293. Chamberlain MC, Glantz MJ, Chalmers L, Van Horn A, Sloan AE. Early necrosis following concurrent temodar and radiotherapy in patients with glioblastoma. *J Neuro-Oncol*. 2007;82(1):81–3.
294. Barajas RF Jr, Chang JS, Segal MR, Parsa AT, McDermott MW, Berger MS, et al. Differentiation of recurrent glioblastoma multiforme from radiation necrosis after external beam radiation therapy with dynamic susceptibility-weighted contrast-enhanced perfusion MR imaging. *Radiology*. 2009;253(2):486–96.
295. Forsyth PA, Kelly PJ, Cascino TL, Scheithauer BW, Shaw EG, Dinapoli RP, et al. Radiation necrosis or glioma recurrence: Is computer-assisted stereotactic biopsy useful? *J Neurosurg*. 1995;82(3):436–44.
296. McGirt MJ, Bulsara KR, Cummings TJ, New KC, Little KM, Friedman HS, et al. Prognostic value of magnetic resonance imaging-guided stereotactic biopsy in the evaluation of recurrent malignant astrocytoma compared with a lesion due to radiation effect. *J Neurosurg*. 2003;98(1):14–20.
297. Wang S, Martinez-Lage M, Sakai Y, Chawla S, Kim SG, Alonso-Basanta M, et al. Differentiating tumor progression from pseudoprogression in patients with glioblastomas using diffusion tensor imaging and dynamic susceptibility contrast MRI. *AJNR Am J Neuroradiol*. 2016;37(1):28–36.
298. Boxerman JL, Ellingson BM, Jeyapalan S, Elinzano H, Harris RJ, Rogg JM, et al. Longitudinal DSC-MRI for distinguishing tumor recurrence from pseudoprogression in patients with a high-grade glioma. *Am J Clin Oncol*. 2017;40(3):228–34.
299. Thomas AA, Arevalo-Perez J, Kaley T, Lyo J, Peck KK, Shi W, et al. Dynamic contrast enhanced T1 MRI perfusion differentiates pseudoprogression from recurrent glioblastoma. *J Neuro-Oncol*. 2015;125(1):183–90.
300. Bisdas S, Naegel T, Ritz R, Dimostheni A, Pfannenbergs C, Reimold M, et al. Distinguishing recurrent high-grade gliomas from radiation injury: a pilot study using dynamic contrast-enhanced MR imaging. *Acad Radiol*. 2011;18(5):575–83.
301. Chung WJ, Kim HS, Kim N, Choi CG, Kim SJ. Recurrent glioblastoma: Optimum area under the curve method derived from dynamic contrast-enhanced t1-weighted perfusion MR imaging. *Radiology*. 2013;269(2):561–8.
302. Ye J, Bhagat SK, Li H, Luo X, Wang B, Liu L, et al. Differentiation between recurrent gliomas and radiation necrosis using arterial spin labeling perfusion imaging. *Exp Ther Med*. 2016;11(6):2432–6.
303. Choi YJ, Kim HS, Jahng GH, Kim SJ, Suh DC. Pseudoprogression in patients with glioblastoma: added value of arterial spin labeling to dynamic susceptibility contrast perfusion MR imaging. *Acta Radiol*. 2013;54(4):448–54.
304. Ellingson BM, Chung C, Pope WB, Boxerman JL, Kaufmann TJ. Pseudoprogression, radionecrosis, inflammation or true tumor progression? Challenges associated with glioblastoma response assessment in an evolving therapeutic landscape. *J Neuro-Oncol*. 2017;134(3):495–504.
305. Lacerda S, Law M. Magnetic resonance perfusion and permeability imaging in brain tumors. *Neuroimaging Clin N Am*. 2009;19(4):527–57.
306. Saut O, Lagaert JB, Colin T, Fathallah-Shaykh HM. A multilayer grow-or-go model for gbm: effects of invasive cells and anti-angiogenesis on growth. *Bull Math Biol*. 2014;76(9):2306–33.
307. Lanzman B, Heit JJ. Advanced MRI measures of cerebral perfusion and their clinical applications. *Top Magn Reson Imaging*. 2017;26(2):83–90.